

CHAPTER I
INTRODUCTION

1.1 General Introduction

1.1.1 Historical Development

1.1.1.1 Methanol as an Industrial Fuel

Methanol or methyl alcohol (CH_3OH) was originally produced by destructive distillation of wood in 1830. This primitive process was replaced in 1923 by a German company Badische Anilin-und-Soda-Fabrik or BASF with the establishment of the first synthetic methanol plant that produced methanol from water gas as a source of syngas. In the 1940's however, natural gas became the main source of syngas and this revolutionized the methanol production industry [1]. With the introduction of low pressure (5-10Mpa) synthesis route of methanol using copper catalyst, the methanol industry and its chemical derivatives were even largely produced. Since then, not only has it caught the attention of countries with huge natural gas reserves due to its viability of production, but also of the green environmentalists who deem methanol to be a cleaner burning fuel and a better option to replace the conventional gasoline. This was a major agenda in the Clean Air Act 1990 [1], enabling methyl tert-butyl derived from methanol and isobutene to become the most widely used oxygenate in reformulated cleaner gasoline. Thus the methanol is not only an economically profitable but environmentally preferable as well. Thus, Mega-methanol or large capacity methanol production plants have been built to meet the ever increasing demand for methanol.

1.1.1.2 Methanol Synthesis Catalysts

The original methanol synthesis catalysts, $\text{CrO}_3\text{-ZnO}$ were developed by BASF in 1923. These were low activity catalyst and were operated at severe conditions of 300 atm and up to 400°C . These catalysts were soon replaced by the $\text{Cu/ZnO/Al}_2\text{O}_3$ catalyst developed by Balsiak in 1947 and operated still at high pressure. In 1960, a low temperature and low pressure methanol synthesis route was developed by ICI using the same $\text{Cu/ZnO/Al}_2\text{O}_3$ catalyst. This process operated at 50 -100 atm and $230 - 260^\circ\text{C}$ is still a prevalent methanol synthesis route today [2].

1.1.2 Methanol Global and Domestic Demand

Global demand of methanol spans up to 35 million tones per year. Asia is successful the main driver for growth of methanol and its derivatives. Derivative products from methanol worldwide are shown in the chart below.

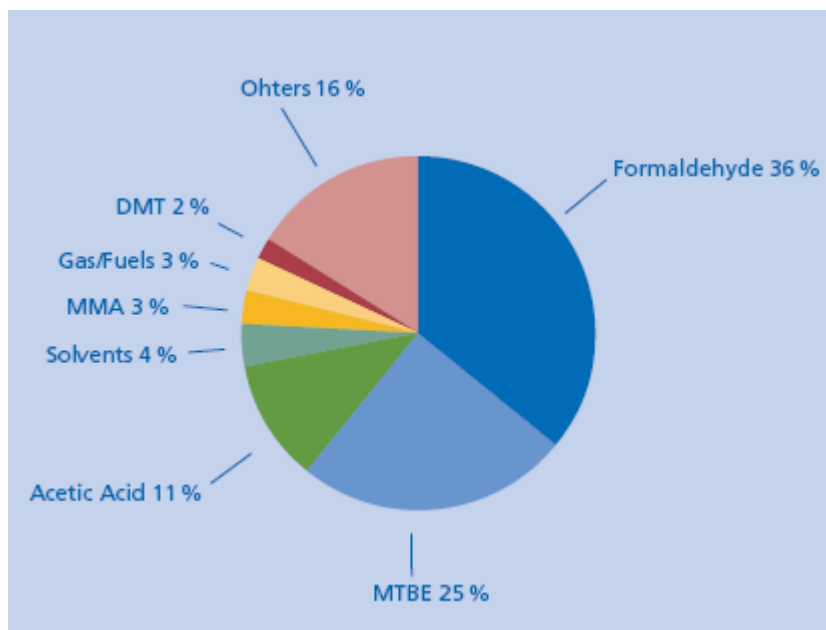


Figure 1.1: Global percentage of products derived from methanol [3].

Average growth rates for methanol and its derivatives are: [3]

- Methanol – 3.8% per annum based on 10 million tones in 2003
- Acetic Acids – 4.85 per annum
- Formaldehyde – 4.4% per annum

In Malaysia, methanol has been largely produced by Petronas Methanol Labuan, PMLSB since 1992 and currently has a methanol output capacity of 1800 t/d and accounts for 35.3% of the total methanol production in South East Asia [4]. It however is on its way to becoming the first Mega-Methanol plant in the region with its expansion project to produce an output of greater than 2500 t/d.

Statistics show that from January to August 2000, Malaysia has supplied methanol to Sri Lanka, Korea, Japan and Indonesia [5].

1.2 Research background

Methanol synthesis catalysts have become a major agenda in the industry as of late. The Cu/ZnO/Al₂O₃ catalyst which predominate the market has had its own share of disadvantages. The limited conversion of up to 0.8% per pass has been for long an issue of academic challenge. The quick deactivation of this catalyst in plants itself has been loudly voiced. The current catalyst has an active life of 4 years and even then its activity dwindles after the first year. This has become an issue and few mitigation methods have been suggested. The need to improve the preparation method of conventional catalysts has heads the list. The most common method which is co-precipitation is quickly being replaced as the product catalyst has low tolerance to poisoning, low thermal stability and low activity period [6-7]. Newer methods such as alternative pH co-precipitation have guaranteed better results and are employed in this study. Also the effect of varying catalyst supports such as ZrO₂ and Al₂O₃ has not been entirely demonstrated. Alumina which stabilizes Cu and ZnO against sintering is also known to stabilize Cu and ZnO against sintering but the acidic sites in alumina encourage production of dimethyl ether as a byproduct. Thus, ZrO₂ has become a new industrial crave as Cu/ZrO₂ and Cu/ZnO/ZrO₂ catalyst have been reported to have high activities, selectivity and

stabilities relative to Cu/ZnO/ Al₂O₃ [2]. This is explained by the greater Bronstead acid sites on ZrO₂ where methanol is produced by hydrogenation of formate and methoxy species [8]. However, the need to study the activity and properties of the combined Cu/ZnO/ ZrO₂/Al₂O₃ catalyst has been undertaken in this project in comparison with the other catalysts in order to obtain an optimum blend of metals and supports which would have the highest activity and selectivity towards methanol. The activity of this catalyst blend would also be compared to the conventional industrial catalyst obtained. The next step to understand the kinetics and surface reaction of methanol synthesis reaction is necessary to improve catalyst active life. The current operating pressure at 50 -100 atm is too high and encourages sintering of catalysts. The need to improve this by operating at lower pressure presumably below 30 atm is desirable. The surface conditions also need to be studied further to compliment the current bi-metal of Cu and Zn active sites theory. The nature of ZrO₂ which also influences the reaction needs to be outlined further.

1.3 Problem Statement

Methanol production by Lurgi technology are known to be one of the most effecint for syngas conversion. However, a local synthesis Methanol plant is currently facing some problems leading to reduction in methanol production with time on stream over the years on catalyst operation. The volume of methanol produced has steadily reduced up to 100t/d over the period of 4 years of catalyst operation [9]. It was also observed during shutdown that catalyst in the ruby (middle) layer of the reactor were forming large chunks and had the resemblance of pink maroon in colour. The catalysts in the tubes were also jammed in the upper portion of the tubes causing difficulties in cleaning. The catalysts which were recovered in the drums were observed to be heavily powder and coked. The reduction in methanol production amount over the years can be described by a few phenomena:

- Reduction in catalyst activity due to carbon/coke formation and sulfur poisoning (preliminary testing).

- Preliminary testing has showed that sulphur contaminant escaped the desulphuriser unit into the natural gas-syngas and thus poisoned the Cu/ZnO catalyst [2]. The effect of S is that it effectively adsorbs into the catalyst surface of Cu crystal and forms a strong Cu-S bond. This will avoid CO molecules from diffusing and chemisorbing onto the Cu surface. This will inhibit the reaction from progressing further on the now inert surface crystals.
- Sintering of metal crystals on the catalyst surface causing loss of surface reaction area.
 - Sintering of Cu crystals is in tandem with the reduction of surface area of catalyst on the surface at high temperatures operation [2]. Thus increasing operation Temperature above 250-260 °C could cause formation of Cu crystal agglomerates on the surface.
 - The high CO/H₂ and CO₂/H₂ ratio could also trigger deactivation [2]. This is because the high ratio of CO and CO₂ would cause the over reduction of ZnO surface causing the formation of unproductive Cu-Zn surfaces. Hydrothermal degradation also occur at high temperature after loss of O from ZnO to H₂ adsorbed on Cu surface which eventually increases steam concentration in the flow.
- Attrition of catalysts with the wall of the tubes and breakage of catalyst while loading in to the tubes causing the formation of large amount of catalyst dust and chips.

Thus a new catalyst with greater activity, selectivity, enhanced stability and mechanical strength is required enhance the life cycle of each catalyst batch. In addition to the conventional Cu/ZnO/Al₂O₃, ZrO₂ has been identified as a potential metal oxide that could boost conversion of methoxy and formate species into methanol on its surface.

1.4 Research Objectives

Our research Objectives can be simplified as:

- Preparation of novel Cu based Methanol synthesis catalyst with ZnO or ZrO₂ or both present.
- Characterization and activity study of each catalyst prepared
- Investigate the nature of each element in the catalyst and their roles in the hydrogenation of carbon monoxide to produce methanol.

1.5 Scope of Study

The scope of our study can be effectively divided into two phases.

1. The study of the industrial catalyst which includes the characterization and links to its position in the reactor. This would give great insight into the possible series of physical events that could have caused the deactivation of the catalyst.
2. To prepare new catalyst recipes with constant amount of Copper and alumina but varying compositions of ZnO and ZrO₂. The method of preparation is the novel Acid-Alkali Alternative pH Precipitation method [10].

These series of catalysts would all be subject to a series of characterization as well activity study in order to determine the optimum blend of ZnO and ZrO₂ which would give us a new highly active, highly selective towards methanol and thermally stable catalyst. The Thermogravimetric Analysis (TGA) would be conducted on all the dried and calcined catalyst in order to determine the stability of catalyst sample at high temperatures. The Temperature Programmed Reduction (TPR) would be conducted by hydrogen adsorption on catalyst surface in order to determine catalyst reducibility and the peak temperature at which catalyst is reduced. Metal surface area, active copper metal dispersion and mean particle diameter can be quantitatively determined by N₂O adsorptive decomposition on the copper surfaces providing oxygen to form CuO at

constant temperature followed by H₂ temperature programmed reduction (s-TPR) of the CuO surface layers [11]. This method further compliments the TPR done on the surface to determine the accuracy and bulk amount of active Cu sites on the surface. The Scanning Electron Microscopy (SEM) of the catalyst surface would give us the image of the final catalyst and from there the general grain size and symmetry of distribution could be determined. EDX probe or Energy Dispersive Spectrometry in the SEM would allow us to determine the wide area composition of elements on the catalyst surface. This information is particularly useful to determine the Cu to Zn and Cu/Zr ratio which would verify the compositions of our calcined catalysts. The WDX or Wavefunction Dispersive Analysis would give us an elemental mapping of the catalyst surface eventually useful to determine the dispersion of Cu and ZnO and ZrO₂ on the surface.

The catalyst activity and selectivity was determined by the activity test in a packed bed reactor where the reactant gas was 30%CO/H₂. Pressure in the reactor was set to 30 bars and temperature of 250 °C. The effluent gas from the reactor which consists of mixtures of CO₂, H₂, CO, methanol and dimethyl ether would be analyzed by an on-line gas chromatograph, GC. The catalyst with the highest methanol conversion and selectivity was ultimately determine as most active and suggested for further investigation. This final catalyst was also compared to the industrial catalyst as an activity reference.

CHAPTER II

LITERATURE REVIEW

2.1 Methanol Synthesis Reaction

Methanol can be produced via a variety of processes and reactants. Natural gas, coal, biomass and petroleum are a possible group of reactants to produce methanol. Table 2.1 summarizes the general physical and chemical properties of methanol [12].

Table 2.1 Physical Properties of Methanol at 20°C [12]

Molecular Formula	CH ₃ OH
Molar mass	32.04g/mol
Appearance	Colorless liquid
Density	0.7918 g/cm ³ , liquid
Melting Point	-97 °C
Boiling Point	64.7 °C
Solubility in Water	Fully miscible
Acidity (pKa)	~15.5
Viscosity	0.59 mPa·s
Dipole Moment	1.69 D

Common methods for methanol synthesis are usually two step reforming followed by conversion or only single step involving direct oxidation of methane to methanol. The routes are summarized as below:

- a. Two step :
- Natural gas reforming → Syngas → Methanol
 - Coal gasification → Syngas → Methanol
 - Biomass gasification → Syngas → Methanol
- b. One step :
- Methane direct oxidation → Methanol
 - Methane bioprocessing by enzymes → Methanol

2.1.1 Methanol Synthesis from Syngas

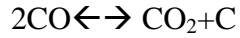
The most common method of methanol production in industry is the two-step process involving natural gas reforming to syngas and syngas conversion to methanol, both are catalytic processes. Common feed composition for methanol synthesis is 70 mol% H₂, 29 mol % CO and 1 mol% CO₂. Trace amount of water and methane is also commonly present. Operating conditions is 250 oC and 50 -80 atm.

Although methanol synthesis from syngas has been available for decades now, the mechanism of production is not entirely understood. Much work has been done to identify the surface species and intermediates in the said process over the years. Methanol synthesis from syngas generally entails a combination of two exothermic equilibrium reactions, which are conversion of CO to CO₂ via a water gas shift (WGS) reaction (2.1) and then the CO₂ hydrogenation to methanol (2.2). The reactions and their enthalpies are given:



The balance between these two reactions would give a net conversion of CO to CH₃OH (2.3).





$$\Delta H_{298\text{K}} = 554.21 \text{ kJ/mol}$$

2.4

The significance CO_2 was largely debated by researchers as many suggested that the main reaction to produce methanol proceeds from CO_2 and most CO is converted before hydrogenation occurs. This however begs the question of the need for low CO_2 concentration and high CO concentration in the feed. Klier *et al* [13] proposed that the water gas shift (reaction 2.1) will occur in the forward direction for low CO_2 feed concentration to convert CO to CO_2 and thus encourage the hydrogenation of methanol. At high concentration of CO_2 however, the reverse water gas shift reaction (RWGS) takes place and reduces CO_2 conversion rate as shown in Figure 2.1. Apart from the WGS and hydrogenation reactions, the Boudouard reaction (reaction 2.4) also takes place in the methanol synthesis process. This reaction causes deactivation of catalyst by the formation of carbon fouling on the active sites. Water is also formed via reaction 2.2, thus requiring liquid-gas separation at the end of the process.

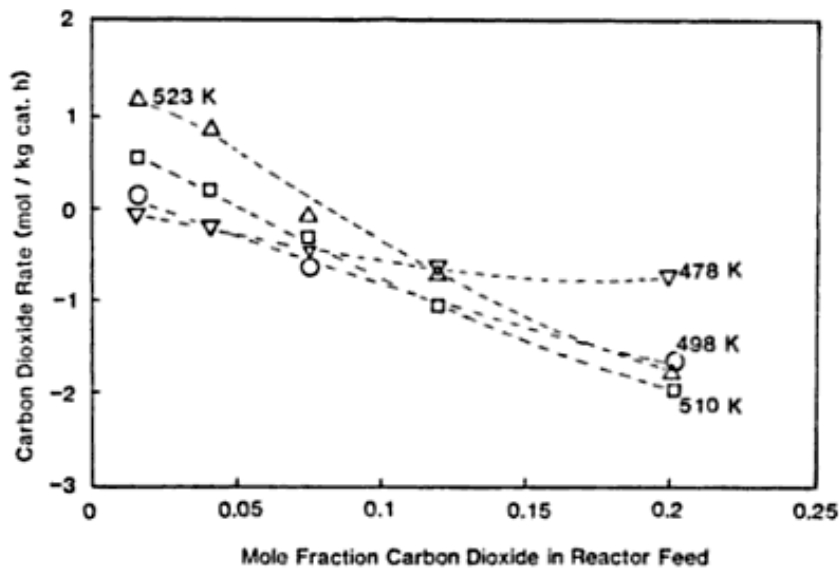


Figure 2.1: Rate of CO_2 consumption (conversion) at varying CO_2 mole fraction in reactor feed [14].

2.1.2 CO₂ hydrogenation to Methanol

Much research has been done in the past involving syngas conversion into methanol. Alternatively, very little attention has been paid until lately to the conversion of CO₂ into hydrocarbons as carbon dioxide is a thermodynamically very stable compound [15]. The equilibrium value for methanol synthesis from CO₂ is about one third of that from CO, and moreover, for temperatures below 250°C, the yield of methanol hardly reaches the equilibrium [16]. The high concentration of CO₂ in flue gas, which comes out from large facilities in the electric power generation plants, the steel, petroleum and cement industries occupies about one third of total CO₂ emission by fossil fuel combustion, is therefore considered as the material for hydrogenation [17]. Public awareness about global climate change caused by greenhouse gas such as CO₂ has raised attention to utilize it more efficiently.

The potential use of CO₂ as an alternative feedstock replacing CO in methanol production has received much attention, as an effective way of CO₂ utilization [18]. Under proper conditions, methanol made from atmospheric CO₂ by its reaction with hydrogen is a promising alternative [19].

The hydrogenation of CO₂ to methanol is shown in reaction 2.2. Generally, reverse water gas shift reaction (RWGS) also occurs simultaneously in CO₂ hydrogenation that led to the formation of CO (reaction 2.5). Nevertheless, CO could be formed from methanol decomposition (reaction 2.6). Therefore, a combination of both reactions gives high concentration of undesired CO. This CO may also react with excess Hydrogen to provide methanol as in the syngas reaction. In addition, water is formed as a by-product from both methanol synthesis and the RWGS.



2.2 Historical Catalyst Development

2.2.1 High pressure Method

Methanol synthesis catalyst of the first generation was developed by BASF in 1923. The catalyst required temperatures of 300 – 400 °C and extremely high pressure of up to 300 atm. This was mainly due to the low activity of the then used zinc/chromium oxide catalyst [2]. Du Pont introduced its own process in 1957, used coal as a feedstock. In this process, zinc/chromium or chromium / copper catalyst were used. This process was abandoned later as the price of natural gas dwindled [20].

2.2.2 Low Pressure Method

The first low pressure and low temperature methanol synthesis catalyst was developed by ICI's research group in the 1960's. This was a Cu/ZnO/Al₂O₃ based catalyst. This new catalyst was operated at about 230 - 260 °C and 50 - 100 atm and thereby favored higher CO and CO₂ conversions. This catalyst had optimum Yield at atomic ratio of 75% Cu (relative to Cu and Zn) [21]. A generic industrial catalyst may contain roughly:

- 30 - 35 wt% CuO
- 45 - 50 wt% ZnO
- 10 - 20 wt% Al₂O₃

A typical industrial catalyst has a very complex multiphase material, and its properties are sensitive to preparation method, pretreatment and operating conditions. ZnO is a textural and chemical promoter in the form of small crystallites (2-10 nm in diameter) and it facilitates formation of small Cu crystallites on its surface (4-8nm in diameter) as well as thermally stabilizing the Cu crystallites against sintering [21]. The high affinity of ZnO towards sulfur and chlorides discourages poisoning on the Cu surfaces. ZnO also

has the ability to neutralize highly acidic sites on alumina phase and therefore minimizing the formation of byproducts such as dimethyl ether. The Cu/ZnO/Al₂O₃ catalyst has very high selectivity (up to 99.9%) towards methanol although common conversion rate per pass is 0.8%. Common byproducts of this reaction are aliphatic hydrocarbons, higher alcohols, esters, ethers and ketones. Catalyst with Cu loaded on other supports may have lower selectivity. Conventional methanol yield for Cu/Cr₂O₃ catalyst is about 96- 97%.

Cu/ZnO/Al₂O₃ is conventionally prepared from aqueous solutions of containing salts of Cu, Zn and Al in a controlled pH precipitation environment. Common preparation pH of near neutral is preferred. Commercial catalysts loaded in the reactor are in the form of cylindrical pellets with diameter 5- 12mm. Bulk densities of commercial catalyst are typically 1.1 -1.4 g/cm³. Methanol yield of commercial Cu/ZnO/Al₂O₃ catalyst at T= 225°C, P= 50 bar and GHSV= 10000 are in the range of 0.3 to 1.5 kg MeOH/ (L_{cat}-h) [22]. Table 2.2 shows methanol yield on different commercial catalysts.

As of late, the Cu/ZnO/Al₂O₃ catalysts have been widely investigated and modified with various metal oxides such as Zirconium, Ceria, Chromium, Vanadium and Titanium [23-32]. Increase in methanol synthesis activity by the inclusion of La₂O₃ and Palladium or Silver was also observed [23-26]. This was mainly due to weak basicity, increasing both the adsorption capacity for CO₂ and is in the increment in the hydrogen spillover through the part of Pd or Ag. The hydrogen spillover gives an influence not only on the proper transportation rate of hydrogen as the reactant but also on the control of the intermediate oxidation state of the catalyst surface during the reaction giving the highest space-time-yield of methanol [7].

It was also reported that the addition of ZnO to the Cu/ZrO₂ catalyst could greatly enhance its activity [37]. Moreover, it was reported that CO₂ kept the copper surface partially oxidized or preventing an over-reduction of the ZnO component [38,39,70]. Ultrafine Cu/ZnO-based catalysts were also obtained using a reduction method in which the dispersion and stability of copper could be improved by doping Cr,

Zn and Th [40]. The Cu/ZrO₂ catalyst series were also studied on its influence of preparation variables on catalytic behavior. High activity and selectivity for methanol synthesis from CO₂ hydrogenation obtained [25,41]. However, the presence zirconia bears the disadvantages of low surface area and poor thermal stability compared to the alumina counterparts. The problem was rectified with the suggestion to spread zirconia over γ -alumina support which has relatively higher surface area [42].

The nature of active sites in the Cu/ZnO/Al₂O₃ has long been an area of controversial dispute. There are two schools of opinion on this matter. One has reported that metallic Cu atoms are homogeneously active for the methanol synthesis [43–48], and the other claims that there exist active sites other than the metallic Cu atoms [49–52]. Researchers such as Chinchin *et al.* [43,44] and Pan *et al.* [45] reported that the activity for methanol synthesis is proportional to the surface area of metallic Cu in Cu/ZnO/Al₂O₃ or Cu/ZnO catalysts and concluded that methanol is formed on a metallic Cu surface. Also, Rasmussen *et al.* [46,47] carried out methanol synthesis by hydrogenation of CO₂ on Cu(1 0 0) at total pressures of 1–4 bar and reported that metallic copper is an active material, and there seems to be no reason to invoke special sites. Askgaard *et al.* [48] formulated a kinetic model for methanol synthesis based on a reaction mechanism deduced from Cu single crystal experiments. Researchers such as Klier *et al.* reported that the active site is a substitutionally dissolved Cu⁺ ion on the surface of the ZnO matrix [49]. Sheffer and King found that addition of alkali metals such as potassium or cesium promotes methanol synthesis by hydrogenation of CO on non-supported Cu catalysts and concluded that cationic Cu is the active site [50,51]. Szanyi and Goodman compared the activity for methanol synthesis on clean Cu (1 0 0) and oxidized Cu (1 0 0) and concluded that Cu ion is the active site [52].

The role of ZnO as a dual active site operating together with the Cu crystals is also well studied. There are four models proposed to explain its functionality in the Cu/ZnO/Al₂O₃ catalyst. They are:

- ZnO addition increases the dispersion of Cu [43,44]

Table 2.2: Methanol yields of Commercial and Developmental catalysts [2].

^a Normalized Yield is normalized to 498 K , 50 bar and GHSV 10,000 h⁻¹

Catalyst/ Manufacturer	Composition Cu _o /ZnO/Al ₂ O ₃ (wt %)	Syngas H ₂ :CO:CO ₂	Temperature (K)	Pressure (bar)	GHSV (h ⁻¹)	Yield (kg/L-h)	Normalised Yield (kg/L-h)
BSAF	22/56/17.4	71/23/6	503	49	10,000	1.28	1.09
BASF	14/69/17.3	71/23/6	503	98	10,000	2.1	1.14
BASF	44/54/2.9	81/18/0.9	503	49	10,000	1.23	1.04
ICI	62/32/6.6	82/4/3.5	513	70	10,000	0.68	0.32
MetGS-AG	60/30/10(CrO3)	77/18/5	503	39	10,000	1.55	1.53
Cu/ZnO/MnO	NA	22.5/5/67	453	50.3	20,000	0.23	0.86
Cu/ZnO/MnO	NA	22.5/5/67	473	70.5	20,000	0.29	0.38
Cu/ZrO ₂	11/89(ZrO2)	75/0/25	500	80	5,400	0.55	0.56
Cu/ZrO ₂ /MnO/La ₂ O ₃	67.5(Cu)	NA	523	60	3,000	2.28	1.89
Cu/Zn/Al/Sc/Zr	43/17/23/11/6	NA	498	80	10,000	1.65	1.22
Raney I	NA	91/5/4	493	44	36,000	1.1	0.62
Raney II	NA	91/5/4	493	44	36,000	0.6	0.34

- ZnO acts as a reservoir for atomic hydrogen spilling over onto the Cu surface to promote the hydrogenation processes [53–55]
- ZnO stabilizes some active planes of Cu or the morphology of Cu particles [56-58]
- ZnO creates active sites on the Cu surface [59-69].

Of all these models, the first model is widely accepted. The others remain controversial in their own respect but have gained much repute lately. For instance Y.Kanai *et al* suggested that the migration of zinc species onto the copper surfaces occurs after reduction. They analyzed this by preparing mixture of Cu/SiO₂ and ZnSiO₂ was prepared separately and then mixed physically and reduced at 723K. The TEM image of the mixture was observed. It shows the migration of ZnO_x species on the Cu surface [63]. A graphical model of the process is shown in Figure 2.1.

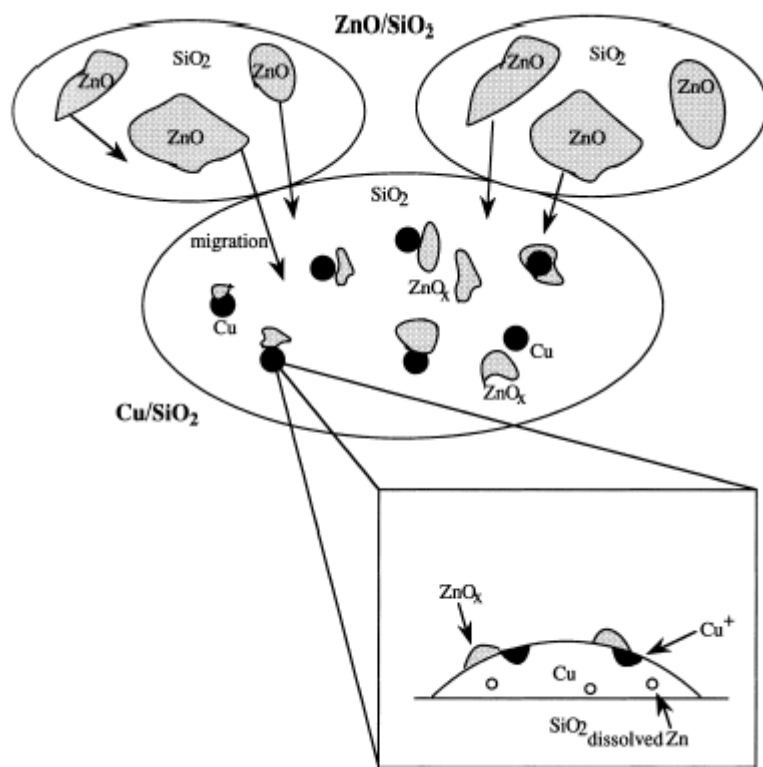


Figure 2.1: Graphical representation of the ZnO_x species migration unto copper surface.

2.3 Catalyst Preparation

Catalyst preparation has evolved since the 20th century to become a major area of research and development. Industries and academics alike have laboured to prepare the perfect catalyst recipe for optimum conversion and high selectivity. In the petrochemical industry itself various achievements have been made in developing newer and more efficient methods of preparing catalyst that would increase product yield. A well prepared catalyst has all the qualities for optimum performance such as:

- High composition of active metal thus higher metal surface area
- High dispersion and homogeneity of metals and low tendency to agglomerate
- High thermal stability to operate at desired temperatures
- High mechanical stability to weather attrition

Preparation of catalyst differs based on the desired usage of the finalized catalyst. A catalyst with good initial activity can lose stability and/or selectivity by poisoning, fouling or ageing. Therefore certain stabilizing compounds must therefore be incorporated in the preparation steps [71]. The need to balance the complexity of preparation technique with the overall cost of catalyst manufacturing is a crucial aspect of catalyst preparation and one that will determine the possible marketing of the finalized catalyst. Two of the most common catalyst preparation methods are as follows:

- 1) Precipitation of the active components and supports through the interaction of aqueous solutions of its chemical compounds.
- 2) Impregnation of the catalyst support using a solution containing a compound of the desired catalyst component.

Each method has developed into major areas of research and the briefness by which they would be mentioned hereafter should be understood as the need to maintain simplicity. The post-treatment of a catalyst precipitate which include drying, crushing, calcination and pelletization are also important aspects of catalyst preparation. However the lack of available details in this area could be attributed to the increasing level of

secrecy among competing catalyst manufacturers. Other methods of copper based catalyst preparation such as the flame combustion synthesis method have been proposed but have reported to be more costly than the conventional precipitation and impregnation methods due to the requirement of flame reactors [72].

2.3.1 Method 1 – Co-Precipitation

The earlier and perhaps a more conventional method of co-precipitation has been employed for decades in the catalyst industry. It can be generally described as the mixing of aqueous salts of active metal and support desired in the catalyst. This would form an acid solution which would then be neutralized by titration of a base solution (such as sodium bicarbonate or ammonium carbonate) to form a precipitate which would later become the catalyst. This process is a means of metal ion displacement from its salts by a more electropositive sodium ion, which then leaves the remaining metal ions of active metals and support to form intricate bonds of multi-metallic complexes. As a result co-precipitation can lead to either adsorption compounds with the microcomponent adhering to the surface of the host, or mixed crystals with the microcomponent free to diffuse through the interior of solid phase [73]. A detailed procedure of catalyst preparation by co-precipitation is shown in Figure 2.1.

There are a few aspects of catalyst preparation by precipitation which need to be highlighted and determined by empirically for optimum results. They are:

- The temperature of precipitation
- The type of agitation (stirring or shaking) and the degree of it
- Aging and its effect on the precipitate
- The effect of washing and soluble salt removal influenced by the particle size of the precipitate.
- Drying rate
- Calcining conditions – period, temperature, ramp rate and gas flow

Catalyst preparation by precipitation is generally preferred as the procedure includes agitation which encourages intimate mixing of the catalyst components and the formation of very small particles for high surface area. The necessary degree of mixing can be achieved either by the formation of very small crystallites, in close proximity, for the different components or by the formation of mixed crystallites containing the catalyst constituents [75]. The only disadvantage of this method is perhaps the lower mechanical strength of the prepared catalyst as compared to the catalyst prepared by wet impregnation method.

As can be noted in Figure 2.1, the addition of gaseous precipitant such as CO₂ is to facilitate the Temperature control in the precipitating vessel. This feature is highly desirable as during the titration, solution may cool down quickly due to addition of cooler base solution. Also, it serves to increase the carbonate content to avoid precipitation of sodium ions.

Although conventional co-precipitation methods are adequate for preparation of copper based catalysts, various modifications have been proposed over the years, attracting much attention. Methods such as forward, reverse, parallel flow and parallel drip co-precipitations have been developed. Even more recent techniques of precipitation are the high speed collision, gel network, and urea hydrolysis precipitations [76-78]. Methods such as insonation of the suspension during precipitation and aging steps could enhance activity of copper based catalyst tremendously [79]. The catalyst preparation method employed in this study is the more recent method of Acid Alkali Alternative pH precipitation method developed C.Yaging et al [10].

The general tools such as a glass beaker with thermometer as well as pH indicator are sufficient in traditional catalyst preparation methods. However a Temperature controlled vessel is desirable to avoid temperature fluctuations during aging [74].

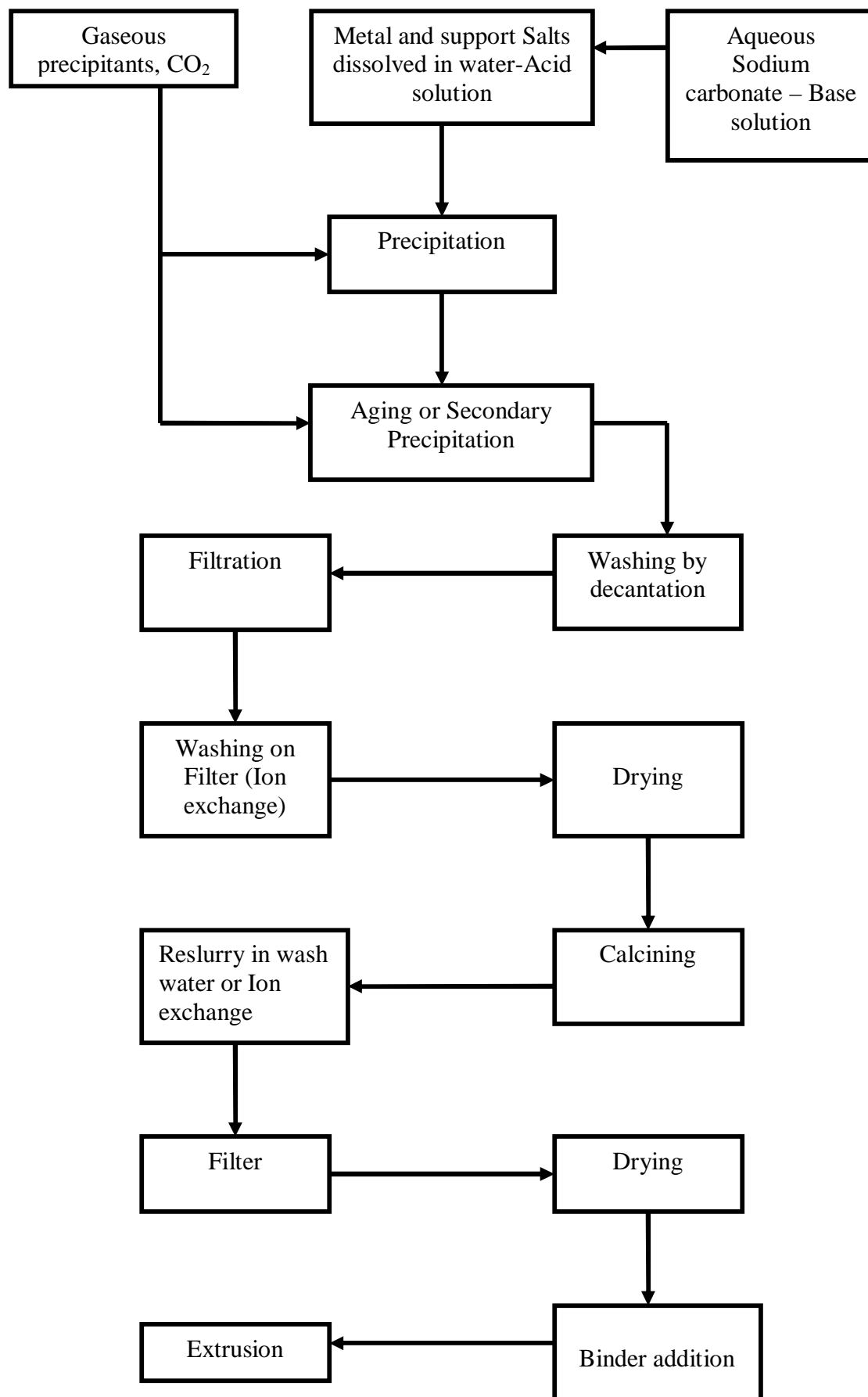


Figure 2.1: Procedure of Catalyst preparation by co-precipitation [74].

2.3.2 Method 2 – Impregnation

The impregnation or sometimes called coating method is another common catalyst preparation method. There is a growing understanding and acceptance of the fact that catalyst when supported on crystallines and oriented structures, they assume the orientation of the support. This can be beneficial and sometimes thought to completely alter the catalytic characteristics of the composite structure. For instance, Ruthenium when supported on γ - or θ -alumina behaves as a hydrogenation catalyst [80]. Thus the method of impregnation serves as a suitable alternative method to prepare catalysts designed for specific reactions.

The desired catalyst orientation is best achieved by suspending support material and then slowly precipitating the active catalytic metals onto the support surface in such a way that the active metal assumes the orientation of the support. This however requires much longer period of ingestion and requires little or no agitation. Various support types are available such as zirconia, magnesia (periclase), spinels of magnesium aluminate, cobalt aluminate as well as barium and calcium sulfates [80].

There are two common methods of impregnation; wet and dry. In dry impregnation, the solution is sucked into the porous support by capillary action and any diffusional transport of the solute, the catalyst precursor is superimposed on the convective flow. In wet impregnation, the pore volume of the support is saturated with water before impregnate and solute is transferred into the support only by means of diffusion [81]. A more elaborate scheme of catalyst preparation by impregnation is described in Figure 2.2.

The stage of drying the catalyst is crucial to facilitate the deposition of salt crystals on the pore surface efficiently. Uneven distribution of salt crystals onto the support surface may result if care is not taken. Calcination finally converts the salt to oxide which is then firmly attached as a thin film on the support surface. The impregnation method is commonly employed when precious metals are involved as the

recovery of precious metals on the surface of support is easier than those multi-metallic complexes prepared by the precipitation method.

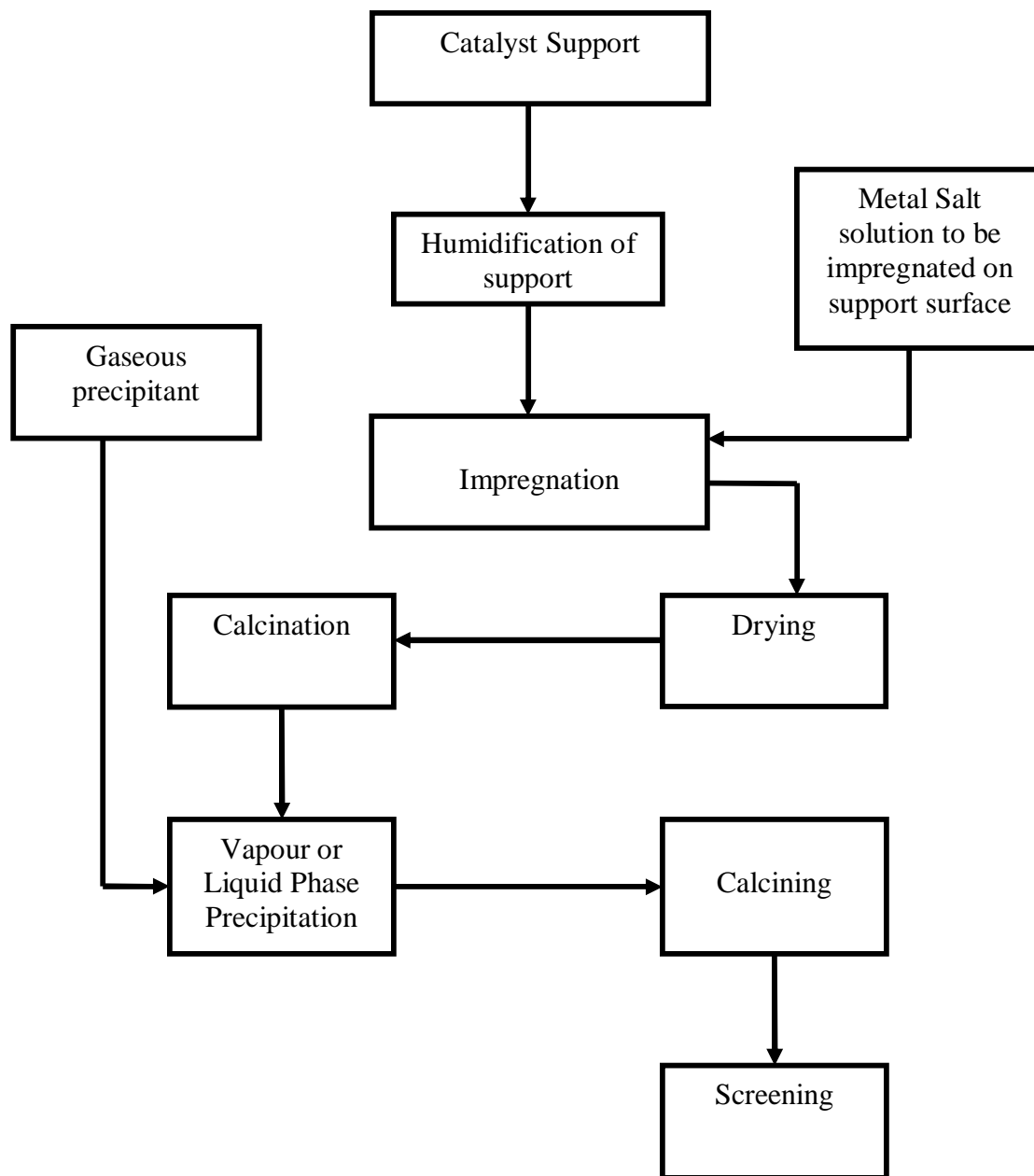


Figure 2.2: Procedure of Catalyst preparation by Impregnation [80].

2.4 Catalyst Carrier / Support

Catalyst support or carriers are known as the backbone of any heterogeneous catalysts. They generally determine the active lifetime of the catalyst and are determined by the mechanical strength and stability under high temperature. The general criteria for a catalyst support are high porosity, high surface area, and high pore volume as well as the ability to ensure a highly dispersed active metal on its surface. Suitable catalyst supports also encourage the stable formation of intermediate gases on the surface of active sites. The most commonly used supports for methanol synthesis catalyst are Al_2O_3 and ZrO_2 . To improve the catalyst for methanol synthesis, it is important to understand the nature of the support at different Temperatures as well as pH.

2.4.1 Alumina

Alumina or Al_2O_3 is the most widely used support for methanol synthesis catalyst as they have an impeccable thermal stability. The alumina group of compounds contains more than a dozen documented amorphous and crystalline structures. They are varied by surface ($0.5 - 600 \text{ m}^2/\text{g}$), pore size, and size distribution as well as surface acidity. These properties of every structure are highly dependent on:

- preparation method,
- level of impurity,
- dehydration
- And especially thermal treatment.

The highly acidic and high surface area aluminas are produced at lower temperature from precipitation by using either acid or base solutions. These high surface area aluminas can be transformed into low surface area and low acidity aluminas by means of dehydration and exposure to high temperatures. The physical and structural properties of some aluminas are given in Table 2.3. γ -alumina is the most common type of catalyst used due to its moderately high surface area and acidity as well as high tolerance to a variety of harsh conditions.

Examples of high surface area and hydrated aluminas are Gibbsite, boehmite, bayerite and diaspore. These aluminas are prepared at low Temperatures and varied pH. Examples of prepared catalysts:

- At pH 11, Alumina precipitates from solution as a trihydrate and is known as bayerite.
- At pH 9, alumina formed is a monohydrate crystal and is known as pseudoboehmite

Table 2.3: Structural and Physical properties of Aluminum Oxide Types [82]

Calcination Temperature, °C	Alumina Phase	Surface Area, m ² /g	V _{pore} , cm ³ /g	d _{pore} , nm	Crystal Structure
250	pseudoboehmite	390	0.5	5.2	Al ₂ O ₃ .H ₂ O
450	γ- alumina	335	0.53	6.4	Cubic, defect spinel
650		226	0.55	9.8	Al ₁₂ (Al ₁₂ H ₄)O ₃₂
850		167	0.58	14	(ABC-ABC stacking)
950	δ- alumina	120	0.50	16.6	Orthorhombic
1050	θ- alumina	50	0.50	28	
1200	α- alumina	1-5	-	-	Hcp-(ABAB Satcking)

Calcination or heating in air determines the final crystal structure, chemical and physical properties of the alumina as is shown in Table 2.3. The alumina boehmite loses its bulk water at 300°C and starts to lose its surface area. This loss of surface area is often related to the migration of Al-OH species. The hydroxyl group plays an important role in increasing the alumina acidity. At around 500 °C, it converts to γ- alumina, which has an internal surface area of 200 -300m²/g. As γ- alumina is heated even further, it loses its hydroxyl groups and by reducing its surface area and to some extent

its acidity to be transformed into δ -alumina at 900°C and θ - alumina at about 1050 °C, with intermediate surface area (50-120 m²/g) and acidity. The final stage is at 1200 °C, where θ -alumina is transformed into α -alumina, which has the lowest surface area and acidity. It also is the most stable form of Al₂O₃.

The nature of aluminas where it has high thermal stability at different temperature ranges as well as the ability to be formed as stable mechanical pellets or extrudates makes it extremely preferable as a methanol synthesis catalyst support. This however needs to be balanced with our need to operate at around 240 – 270 °C and average acidity and high surface area. In methanol synthesis process, the high Al₂O₃ acidity causes the formation of dimethyl ether as a byproduct. This is because the large Bronstead Acid sites (Al-OH) where hydroxyl sites are present and the methanol is catalyzed into dimethyl ether. Our need for a support which has low acidity and high inertness is very crucial. Thus we would prefer either γ - alumina which has high surface area but medium Bronstead acidity or θ -alumina which has low acidity, high inertness despite its lower surface area.

2.5 Catalyst Deactivation

Although catalyst preparation techniques have been greatly improved, to enhance the selectivity, activity and catalyst life time, catalyst deactivation still is considered a problem in the industry. The copper based activity often reduces during the course of operation time, and would consequently require replacement with new catalyst batch. The active period of the locally employed Megamax 700 Sud-Chemie catalyst is 4 years [9].

Cu based catalysts are often catastrophically poisoned by sulfur, chlorine and iron pentacarbonyl. However, sulfur in a methanol production plant is removed before syngas production. The syngas feed and recycle are purified by a ZnO guard bed to remove sulfur up to a required composition of less than 0.1mol%. The ZnO in the catalyst also has the ability to remove sulfur by forming Zn-S compounds and thus

reducing the possibility of Cu surface sulfide formation. Chlorine usually present in catalyst precursors or syngas can greatly accelerates the sintering of Cu and Zn phases in the catalyst, mainly by forming volatile Cu and Zn chlorides. The unusual but possible formation of Fe- pentacarbonyl by reaction of high pressure CO with carbon-steel or rust in the reactor or pipelines needs to be avoided. This is because the Fe-pentacarbonyl compound decomposes to form Iron metal on the catalyst surface, and thus catalyzing the formation of higher hydrocarbons and waxes by exothermic reaction of CO with H₂. These waxes would in turn plug the catalyst pores and reduce its activity. [82].

Sintering of Cu metal phase on catalyst surface has been identified as the main cause of catalyst deactivation in a commercial methanol synthesis catalyst [82]. Sintering of metal crystallites can be greatly reduced by operating at low reaction temperatures in the range of 250 – 260°C. The need to include both CO and CO₂ in the syngas is also crucial as the existence of CO only would encourage the over-reduction of catalyst oxides, while CO₂ only present would produce excessive steam which can lead to hydrothermal degradation [21, 82]. Both these scenarios would aggravate the metal sintering on catalyst surface. Even with all the necessary precaution, low amount of catalyst sintering is unavoidable, leading to 30% of reported activity loss after 600 hours of catalyst operation [21].

As the catalyst activity decreases over time, standard practice dictates the increase in operation Pressure in the reactor with time to maintain methanol yield [82].

2.6 Characterization Techniques

2.6.1 FESEM

Electron Microscopy is a powerful tool that allows us to observe the chemical structure, morphology, surface texture and crystalline size of catalysts from resolution in the range of micro to nanometers. In brief it allows not only aerial image of the surface

that is invisible to the naked eye but also the angular topology which enables us visualize the catalyst in a 3 dimensional point of view.

The diagram in Figure 2.3 shows the major components of a conventional SEM. These components are part of seven primary operational systems: vacuum, beam generation, beam manipulation, beam interaction, detection, signal processing, and display and record. These systems function together to determine the results and qualities of a micrograph such as magnification, resolution, depth of field, contrast, and brightness.

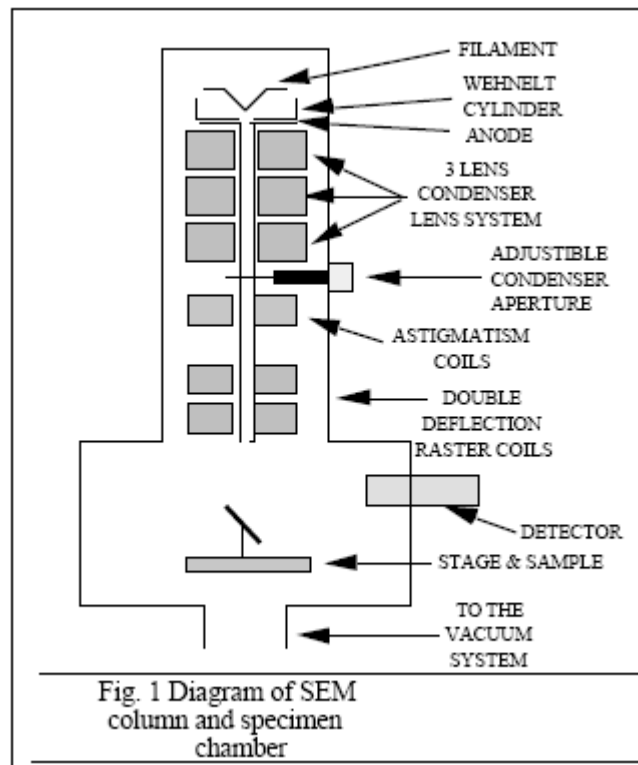


Figure 2.3: Functional parts of a Scanning Electron Microscope, [83]

Electrons in a SEM are ejected by a thermostat after it is heated and these electrons are focused into a fine beam by a magnetic lense. Field Emission Scanning Electron Microscope (FESEM) is a special kind of electron microscope whose electrons are ejected after a strong electric field is applied to the source causing the electrons to gain sufficient energy to overcome its atomic forces to the atoms. The ejected electron

field of an FESEM is also focused not by a magnetic but an electrostatic lense. FESEM also gives much higher resolution than the conventional SEM as well as better imaging of trenches and deep holes [84].

The ejected beam from the electron gun is bombarded to the surface of the sample that needs investigating. The backscattered and/or secondary electrons from the surface at particular energies could determine the composite material that makes the surface. Backscattered or reflected source electrons are detected by the BSE detector while the secondary electrons ejected from the sample are detected by the SE detector. The SE detector is placed at an angle above horizontal so as to enable topographical information to be analyzed [84].

Another detector, the in lens detector is placed vertically and inside the electron acceleration column to detect high energy secondary electrons which provides extremely high resolution of the sample surface.

Quantitative compositional analysis of materials that make up the catalyst on the surface assuming homogeneity can be determined by the Energy Dispersive Spectrometer (EDS) which detects X-rays released by the surface after electron bombardment and the X-rays are characteristic of an element. Also, Wavelength Dispersive Analysis (WDS) allow elemental mapping on the sample surface by introducing false colors for each element.

2.6.2 XRD

X- Ray diffraction is often cited as the fundamental tool in the study of solid states. Solid can be divided in two main categories, crystallines and amorphous solids. In crystalline solids, atoms are arranged in a regular pattern, and there is as smallest volume element that by repetition in three dimensions describes the crystal. This smallest volume element is known as a unit cell. The dimensions of the unit cell are described by three axes, a, b, c and the angles between them alpha, beta, and gamma. On

the contrary, in crystalline solids, the atoms are arranged in a random way similar to the disorder we find in a liquid. Glasses for instance are amorphous materials.

About 95% of all solid materials can be described as crystalline [85]. When X-rays interact with a crystalline substance (Phase), one gets a diffraction pattern. The X-Ray diffraction of a pure substance is thus more generally described as its fingerprint. The powder diffraction method is therefore an ideal tool to characterize and identify polycrystalline phases.

Today about 50,000 inorganic and 25,000 organic single components, crystalline phases, and diffraction patterns have been collected and stored on magnetic or optical media as standards [85]. The main use of powder diffraction is to identify components in a sample by a search/match procedure. Furthermore, the areas under the peak are related to the amount of each phase present in the sample.

Once the material has been identified, x-ray crystallography may be used to determine its structure (how the atoms pack together in the crystalline state and what the interatomic distance and angle are). Figure 2.4 shows the reflection of x-rays from two planes of atoms in a solid. During diffraction, x-rays impinge on the crystal and are coherently scattered [86]. The scattered radiation can be well observed only in directions in which the beams reflected from the crystal plane under each other are amplified by interference.

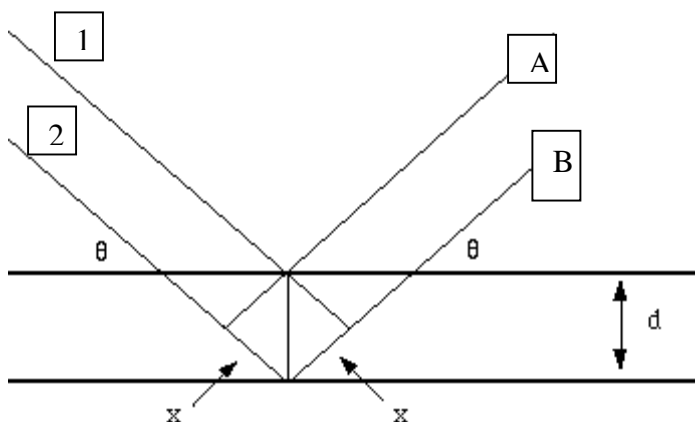


Figure 2.4: X-ray reflection on two atomic planes of a crystalline solid.

The two parallel incident rays 1 and 2 make an angle θ with these planes. A reflected beam of maximum intensity will result if the waves represented by the x-ray termed 1 and 2 are in phase. The difference in path length between 1 to A and 2 to B or simply labeled as d must then be an integral number of wavelengths, λ [87]. This relationship is described mathematically by Bragg's law as:

$$n\lambda = 2d_{hkl} \sin \theta \quad [2.7]$$

Where n is an integer, hkl is the Miller indices of the plane. This equation is a general simplification of a now more elaborate field of x-ray crystallography.

2.6.3 TPR

Temperature Programmed Reduction or TPR is a common analytical method used to investigate and identify reduction conditions of a catalyst sample. Overall it allows quantitative measurement of a samples' changes namely chemical structure under given thermal conditions, with the presence of reductive gases flown over it [88]. The gas used for reduction of a catalyst sample is usually a mixture 5% Hydrogen in an inert gas. A TPR study unit can more generally be classified as a miniature reactor together with a furnace for sample heating as well as a Thermal Conductivity Detector (TCD).

The reaction of the reducible materials with H_2 is a surface chemical reaction. This allows us access to a great deal of information on the material under investigation [89]. Consequently, it is widely employed for the verification of the nature of species in calcined catalysts [90-92].

Common information which can be obtained from the TPR study is:

- Optimum Reduction Temperatures
- Amount of active sites present
- Dispersion of Active metals on catalyst surface.

- Active metal particle size in catalyst (nm)

The reactions are usually carried out to match its industrial or lab reactor experiment as much as possible. A detailed diagram of the instrument for TPR analysis, Thermo Finnigan's TPDRO 1100 is shown in Figure 2.3.

Usually the sample is previously oxidized or pretreated to eliminate possible contaminants and completely oxidize the metal portion of the catalyst. Also, the sample is submitted to a linear increase of temperature and to a constant flow of the gas mixture. The reaction generally starts at room temperature, but at an extremely low speed, therefore negligible. At a certain temperature, the reaction speed becomes considerable and the hydrogen consumption can be monitored through the TCD detector. A thermal conductivity detector measures the H₂ concentration in the effluent gas with respect to the initial percentage, monitors the reaction progress [93]. The signal integration allows us to calculate the quantity of hydrogen consumed and therefore the number of reacting sites. A quadrupole mass spectrometer can also be used as a detector. Due to the large difference in thermal conductivities between hydrogen and nitrogen, it was possible to detect hydrogen consumption as low as 1 μmol. This ensured high detection sensitivity and consequently, a low detection limit for the TPR technique [94]. The TPR analysis also enlightens the presence of different states of oxidation of the contained metals

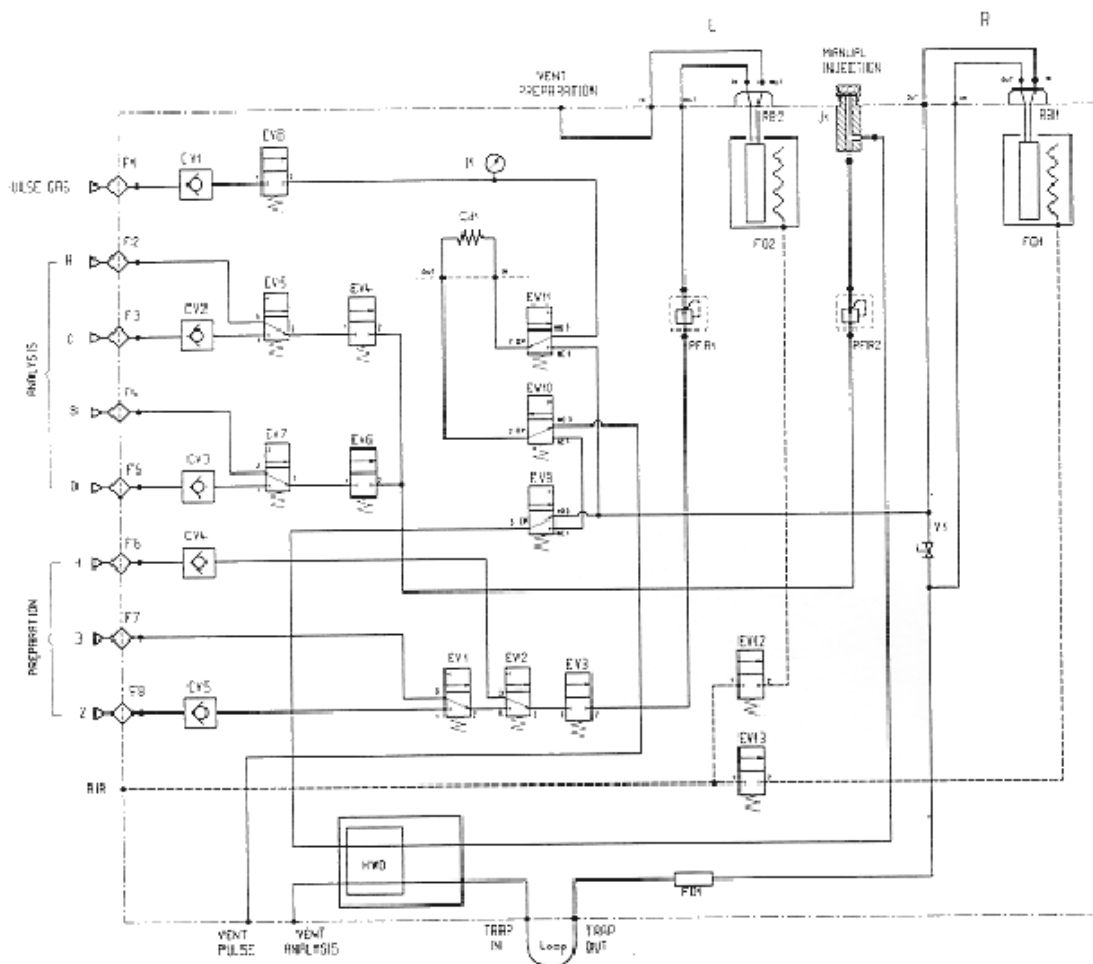


Figure 2.5: A detailed diagram of a Thermo Finnigan's TPDRO 1100 unit [88].

2.6.4 Density Measurement

Density of catalyst particles is essential information in characterizing and outlining its physical properties. Archimedes developed a principle that allowed for solid density to be measured by displacement of fluid volume by that solid. This allowed for a semi-accurate measurement of its density. Usually, when catalysts are concerned, a gas is used as the displacing fluid as catalysts consists of large and small pores which could be easily be penetrated by an inert gas. Helium is recommended since it is chemically inert and has small atomic diameter allowing entry into crevices and pores approaching one Angstrom (10^{-10} m). The Quantachrome Ultrapycnometer 1000 instrument was used to measure the density of catalyst samples. An image of the

instrument is shown in Figure 2.6 and a flow diagram of its operation is shown in Figure 2.7.



Figure 2.6: Ultracycrometer 1000 instrument image.

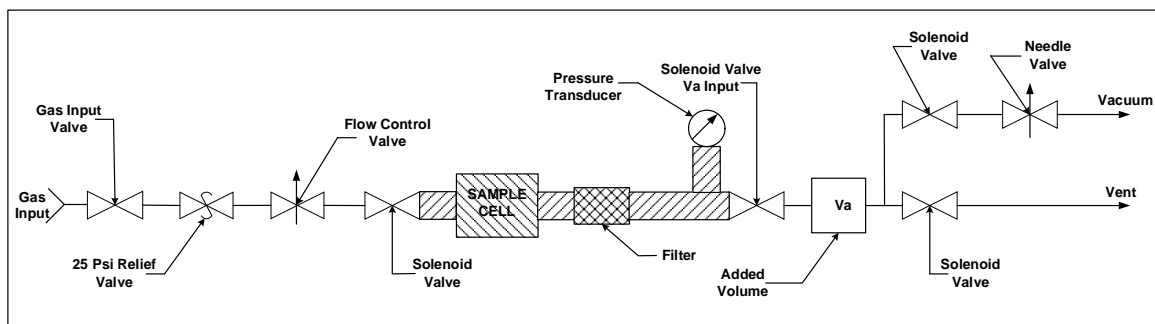


Figure 2.7: Flow diagram of the Ultracycrometer 1000 instrument

2.6.5 s-TPR

Catalyst performance is closely related to the dispersion of its active sites, in this case, copper dispersion (D_{Cu}). Therefore, the search for reliable methods for determining D_{Cu} and related parameters such as specific Cu metal surface area (MSA), and average diameter of the copper aggregates ($\bar{\phi}_{av}$) is essential to interpret their activity in terms of turnover frequencies. There has been a large continuing debate for decades about the most suitable adsorbate to be used to determine the Cu dispersion through chemisorption

method [95–102]. The existence of weak reversible chemisorption and uncertain adsorption stoichiometries is associated with adsorbates, such as H₂ and CO [98, 100]. Low-temperature O₂ chemisorption at -195 or -136 °C has been proposed as a reliable technique for the measurement of Cu surface areas [95, 103]. This procedure however has been deemed time-consuming. To overcome this problem, Pernicone et al. suggested O₂ chemisorption at -130 °C through the pulse flow technique, which should be more suitable for routine measurements [104]. However, Bartley et al showed that even O₂ chemisorption can be unreliable for catalysts containing lower loadings of copper or for catalysts in which the support is partially reducible [105].

Adsorptive decomposition of N₂O is a technique used frequently for catalyst dispersion determination [96, 97]. Different operating procedures have been applied to determine the extent of the reaction of N₂O with the surface copper. One method involves volumetric determination of the N₂ produced by decomposition of N₂O or titration [97, 99]. The more commonly used method involves the chromatographic separation of unreacted N₂O and N₂ formed and is known as Reactive Frontal Chromatography (RFC) [96, 102].

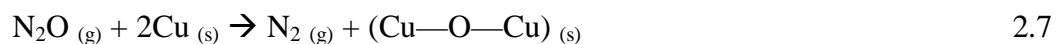
There are problems related to the N₂O use. This is because it is difficult to identify the exact Temperature at which only the first copper surface layer is oxidized without deeper bulk Cu oxidation. Chinchén et al. showed that by cutting-off the N₂O decomposition at half-monolayer coverage, Cu bulk oxidation can be avoided [107]. Temperatures between 30 and 90 °C are the most frequently used to conduct N₂O adsorptive decomposition. However, even in this temperature range, oxidation of bulk copper could lead to overestimation of copper dispersion. Sato et al. have recently shown that slow bulk oxidation may proceed during N₂O oxidation even at temperature as low as 30 °C [101]. At temperatures above 100 °C, Cu oxidation by N₂O is not restricted to the surface and bulk oxidation happens almost completely [99, 105].

A. Gervasini *et al* designed the s-TPR method which is also known as the Temperature Programmed Reduction of Oxidized surfaces to solve the problem of

distinguishing between surface and bulk copper layers. It permits to obtain copper dispersion and specific copper surface area with qualitative and quantitative information on the different surface copper species with as two step procedure [108]:

- a. Isothermal surface oxidation by N₂O (reaction 2.7)
- b. Analysis of H₂ temperature-programmed-reduction of the partially and fully oxidized Cu surfaces (reaction 2.8 and 2.9)

The surface copper species can be well distinguished from the bulk copper species in this s-TPR method. Copper catalysts were encouraged to be studied at low-temperature range, 30 – 50 °C [108].



2.6.6 TGA

Thermal gravimetric analysis or TGA is a method where the mass of a sample is measured as a function of sample Temperature over time. The sample is either heated at a constant heating rate (dynamic measurement), held at constant temperature (isothermal measurement) or subjected to a non-linear temperature programs. The type of heating program would depend on the type of information required of the sample [109].

In addition, the gas supply to the sample during the heating would have to be suitable to the desired analysis whether oxidizing, reducing or inert. A choice of reactant gas to observe thermal degradation during reaction is also possible.

TGA measurement results are displayed as a plot where mass is plotted against Temperature of time. Alternatively, mass change or differential can be plotted against time or temperature to analyze mass change at every given Temperature or moment in time. This method is known as the differential thermogravimetric or DTG analysis. A schematic of a thermo analysis setup is shown in Figure 2.8.

Mass of the sample changes in many ways as it interacts with its surrounding gas at a given Temperature. The sample mass can increase or decrease depending on the type of interaction it has with its surrounding gas or the effect of variable temperature on it. Oxidation of metals is an example of sample mass increasing whereas oxide reduction and thermal decomposition is an instance of sample mass decreasing over time. The decomposition process often occurs in several steps as shown in Figure 2.9d. Thermal analyses of catalysts were conducted on the Pyris 1 TGA model by Perkin Elmer.

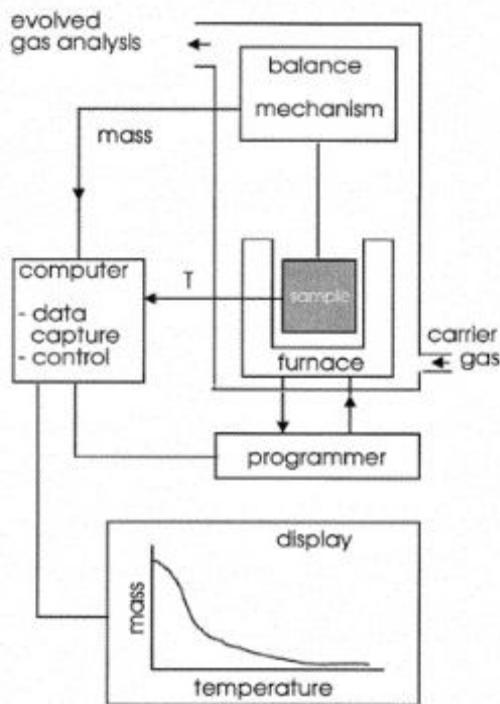


Figure 2.8: A schematic of a thermo analysis setup [110]

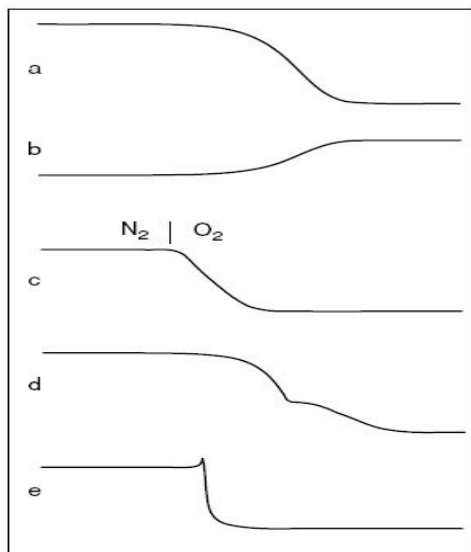


Figure 2.9: TGA spectrum of multiple process types. (a) Thermal decomposition with the formation of volatile compounds. (b) Metal oxidation. (c) Combustion when gas switches from N₂ to O₂. (d) Multi step decomposition. (e) Explosive decomposition with recoil effect [109].

CHAPTER III

METHODOLOGY

3.1 Chemicals and Gases Employed

The chemicals used in the preparation of the catalyst are shown in Table 3.1. All nitrates are used in the acid solution while Sodium Carbonate is a titrating agent.

Table 3.1 Table of chemicals applied in catalyst preparation

Chemicals	Chemical Formula	Purpose
Copper nitrate trihydrate	$Cu(NO_3)_2 \cdot 3H_2O$	Catalyst reagent – Acid solution
Zinc nitrate hexahydrate	$Zn(NO_3)_2 \cdot 6H_2O$	Catalyst reagent – Acid solution
Aluminum nitrate nonahydrate	$Al(NO_3)_3 \cdot 9H_2O$	Catalyst reagent – Acid solution
Zirconium Nitrate hydrated	$N_2O_7Zr \cdot xH_2O$	Catalyst reagent – Acid solution
Sodium carbonate	Na_2CO_3	Base solution for Acid titration

The gases used in the characterization, and activity study of catalyst sample are shown in Table 3.2. 5% H₂ in excess N₂ is used as reduction as well as characterization (TPR, s-TPR) gas.

Table 3.2 Table of gases used in characterization and methanol synthesis reaction

Gases	Composition	Purpose
Hydrogen	5% in excess N ₂	Reduction / Characterization
Nitrous oxide	2.13% in excess He	Characterization
Nitrogen	pure	Characterization/ Purging
Helium	pure	Characterization
Syngas	30% CO, 70% H ₂	Chemical Reaction

3.2 Catalyst preparation

A series of Cu/ZnO/Al₂O₃, Cu/ZnO/ZrO₂/Al₂O₃ and Cu/ZrO₂/Al₂O₃ catalysts were prepared. The objective is to determine the effect on activity of Zn or Zr or both in varied quantity in the catalyst sample. Commercial Cu/ZnO/Al₂O₃ catalyst was used as reference in activity study.

Sample A is the prepared Cu/ZnO/Al₂O₃ catalyst sample. Sample B, C, D and E are Cu/ZnO/ZrO₂/Al₂O₃ catalysts. From sample B to E Zr composition in catalyst sample increases. Only prepared catalyst F is from the Cu/ZrO₂/Al₂O₃ catalyst series. This catalyst has no ZnO present. The catalyst classification and composition is outlined in Table 3.3.

The method of catalyst preparation applied is a novel Acid Alkali Alternating pH precipitation method developed recently by CEN Yaging et al [10]. The reactants used

for catalyst preparation were copper nitrate trihydrate $[Cu(NO_3)_2 \cdot 3H_2O]$, zinc nitrate hexahydrate $[Zn(NO_3)_2 \cdot 6H_2O]$, aluminum nitrate nonahydrate $[Al(NO_3)_3 \cdot 9H_2O]$ and zirconium nitrate hydrated $[N_2O_7Zr \cdot xH_2O]$. These chemicals were mixed to prepare the acid site solution whilst the base titrating solution was sodium carbonate $[Na_2CO_3]$.

Table 3.3: Catalyst series type and their metal atomic composition

Sample	Series	Composition (metal atomic %)			
		Cu	Zn	Al	Zr
Ind (Commercial)	Cu/ZnO/Al ₂ O ₃	64.46	29.02	6.52	0.00
A		42.86	47.62	9.52	0.00
B	Cu/ZnO/ZrO ₂ /Al ₂ O ₃	42.06	46.73	9.35	1.87
C		40.91	45.45	9.09	4.55
D		39.82	44.25	8.85	7.08
E		40.91	36.36	9.09	13.64
F		Cu/ZrO ₂ /Al ₂ O ₃	42.86	0.00	9.52

Amount of Copper nitrate trihydrate, Zinc nitrate hexahydrate, Aluminum nitrate nonahydrate and Zirconium nitrate hydrated as shown in Table 3.4 were dissolved in 150 mL of distilled water separately to form their salt solutions. The detail calculation of nitrate salt amount for catalyst samples is shown in Appendix A. These nitrate solutions of copper, zinc, aluminium and zirconium were then mixed together in a beaker to form the acid site solution. 20g of Sodium carbonate was dissolved in 500mL of water to form the base solution.

The acid site solution was added into a 200mL mother solution (distilled water) beaker until the pH of the solution reaches 4.88. Then, the Base solution was added into the mother solution until the pH of mother solution reached 8.8. This procedure of alternative addition acid and base solution addition into the mother solution was repeated until all the acid site solution was consumed and the Base solution was added for the last time increase the pH of the mother solution to 7.1. The base solution contains the highly electropositive Na⁺ ions, which would displace Cu²⁺, Zn²⁺, Zr⁴⁺ and Al³⁺ ions

from their respective nitrate anions. The purpose of this displacement is to allow the Cu^{2+} , Zn^{2+} , Zr^{4+} and Al^{3+} cations to disperse and mix as much as possible to obtain a high metal dispersion in the final precipitate.

Table 3.4: Amount of chemicals used in preparation of sample catalysts

Sample	Chemical Mass, g			
	$\text{Cu}(\text{NO}_3)_2 \cdot 3\text{H}_2\text{O}$	$\text{Zn}(\text{NO}_3)_2 \cdot 6\text{H}_2\text{O}$	$\text{Al}(\text{NO}_3)_3 \cdot 9\text{H}_2\text{O}$	$\text{N}_2\text{O}_7\text{Zr} \cdot x\text{H}_2\text{O}$
A	9.5050	3.5569	3.2796	0
B	9.5050	3.5569	3.2796	0.2154
C	9.5050	3.5569	3.2796	0.5386
D	9.5050	3.5569	3.2796	0.8618
E	9.5050	2.8455	3.2796	1.6159
F	9.5050	0	3.2796	5.3862

The mother solution was continuously stirred and its temperature was maintained at 70°C. The solution was aged at 80°C for 2 hours under continuous stirring followed by filtered. The filtrate was washed with distilled water several times to remove residual sodium ions from its surface. The filtrate was then dried at 110 °C for 12 hours. Consequently, the dried sample was pressed under hand pressure and grounded to mesh size 60–80 and then calcined in air at 370°C for 9 hours. Some amount of the dried sample C was subjected to different calcination Temperatures of 200 °C, 300 °C, and 400 °C to study the effects of calcination Temperature on species type formation. The catalyst preparation procedure is shown graphically in Figure 3.1.

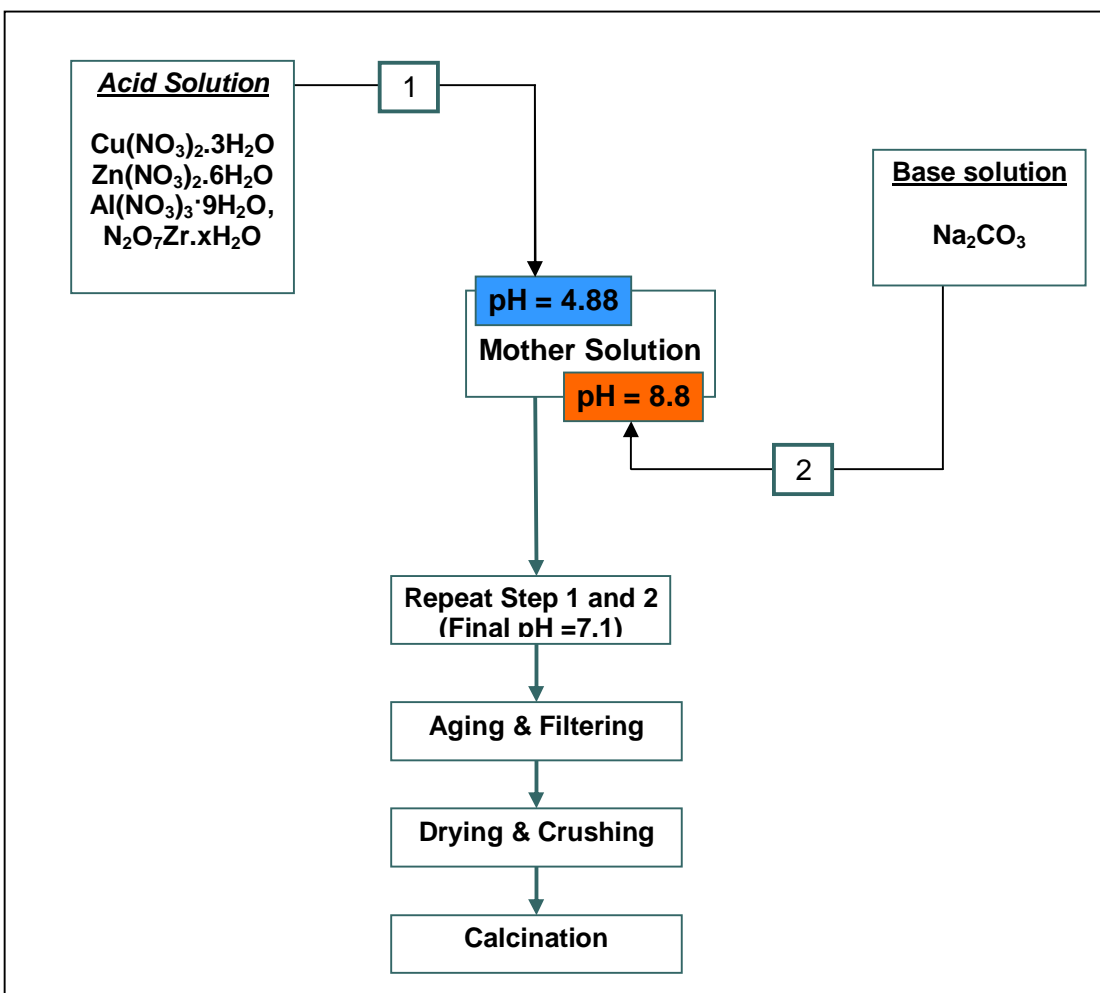


Figure 3.1: Flowchart of catalyst preparation procedure

3.3 Physio-Chemical Characterization

3.3.1 Catalyst Density Determination

Catalyst density was determined by means of the Quantachrome Ultracycrometer 1000 instrument. The relatively simple procedure of density measurement is as follows:

- Catalyst sample was loaded into the small sample cell until $\frac{3}{4}$ of the cell volume was filled.
- The mass of catalyst sample in the cell was weighed.

- The sample cell was placed in the cell holder in the Pyconometer.
- The cell was tightly capped and Helium gas supply was initiated
- The cell was vented to ambient and when stable pressure was reached, the unit stored a zero pressure reading.
- Subsequently, the system was pressurized to the target pressure, 18psi. Helium gas flow into the cell would determine the difference between Volume of cell and the Volume of gas in the cell. This resultant would be the true volume of the catalyst in the cell.
- The catalyst density, ρ would be calculated using the formula:

$$\rho = \frac{\text{Sample mass}}{\text{Sample volume}}$$
- Three measurements of density were taken for each sample for greater accuracy.

3.3.2 Temperature Programmed Reduction (TPR)

Temperature Programmed Reduction or TPR is a crucial method to analyze the surface reducibility and optimum reduction Temperature of a catalyst species. It involves the adsorption of H₂ on the active metal surface and allows for qualitative analysis of reduction conditions on catalyst surfaces.

The TPR analysis was conducted on the catalyst by means of the Thermo Finnigan TPDRO 1100 equipment. The procedure requires the pretreatment of catalyst sample before the TPR study could be conducted on its surface. 0.15g of catalyst was weighed and packed into a quartz sample reactor in between two layer of quartz wool. A gas volume reducing tube was inserted into the reactor and the set was place in a reactor holder. This reactor holder was equipped with a surrounding electric furnace, which is operated by a programmable temperature controller.

The catalyst sample in the reactor was pretreated from room Temperature to 300°C at ramp rate of 10°C/min under the flow pure nitrogen gas. The gas flow rate was 20cm³ /min. The sample temperature was maintained at 300°C for another 30 min with

gas flow. The sample was finally cooled to room temperature with gas flow. This pretreatment procedure is important to remove moisture and impurities from the catalyst sample surface.

Once the pretreatment step was complete, the TPR step was commenced. TPR analysis was conducted in a 5% H₂ in N₂, which is a reducing hydrogen gas in inert nitrogen. The catalyst sample was heated from room Temperature to 600°C at a ramp rate of 10°C with the gas flowing at 20cm³/min and was held at final temperature for 10 minutes. The analysis gas consisting Hydrogen and nitrogen have a thermal conductivity of 39.6x10⁻⁵ and 5.68 x10⁻⁵ each at 0°C temperature. The difference between the thermal conductivities of the two gases is detected by the Thermal Conductivity Detector (TCD) as a voltage signal in mV. The concentration of hydrogen in the gas mixture decreases as it adsorbs on catalyst surface. This change in gas concentration is detected by the TCD as a positive change in signal (mV) as the Thermal conductivity difference in the gas mixture is reduced [88]. The highest peak in the spectrum is identified as the optimum reduction Temperature where highest amount of hydrogen gas is adsorbed. The area under the spectrum curve is defined as the total amount of gas adsorbed in mV and the signal is converted to mmol of gas adsorbed by a pre-calibrated factor of 1.06745307416578899x10⁻⁷ mmol/mV.

3.3.3 TPR of oxidized surfaces (s-TPR)

The technique of nitrous oxide titration has enjoyed prolonged period of success as a means to determine active metal dispersion (D_{Cu}), metal surface area (MSA), and average diameter of the Cu aggregates (\varnothing_{av}) for copper-based catalysts. However, the existence of multiple Cu states on the catalyst surface begs the need to distinguish between partially oxidized surface Cu₂O layers, which are actively involved in the methanol synthesis reaction from the fully oxidized bulk CuO layers, which remain mostly inactive. Thus, the s-TPR method allows the quantification of these two different states to obtain a more conservative estimate of the Cu metal surface area. This

procedure was conducted on the Thermo Electron TPDRO 1100 instrument. The sample packing method is similarly described in the TPR analyses in section 3.3.

Generally, the s-TPR method is a two-step process involving:

- c. Isothermal surface oxidation by N_2O (reaction 2.7)
- d. Analysis of H_2 temperature-programmed-reduction of the partially and fully oxidized Cu surfaces (reaction 2.8 and 2.9)

Before the s-TPR study is conducted, the sample was pretreated to remove impurities and moisture. Pure nitrogen gas was flowed at Temperatures up to 300°C with ramp rate of $10^\circ\text{C}/\text{min}$. The gas flow rate was $20\text{cm}^3/\text{min}$. The second pretreatment procedure involves the reduction of the catalyst sample. The catalyst sample was exposed to 5% H_2 in N_2 gas at $15\text{cm}^3/\text{min}$ flow rate with the sample temperature increasing from room to 400°C . The temperature was maintained constant for another 30minutes before cooling to 60°C .

The first step in the s-TPR process involves the isothermal catalyst surface oxidation by nitrous oxide. A calibrated amount of oxidizing gas (2.13% N_2O in He) was injected into the catalyst sample cell at a constant isotherm of 60°C . 60°C was the recommended isotherm Temperature for the s-TPR study [108]. This gas was injected every 5 minutes and the total amounts of injections were 12. The nitrous oxide gas would oxidize the catalyst metal surface until saturation point is reached. The layers of Cu oxidized would include the surface and bulk Cu layers.

Once the surface oxidation by nitrous oxide is complete, the final TPR stage was commenced. 5% H_2 in N_2 gas at $20\text{cm}^3/\text{min}$ flow rate was flown over the oxidized sample from room temperature to 800°C at a ramp rate of $10^\circ\text{C}/\text{min}$. The signal was converted from mV to mmol by using a pre-calibrated factor of $1.06745307416578899 \times 10^{-7}$ mmol/mV. The reducing hydrogen gas would reduce the previously oxidized Cu_2O and CuO surfaces. The surface copper species, Cu_2O can be

well distinguished from the bulk copper species, CuO in this s-TPR method as two distinct TPR peaks were produced at the end of this procedure.

The metal surface area, MSA (equation 3.1) was calculated by using the method described by Gervasini et. al. The stoichiometric factor, S.F that corresponds to Cu/O ratio is assumed to be 2 to account for Cu₂O decomposition into Cu (0) state and 1 for CuO decomposition into Cu (0) state [108]. For surface Cu (Cu₂O) metal area the mol H₂ adsorbed corresponds to the amount of H₂ adsorbed at Low Temperature only. For Bulk Metal Cu (CuO) Area, the mol H₂ adsorbed corresponds to amount of H₂ adsorbed at High Temperature conditions. The sum of the surface and bulk metal Area would constitute the total metal are available to the catalyst.

$$MSA\left(\frac{m^2}{g_{Cu}}\right) = \frac{\text{mol H}_2 \times \text{S.F} \times N_A}{10^4 \times c_m \times W_{Cu}} \quad 3.1$$

Where,

Mol H₂ = moles of hydrogen consumed per unit mass catalyst, (μmol_{H₂}/gcat)

N_A = Avogadro's no

S.F = Stoichiometric factor, 2

c_m = No. of surface Cu atoms per unit area, 1.47x 10¹⁹ atoms/m²

W_{Cu}= Cu metal content, wt%

Cu metal dispersion however, is defined separately by two different sources. Gervasini et al. defined dispersion of Cu metal as the ratio of surface copper sites, Cu₂O to the total Cu present in the catalyst sample (equation 3.2) [108]. This was experimentally determined by calculating Low temperature peak area of the s-TPR spectrum, which represents surface copper sites and divide it by the total area under the curve representing the total metal surface area. The second source of metal dispersion definition was the Thermo Finnigan Instruction suite (equation 3.3) [88]. Here, metal

dispersion is defined as the ratio of adsorbing Cu or active Cu atoms over the total Cu atoms present in the catalyst sample.

$$D_{Cu}^1 = \frac{\text{Surface Cu (Cu}_2\text{O)}}{\text{Surface Cu (Cu}_2\text{O) + Bulk Cu (CuO)}} \times 100\% \quad 3.2$$

$$D_{Cu}^2 = \frac{\text{adsorbing Cu atoms}}{\text{total Cu atoms}} = \frac{MSA \times MW_{Cu} \times c_m}{N_A} \quad 3.3$$

Where,

MW_{Cu} = Cu molecular weight.

Finally, average copper particle size, ϕ_{av} can be determined using the definition given by Gervasini et al. (equation 3.4). SK is a constant that depends on the Cu particle shape. The value 6 for SK refers to the spherical or cubic shape of copper aggregates. Copper density, ρ_{Cu} has the value of 6.64 g/cm³.

$$\phi_{av} (nm) = \frac{10^7 \times SK \times c_m \times W_{Cu}}{S.F \times mol H_2 \times N_A \times \rho_{Cu}} \quad 3.4$$

3.3.4 X-Ray Diffraction (XRD)

The X-Ray diffraction method is conventionally employed to analyze and determine the species type present in the sample as well as its extent of crystallinity. Each species has a different crystal structure and corresponds to a different Bragg's angle (2θ) in the graph. The rate of crystallinity is represented by the Integral of a peak, which is the area under the peak. Greater area under the peak would signify greater extent of crystallinity of the particular species.

The XRD analysis was conducted through the Bruker D8 Advanced Diffractometer instrument that uses $\text{CuK}\alpha$ radiation as its source. The range of the scanning angle was $2 - 80^\circ$ and the scanning speed was $1.2^\circ/\text{min}$. The crystallite types present in the catalysts were identified by comparing the scanning angles and d-spacings of each peak in the resultant curves with the ones existing in the material library.

All six prepared catalyst samples as well as the commercial catalyst were subjected to the XRD analysis in order to identify the crystal types present in its powder. The existence and increment of the Zirconium species in every sample was of the greatest interest.

Prepared catalyst sample C was calcined at four different calcination Temperatures and they were individually analyzed with the XRD to investigate the effects calcination temperatures. The temperatures were 200, 300, 350 and 400°C .

3.3.5 Thermal Gravimetric Analysis (TGA)

Thermal gravimetric method or TGA is an analytical method to measure the thermal stability or thermal mass loss of a sample under heating over a range of Temperatures. The weight or differential weight of the sample is plotted against the sample Temperature to study the effect of heating at different temperatures on the sample.

Thermal gravimetric analyses of the samples prepared were conducted using the Pyris 1 TGA equipment developed by Perkin Elmer. Initially, the empty pan was inserted into the TGA equipment and the furnace was raised to close the chamber. This was done to set the weight of the empty pan to zero as reference. The furnace was then lowered and the pan was removed to insert 10mg of catalyst sample into the pan.

Next, the pan was the inserted into the TGA equipment and the furnace was raised. The temperature inside the pan was allowed to reach equilibrium at room conditions before the heating was started. The heating was done from Room

Temperature to 800°C and the weight of the catalyst was recorded at 5°C interval. Helium was flowed over the surface of the sample throughout the heating process.

The graph of catalyst weight change (%) vs. Temperature was plotted. The analysis was conducted on dried catalyst sample as well as sample calcined at 350°C of Trial C to study the effectiveness of calcination to remove salts. Also, a comparison of thermal stability between Trial A and Industrial fresh catalyst sample was done by of thermal gravimetric method.

3.3.6 Field Emission Scanning Electron Microscopy (FESEM)

Field Emission Scanning Electron Microscopy (FESEM) is a technology used to capture the image of the surface of a solid sample, determine its elemental composition as well determine the distribution of the elements on its surface. The model of the FESEM used for analysis was the SUPRA 55VP by Carl Zeiss. The electrons are ejected from a GEMINI (vacuum pressure) column that houses the electron gun and the electron beam were then accelerated by an electrical field and focused by an electrostatic lens. Electrons were ejected from the column at an EHT (acceleration voltage) of 5kV. Working distance between lense and sample was 3.6mm.

The image of the sample was captured by the SE (secondary electron) detector that is situated at an angle from the sample to capture secondary and backscattered electrons emitted by the sample. These electrons then hit a phosphor screen which emits photons that are converted into electrical currents by a photo multiplier (PMT). This electrical signals are finally processed to form an image. SE detectors gives good topographical image of the sample. The image of the sample was magnified 20000x and at a resolution of 200nm.

X-Ray Energy Dispersive Analysis (EDX) was done to obtain elemental composition of the sample at its surface. X-rays are released by the sample surface after electron bombardment and each element releases x-rays of a particular energy (keV).

The amount of x-ray at every particular keV are detected by the EDX detector are then used to determine the identity and amount of each element present. EDX was conducted on an image of width 6 μ m. WDX or X-ray Wavefunction Dispersive Spectrometry method was used to map the distribution of each element on sample surface based on the locations from which characteristic x-rays are detected.

3.4 Micro Tubular Reactor (MTR) / GC System – Catalyst Evaluation

3.4.1 System Description

The High Pressure Reactor Analysis system involves a Multi tubular reactor (MTR) and an on line gas Chromatograph used to analyze the gaseous products from the reactor. Figure 3.2 shows the ensemble of the system placed in a room specially designed for Hig pressure systems. The micro reactor is housed in a mounted cabinet with $\frac{1}{8}$ thick stainless steel roof, floor and sidewalls. There are two doors on opposite side of the reactor made of scatter proof glass that allows access to the reactor tubes and other components of the system. The gas inlets of the reactor are placed on the top of the and the exhaust system connected to a vacuum suction is also placed at the top of the cabinet.

The reactor is connected to a panel that houses the electronics of the reactor as shown in Figure 3.3. The control panel consists of information directly from the reactor such as Temperature display, temperature Controller, Pressure display, Main switch, Safety switch, and switches for all the solenoid valves in the reactor. The Reactor pressure can be monitored via the Indicator present on the control panel. The Hengstler digital temperature indicator and a temperature controller is supplied by Fuji Electric. Information from the reactor such as the mass flow readings, Reactor Temperature as well as Pressure can also be seen on the LabView data acquisition and control software in the pc connected to the control panel.



Figure 3.2: Micro Tubular Reactor with an on-line GC system



Figure 3.3: MTR Control panel

3.4.2 Micro Tubular Reactor

The micro tubular reactor is supported on the top by a support flab with a cylindrical opening. This cylindrical opening is connected to the reactor tube via a lock-system with Allen type bolts, which keeps the reactor tube suspended in mid-air. The micro tubular body of the reactor consists of an outer shell and inner shell. There are four inlet openings at the top of the reactor which are connected to all the inlet gases. The inner and outer shells were fabricated from stainless steel SS 316. At the bottom of the reactor, there is another lock system, which connects the bottom of the shells to the Reactor outlet. The top and bottom of each lock system are secured tightly by a gasket in between each lock system and six Allen bolts that together ensure that the reactor is air tight. The dimensions of the outer reactor shell are 2.55cm I.D., 4.90cm O.D and Height of 45.5 cm. The dimensions of the inner shell are 1.3cm I.D., 2.5cm O.D., and a Height of 47.4. The volume of the inner shell is 62.92 cm³. Catalyst sample is placed in the centre of the inner tube. At the bottom of the inner tube, a filter of the mesh size 90µm is placed to avoid catalyst powder from escaping the reactor into the product line. The cross sectional top and side view of the Micro Tubular Reactor is shown in Figure 3.5.

The dual sensor thermocouple is placed in between the outer and inner shell of the reactor bottom as to maintain the accuracy of the reading and avoid damage to its body. One sensor of the thermocouple is placed at the centre of the reactor as to allow control of the catalyst bed temperature. This reactor system is equipped with a split-type electric tubular heating element with controllable temperature from ambient to 600°C and accuracy of $\pm 0.5^\circ\text{C}$. The reactor has a design Temperature of 50 bars.

The inner shell that holds the catalyst is a hollow cylinder as described earlier. The catalyst is placed in the middle of the reactor in between two layer of quartz wool to avoid catalyst diffusion. The top and bottom of the tube are filled with inert alumina

balls as support to the catalyst in the middle. Figure 3.4 shows the magnified image of the inner shell system.

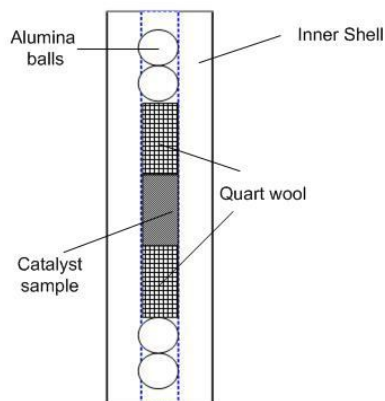


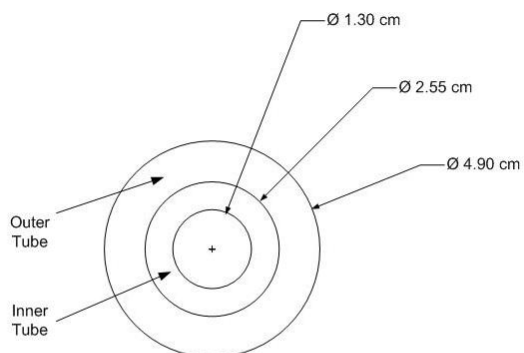
Figure 3.4: Reactor Inner Shell

3.4.3 Reactor Inlet System

The reactor inlets are used to flow 3 types of gas into the systems listed in Table 3.1.a. They are the reduction gas, purge gas and reactant gas. The reduction gas used to activate the catalyst is 5% H_2 in excess N_2 while the purge gas is pure N_2 gas. The reactant gas is a mixture with the composition 30% CO and 70% H_2 for methanol synthesis reaction. All these gases were supplied by MOX Malaysia Bhd. The gas cylinders were connected to the reactor inlets via $\frac{1}{4}$ inch high-pressure stainless steel tubing. High-pressure gas regulators were used to control the outlet pressure from gas cylinder to 30 bars. The design pressure of the MTR is 50 bar and its equipped with a pressure relief valve that evacuates the reactor gas if pressure exceeds that limit.

The reactor flow was controlled using the Swagelok type $\frac{1}{4}$ -inch needle valve and gas flow is measured by the Brooks 5860i series mass flow meter that has a flow rate range between 1-200 sccm. The pressure in the reactor was indicated by a Pressure gauge located at the top of the reactor cabinet as well as the pressure transducer that

displays the Pressure digitally on the control panel. Figure 3.6 outlines the flow system and all the parts of the Micro tubular reactor.



Cross Section -
Top View

Figure 3.5.a: High-pressure micro tubular reactor schematic diagram – Top view

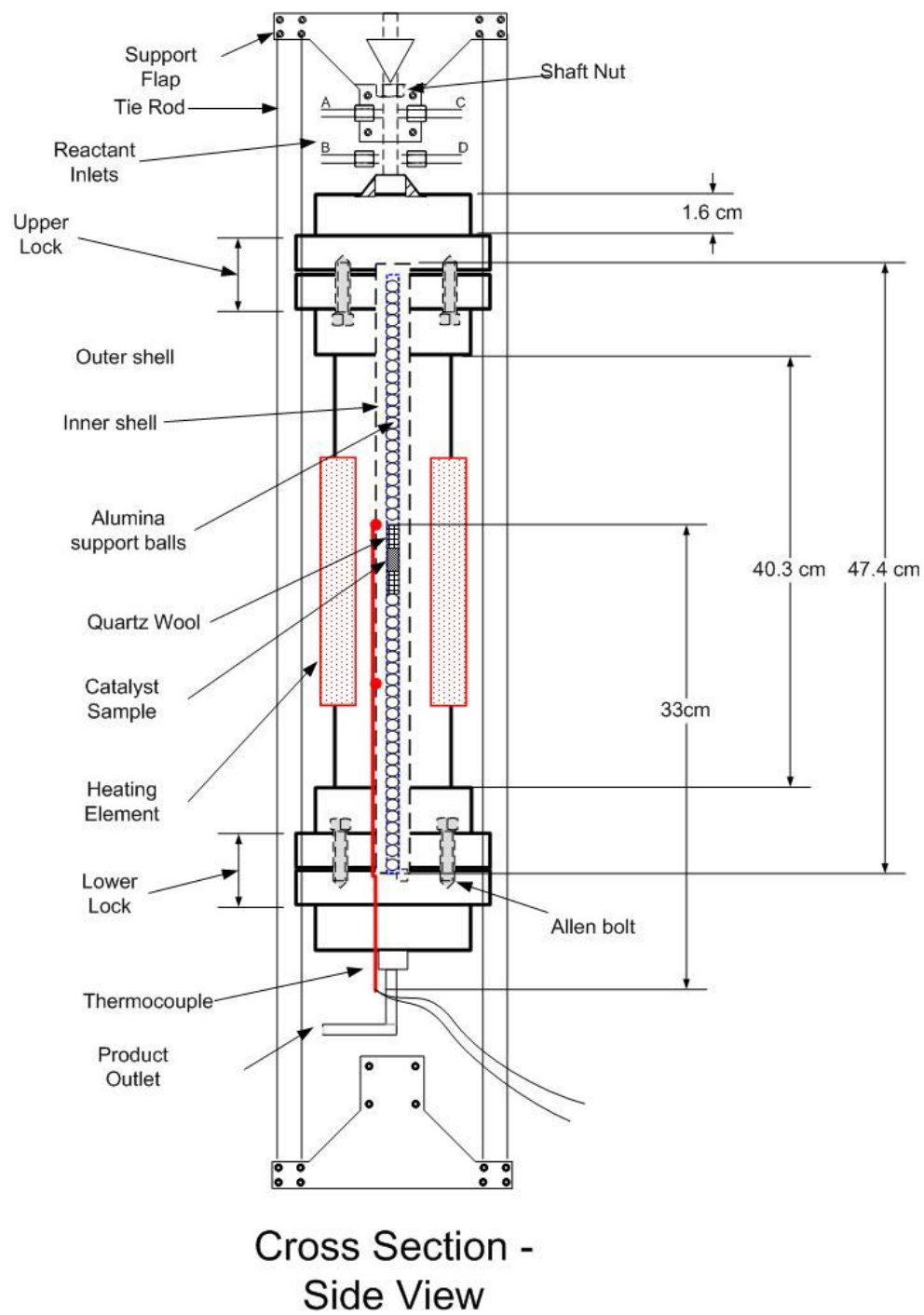


Figure 3.5.b: High-pressure micro tubular reactor schematic diagram - Side view

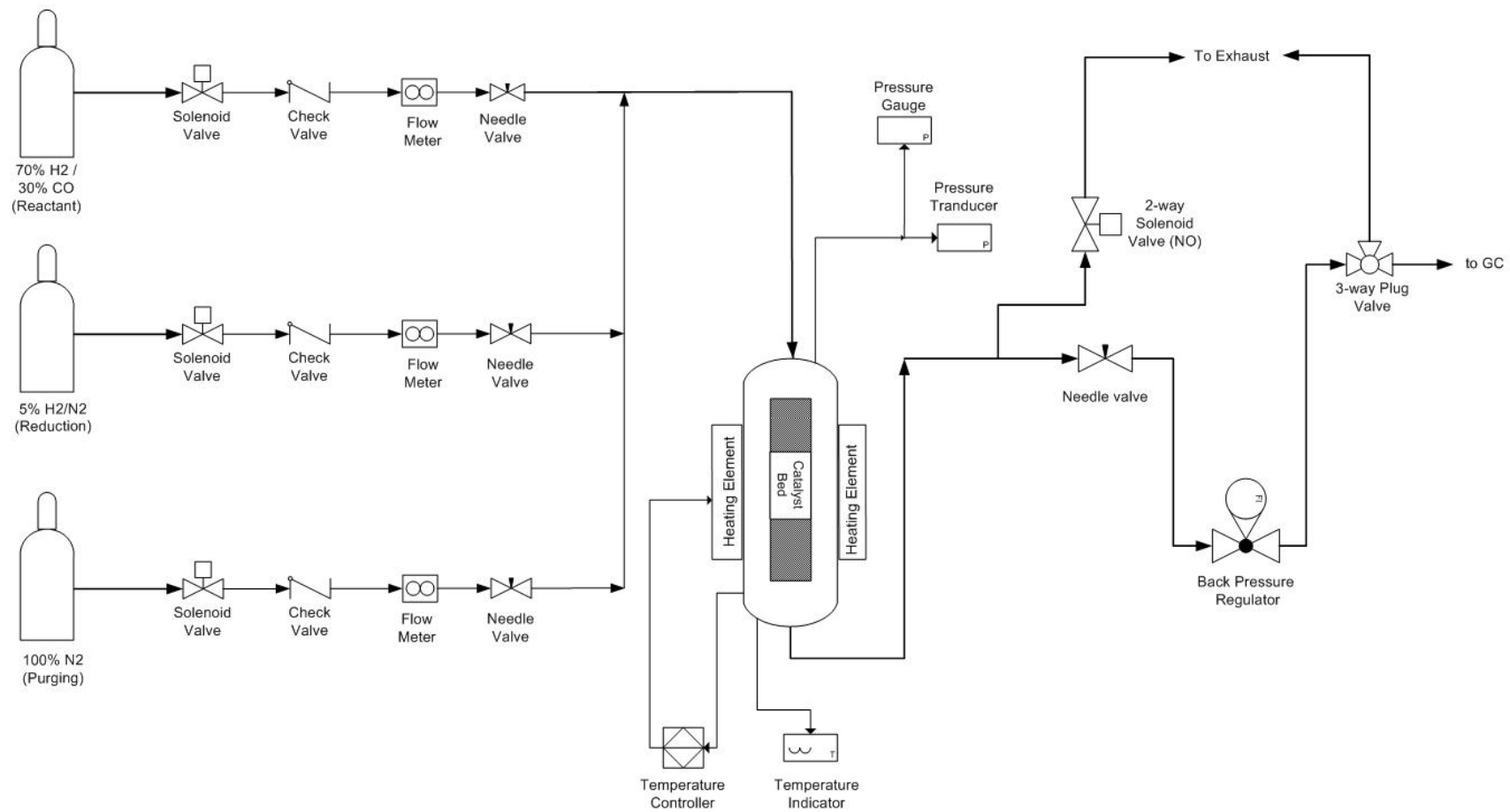


Figure 3.6: Process Flow diagram of the Micro Tubular Reactor

3.4.4 Gas Chromatography

Gas chromatography (GC) is a useful mechanism to analyse qualitatively and quantitatively gaseous product by means of retention in multi-coiled columns. It is a separation method in which components of a sample partition between two phases. One of these phases is a stationary bed with a large surface area and the other is a gas that filters through the stationary bed. The sample is vaporized and carried by the carrier gas through the column. Sample partition into the stationary liquid phase based on their solubilities at any given Temperature. The components of the sample separate from one another based on their relative vapor pressures and their affinities for the stationary bed. This chromatographic process is called elution [111].

The gas chromatograph (GC) employed for the identification and quantification of the reaction effluents was the GC 6890 series by Hewlett Packard as shown in Figure 3.8. A 3-way valve connected the reactor outputs with the GC gas-sampling valve creating an online gas sampling system. The reactor was connected to the GC by a ¼ inch stainless steel tub which was heated by a heating element and Temperature controlled by a Watlow Controller. The temperature of the line was maintained at 150°C to maintain the gaseous phase of the reactor outputs.



Figure 3.7: The GC 6890 series by Hewlett Packard

The 890 GC was equipped with 3 columns for gas retention. They were the DB-1, HP-Plot U and HP-Molesieve columns. In addition, 2 detectors to determine gas types are included, the thermal conductivity detector (TCD) and a flame ionization detector (FID). The details of the GC columns are shown in Table 3.5.

Table 3.5 Details of the 6890 GC column

Type	Model No.	Column Details			Max Temp. (°C)	Gas Flow (ml/min)
		Length (m)	Film (µm)	I.D. (µm)		
HP-Plot U	19095P-U04	30	20	530	190	3
HP-Molesieve	19095P-MS9	15	50	530	300	3
DB-1	125-1034	30	3	530	280	5

HP-PLOT U consists of bonded, divinylbenzene/ethylene glycol dimethacrylate coated onto a fused silica capillary, and is suitable for analyzing hydrocarbons such as natural gas, refinery gas, C1-C7, all C1-C3 isomers except propylene and propane as well as CO₂, methane, air, CO, water and polar compounds.

HP Molesieve is a PLOT column for the analysis of permanent gases such as O₂, N₂, CO and CH₄ that are resolved in less than 5 minutes. This column has a durable molecular sieve 5A coating that minimizes baseline spiking and damage to multiport valves.

DB-1 column is made of 100% Dimethylpolysiloxane. It is suitable for analyses of non-polar molecules such as methanol and dimethyl ether. It has a High temperature limit and is bonded and cross-linked. It is also rinsable with solvent for cleaning [112]. Figure 3.8 shows an image of a column with its coiled capillary tubes.



Figure 3.8: Image of a Gas chromatograph column [112].

3.4.5 Product Sampling Description

The gas products from the reactor into the GC were flowed through a series of pneumatic 6-port sample valves to constraint gas flow into the gas columns. They are 3 valves labeled valve 1, 2 and 3. The process diagram outlining the gas flow in the GC is shown in Figure 3.9.

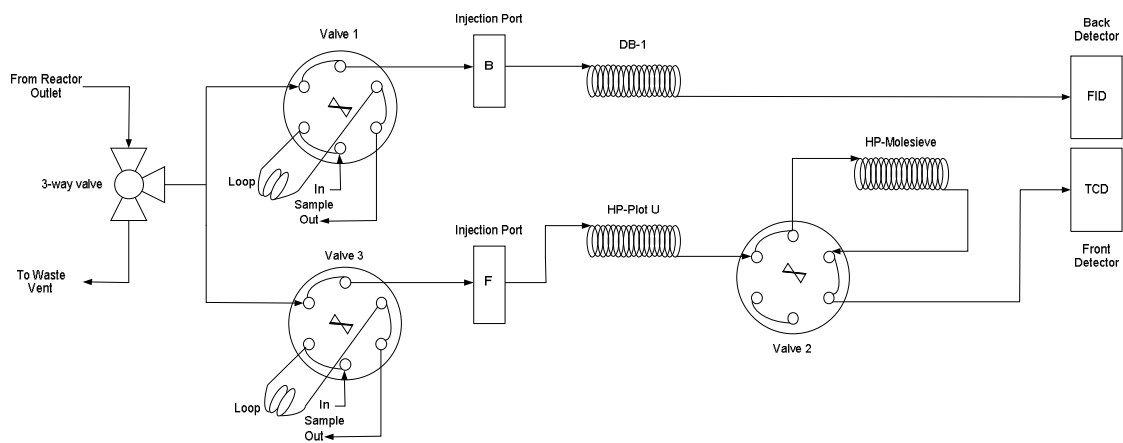


Figure 3.9: Gas Chromatography sampling valve diagram

Initially the gas from the reactor filled both loops in Valve 1 and Valve 3. GC analysis began when these valves were in Inject position at run time **0.00 min**. This allows gas to be directed into the front columns (HP-Plot U and HP-Molesieve) and back column (DB-1). DB-1 column was used to separate hydrocarbons such as dimethyl ether (DME), methanol and methyl formate, which were eventually detected by the FID. Other compounds such as CO₂, CO and H₂ were separated to the HP-Plot U and HP-Molesieve and detected by TCD.

CO₂, DME and methanol were held back in the HP-Plot U column but H₂, CO and CO₂ traveled through quickly into the HP-Molesieve column. At **2.10 min** run time, the HP-Molesieve column was then isolated (Figure 3.10a) to prevent DME and methanol from entering this column. A restrictor valve replaced the HP-Molesieve column to restrict gas overflow into the TCD as shown in Figure 3.10a.

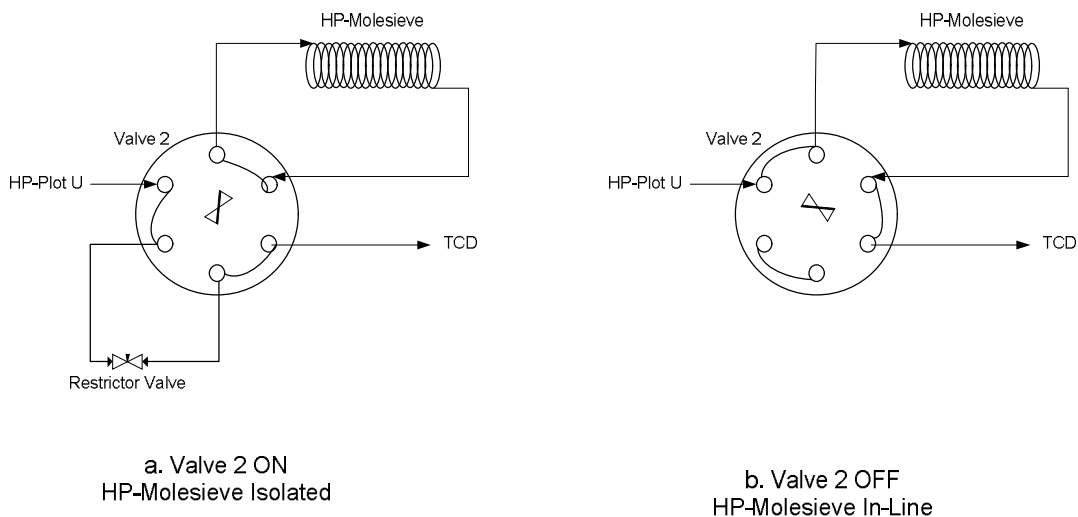


Figure 3.10: Valve 2 Configurations

When the dimethyl ether and methanol have eluted, valve 2 was turned off (Figure 3.10b) at run time **3.00 min** to allow gas HP-Molesieve column into the flow path. H₂, CO and CO₂ were then separated and detected by the TCD.

Table 3.6: Gas sampling valve run time

Run Time (min)	0	0	1	1	2.1	3
Valve No.	1	3	1	3	2	2
State	On	On	Off	Off	On	Off

Gas calibration was conducted with standard gas mixtures which have known amount of desired reactant and expected product gases as shown in Table 3.5. The standard gases were injected into the GC to identify gases by its retention time as well its quantity in mol%.

Table 3.7: Calibration of gas retention time and its amount

No.	Retention Time (min)	Detector	Gas detected	Quantity (Mol %)	Integrated Area
1	1.521	FID	Methane	30	2433.7
2	1.789	FID	Dimethyl Ether	0.01262	17.323
3	1.841	FID	Methanol	14.896	2849.9
4	1.976	FID	Methyl Formate	0.0010031	2.313
5	2.019	FID	Ethanol	0.03074	3.980
6	2.651	TCD	Carbon Dioxide	30.00	2433.7
7	3.767	TCD	Hydrogen	40.00	220.58
8	4.892	TCD	Carbon Monoxide	33.00	7276
9	8.556	TCD	H ₂ O	100.00	466.620

3.5 Activity Study

The micro tubular reactor was employed to study the catalyst activity i.e. methanol selectivity, methanol yield and CO conversion. The standard Operating procedure for catalysts loading and reactor operation is shown in Appendix E.

1g of catalyst was inserted into the inner tube of the reactor and sandwiched immediately between cotton wool and then alumina balls. The location of the catalyst samples was in the center of the inner tube.

Catalyst activation which was conducted to reduce the catalyst surface was done with a 5% H₂ in N₂ gas stream at a flow rate of 76.5 ml/min from Room Temperature to the sample reduction Temperature (obtained from the TPR analysis as discussed in Section 4.1.5) at a ramp rate of 10°C/min. The bed temperature was maintained for the next 1 hour. This is followed by reactor line purging and sample cooling with pure nitrogen gas at 110ml/min and 10 bars for 1 hr.

A gas mixture of 30% CO and 70% H₂ (syngas) was then flowed in to the system at a flow rate of 210 ml/min and Temperature was maintained at 250°C and 30 bars. The product line was heated to 150°C to maintain product gaseous phase. An on-line GC analyzed effluent gases from the reactor outlet at every ½-hour interval to obtain the gas concentration in mol%.

CHAPTER IV
RESULTS AND DISCUSSION

4.1 Catalyst Physio-Chemical Properties

4.1.1 Density of Catalysts

Catalyst density was measured for the 3 catalyst series prepared by the Acid Alkali Alternating pH precipitation method [10]. The Cu/ZnO/Al₂O₃, Cu/ZnO/ZrO₂/Al₂O₃ and Cu/ZrO₂/Al₂O₃ catalyst series were prepared to determine the quantitative influence of Zn and/or Zr in the catalyst. Catalysts' density was measured by the Quantachrome Ultrapycnometer 1000 instrument. The density for each sample was measured 3 times to account for deviation in densities of different sample group. The average of these 3 readings was taken as the density of the catalyst sample. The resultant densities, average densities and standard deviation are tabulated in Table 4.1.

As can be seen in Table 4.1, the standard deviation of 3 density readings for every sample is between 0.01 to 0.19 g/cm³. This is a small deviation range and thus the average density values are acceptable. Figure 4.1 is a graphical representation of average density for all catalyst samples. From the figure, it can be seen that Sample F has the highest density of 18.9 g/cm³ while commercial catalyst sample (Ind) has the lowest density of 4.72g/cm³. For, commercial catalyst sample A, it has been found through FeSEM-EDX study, that it contains 4.21 wt% surface graphitic carbon possibly inserted into the catalyst as a binding agent during pelletization process. Since graphite has low

density (2.26 g/cm^3) [113], it would significantly reduce the catalyst weight and hence lower its density. For catalyst sample F on the other hand, the presence of ZrO_2 (density range $5.49 - 6.0 \text{ g/cm}^3$) [113] instead of ZnO (density 5.47 g/cm^3), might account for its higher density than other catalyst samples. Other catalyst samples, A to E, however have density similar to each other as they have the same amount of CuO , alumina as well as the same range of ZnO and/or ZrO_2 as can be seen in Table 3.3.

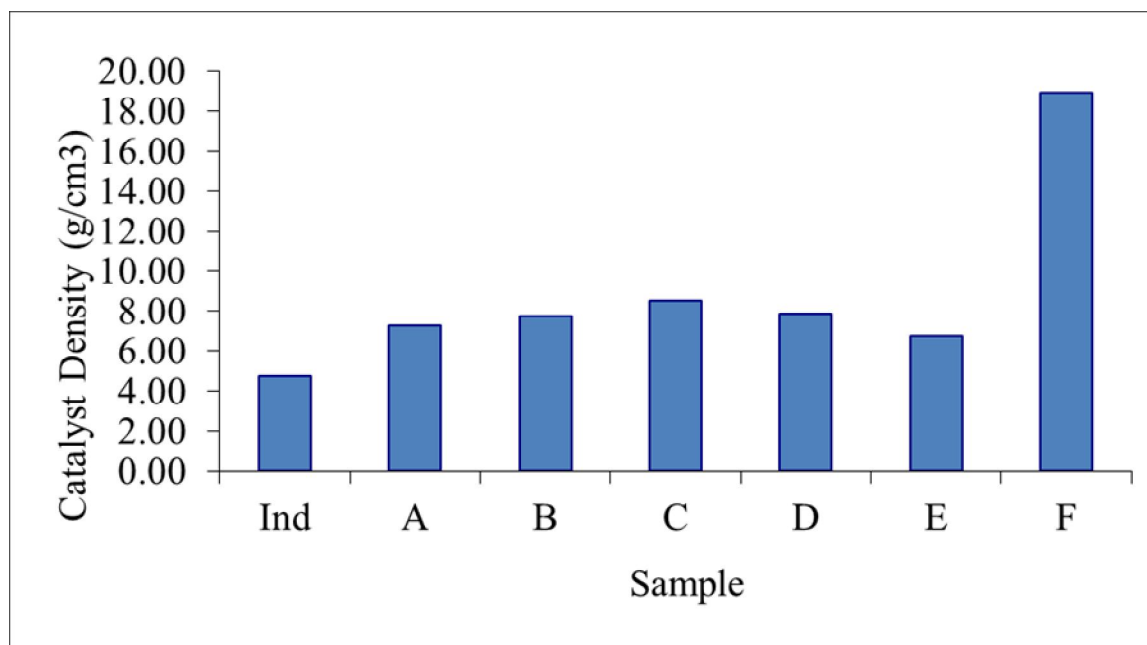


Figure 4.1: Density of all catalyst samples

Table 4.1: Densities of catalysts from all 3 catalyst series

Catalyst Series	Catalyst sample	Run	Density , ρ (g/cm ³)	Average Density , ρ_A (g/cm ³)	Standard Deviation (g/cm ³)	
Cu/ZnO/Al ₂ O ₃	Ind	P ₁	4.73	4.72	0.01	
		P ₂	4.73			
		P ₃	4.71			
	A	P ₁	7.32	7.31	0.02	
		P ₂	7.32			
		P ₃	7.28			
Cu/ZnO/ZrO ₂ /Al ₂ O ₃	B	P ₁	7.55	7.76	0.19	
		P ₂	7.83			
		P ₃	7.90			
	C	P ₁	8.49	8.52	0.06	
		P ₂	8.47			
		P ₃	8.59			
	D	P ₁	7.82	7.86	0.03	
		P ₂	7.87			
		P ₃	7.87			
	E	P ₁	6.63	6.73	0.14	
		P ₂	6.66			
		P ₃	6.89			
	Cu/ZrO ₂ /Al ₂ O ₃	F	P ₁	18.92	18.90	0.09
			P ₂	18.80		
			P ₃	18.98		

4.1.2 TPR of oxidized states (s-TPR)

Copper metal area was determined quantitatively by Temperature Programmed Reduction (TPR) of oxidized states or s-TPR method [108]. This method not only determines the number of copper sites available, but also gives the advantage of distinguishing the surface and bulk copper active sites. The surface copper active sites or Cu_2O are partially oxidized copper active sites, are easily available during reaction are detected as the low temperature copper active sites. This is because they adsorb and desorb copper active sites at low temperature (Section 2.6.5, Equation 2.8). Bulk copper active sites however are only reduced at high temperatures and marginally active during methanol synthesis reactions. These are fully oxidized CuO and they are called the High Temperature Active sites (Section 2.6.5, Equation 2.9). These reactions (Section 2.6.5, Equation 2.7-2.9) are explained in detail in Section 2.6.5.

. Generally, the s-TPR method is a two-step process involving:

- a. Isothermal surface oxidation by N_2O (Section 2.6.5, Equation 2.7)
- b. Analysis of H_2 temperature-programmed-reduction (TPR) of the partially and fully oxidized Cu surfaces (Section 2.6.5, Equation 2.8 and 2.9)

The surface copper species, Cu_2O can be well distinguished from the bulk copper species, CuO in this s-TPR method as two distinct TPR peaks were produced as shown in Figure 4.2.

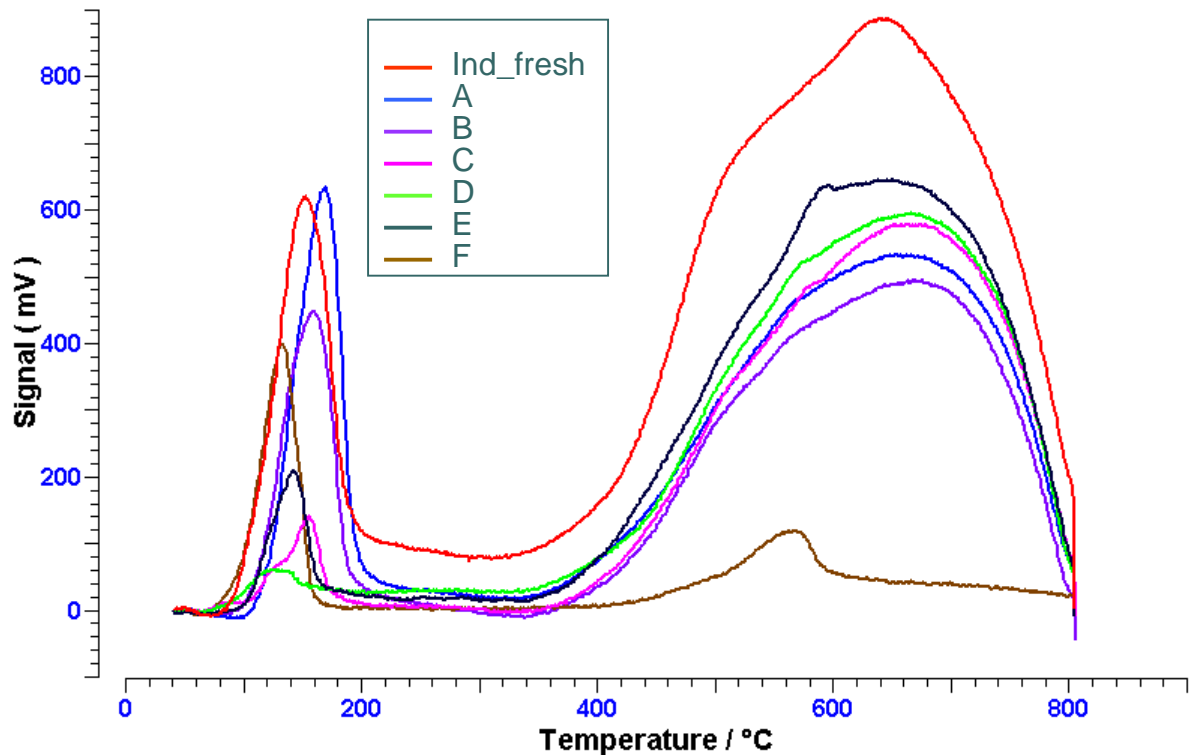


Figure 4.2: s-TPR spectrum of catalysts after N_2O adsorption. Catalysts are labeled above the graph.

Figure 4.2 clearly shows the distinction between Low Temperature and High Temperature copper active sites. The Low Temperature active sites are reduced and activated at a temperature range of 150-200°C. High temperature copper active sites however are only reduced and activated at the temperature range of 400-800 °C. This range is far above the methanol synthesis reaction temperature of 250°C. Therefore copper sites in the high temperature range would be less easily available during reactions compared to low temperature copper active sites.

Area under the curve for the low and high temperature peaks in Figure 4.2 which is the sum of signals (mV/g_{cat}) reading from the TCD is the total amount of H_2 gas adsorbed under those Temperatures and thus represents the amount of copper active sites at Low and High Temperatures conditions. This signals for Low Temperatures and High Temperatures has been plotted in Figure 4.3. Also plotted is the sum of those two signals representing the total copper active sites available in the catalyst samples.

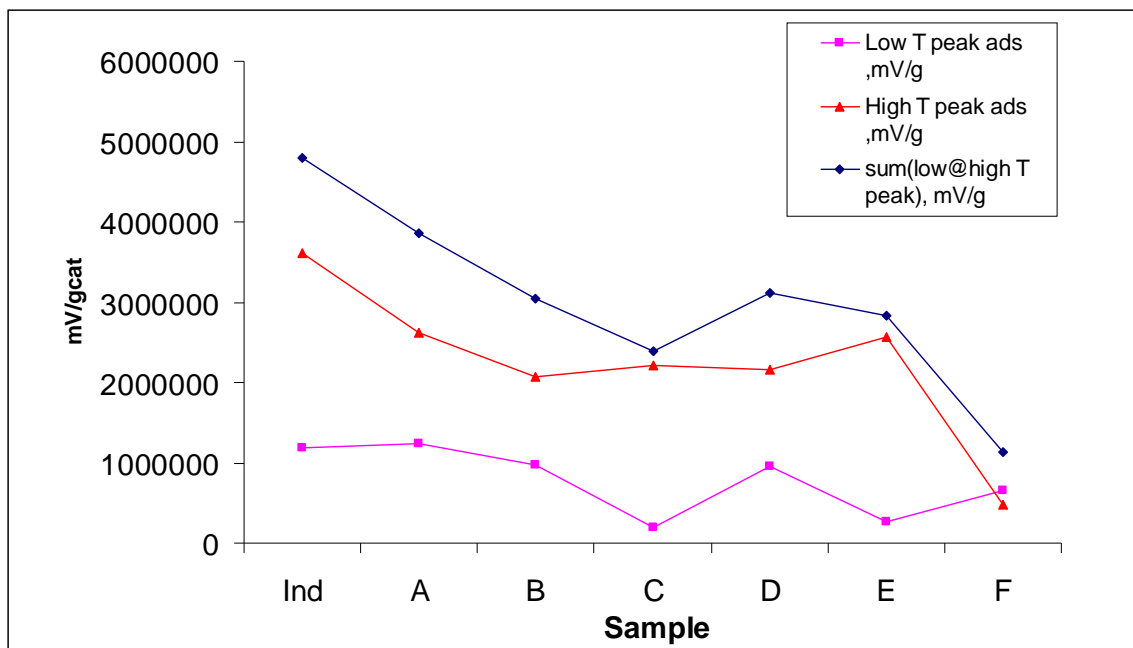


Figure 4.3: Low Temperature signals, High Temperature signals and their sum from the s-TPR analysis for all catalyst samples

From Figure 4.3, it can be seen that commercial catalyst (Ind) has the highest amount active copper sites in high temperature conditions. This can be largely because the Industrial sample has the largest metal atomic percentage of Cu, 52.66 atomic% obtained from SEM-EDX analysis in comparison with other prepared samples which have only around 40 atomic% copper metal in them (Section 4.2.3, Table 4.4). This suggests that a lot of its metal Cu is present in the form of CuO which would indicate lower activity. Among prepared samples, sample A which has no Zr present has the highest low temperature and high temperature sites. This suggests that this sample has a lot of readily available surface copper as well as less available bulk copper active sites. This could be due to the absence of Zr and the abundance of Zn as agent of metal dispersion encouraging more copper to be available in partially oxidized states, Cu₂O.

For samples B to E, which have both Zn and Zr present in them it can be seen that sample B and D have high surface area low temperature copper sites while C and E

has less of these sites. From SEM-EDX study (Section 4.2.3, Table 4.4), it was confirmed that only samples B and D have high Zn/Cu ratio of 1.25 and 1.23 each. For samples C and E however, they both have lower Zn/Cu ratio of 1.1 and 1.0 each. This low amount of Zn in samples C and E could have affected the dispersion of Copper active sites and thus they are available in mostly CuO phase which remains largely inactive during reactions. This can be seen in Figure 4.3 as sample E has large High Temperature bulk sites but lower Low Temperature surface sites.

Sample F is unique compared to other catalyst samples as it is the only Cu/ZrO₂/Al₂O₃ sample and also because it has larger amount of Low Temperature surface sites than it has High Temperature bulk sites as can be seen in Figure 4.3. This could be due to the unique arrangement of Cu-Zr metallic matrixes which allows copper sites to be present greatly in partially oxidized states, Cu₂O.

4.1.3 Copper Metal Area

From the method of s-TPR, surface oxidized copper sites, Cu₂O as well as bulk oxidized copper sites, CuO were determined by N₂O titration and subsequently TPR with H₂ which provides a low and high temperature adsorption signal peaks. The signal was converted from mV to mmol H₂ adsorbed by using a pre-calibrated factor of $1.06745307416578899 \times 10^{-7}$ mmol/mV. This would give the amount of adsorbed H₂ in mmol which would be then used to calculate the copper metal surface area.

The metal surface area, MSA (Section 3.3.3, Equation 3.1) was calculated by using the method described by Gervasini *et.al* [108]. The stoichiometric factor, S.F that corresponds to Cu/O ratio is assumed to be 2 to account for Cu₂O decomposition into Cu crystal state and 1 for CuO decomposition into Cu crystal state. For surface Cu (Cu₂O) metal area, the mol H₂ adsorbed corresponds to the amount of H₂ adsorbed at low temperature only. For Total Metal Cu Area, the mol H₂ adsorbed corresponds to amount of H₂ adsorbed on surface and bulk copper sites.

Sample calculation for Metal Cu Area of surface (low temperature Cu₂O) and bulk (high temperature CuO) as well as the Total Cu area is included in Appendix A. Results of surface and total Metal Copper sites is shown graphically in Figure 4.4. As can be seen the highest amount of both surface and total Cu active sites are observed in catalyst sample A with 23.60 and 43.79 m²/g_{cat} each. This belongs to Cu/ZnO/Al₂O₃ catalyst type. The values are higher even than the commercial catalyst (Ind).

Commercial catalyst as can be seen in the Figure 4.4, has fairly increased amount of Total Cu Area with respect to Sample A. This is because it has a fairly large amount of bulk copper sites (CuO) which are largely inert during reactions. As for the Cu/ZnO/ZrO₂/Al₂O₃ series i.e sample B to E, it can be seen that sample D has both highest amount of surface and total Cu active Area at 19.14 and 40.52 m²/g_{cat} each. This would indicate that it may have the highest activity among that catalyst series.

Sample F shows an interesting property of as it has the lowest amount of total Cu area but relatively high amount of surface Cu area. It suggests a unique feature of Cu/ZrO₂/Al₂O₃ catalyst type which increases bonding of Zr to Cu metal as to allow for Cu to be present in partially oxidized states, Cu₂O.

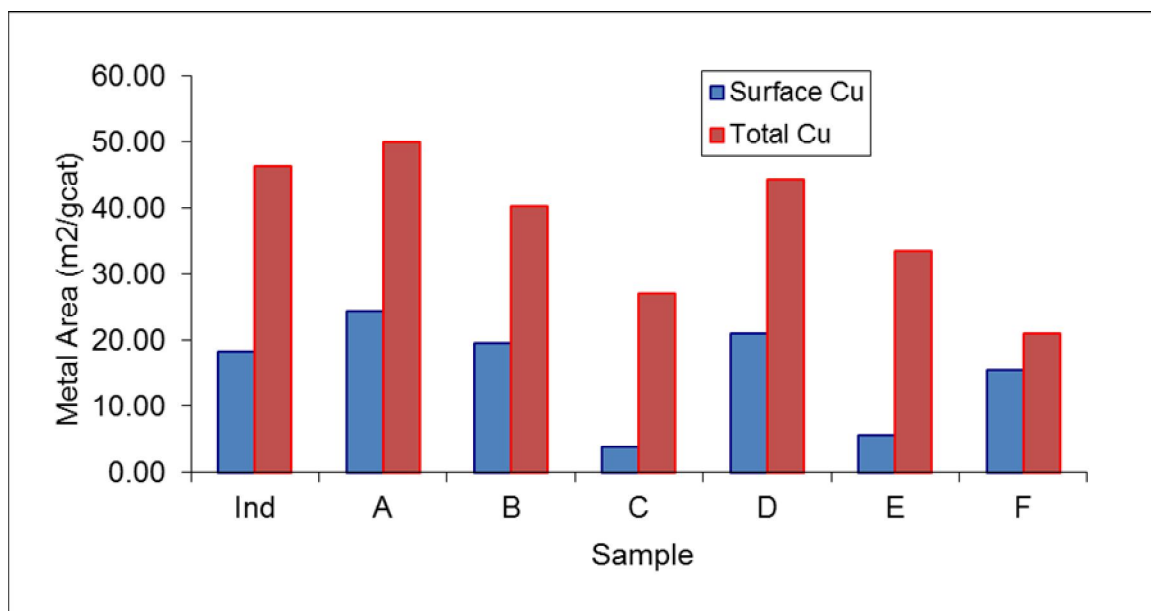


Figure 4.4: Surface and Total Metal Cu Area available in all catalyst sample types.

4.1.4 Dispersion and Particle Size Analysis.

Cu metal dispersion however, is defined separately by two different sources. Gervasini et al. defined dispersion of Cu metal as the ratio of surface copper sites, Cu₂O to the total Cu present in the catalyst sample (Section 3.3.3, Equation 3.2) [108]. This was experimentally determined by calculating low temperature peak area of the s-TPR spectrum, which represents surface copper sites and divide it by the total area under the curve representing the total metal surface area. The second source of metal dispersion definition was the Thermo Finnigan Instruction suite (Section 3.3.3, Equation 3.3) [88]. Here, metal dispersion is defined as the ratio of adsorbing Cu or active Cu atoms over the total Cu atoms present in the catalyst sample. MW_{Cu} in the equations is the Cu molecular weight.

Table 4.2 outlines the dispersions obtained for each sample based on the descriptions given. It can be seen Sample A which is a Cu/ZnO/Al₂O₃ catalyst type has the highest dispersion in D_{Cu}² and second highest in D_{Cu}¹. This would suggest high

activity as the sample has a good distribution of Copper all over its surface which reduces sintering and thus increases available surface area for reactant adsorption.

Sample D with Zr/Cu ratio of 0.18 is of the Cu/ZnO/ZrO₂/Al₂O₃ catalyst series and has the highest dispersion of Cu among that series. This would suggest the 0.18 ratio of Zr/Cu to be the optimum amount in encouraging metal dispersion and hence possibly its activity.

Sample F however presents a curious case as one it has the highest D_{Cu}^1 of 73.55% but has the lowest D_{Cu}^2 dispersion at 3.01%. This is because although surface copper to bulk copper ratio is the highest in sample F, the overall copper sites which are active are indeed limited. This would mean that there exists also Cu sites in Sample F which are entirely non-active at Low or High Temperature reaction conditions. This is a unique feature of Cu/ZrO₂/Al₂O₃ catalyst in sample F.

Mean particle diameters (Φ_{av}) can be determined using the definition given by Gervasini et al. (Section 3.3.3, equation 3.4). SK is a constant that depends on the Cu particle shape. SK has a value of 6 for spherical or cubic shape of copper aggregates. Copper density, ρ_{Cu} has the value of 6.64 g/cm³.

Table 4.2: Two different Dispersion description for catalyst samples D_{Cu}^1 and D_{Cu}^2

Catalyst Series	Sample	Zr/Cu ratio	D_{Cu}^1	D_{Cu}^2
Cu/ZnO/Al ₂ O ₃	Ind	0.00	39.46	7.19
	A	0.00	48.79	7.50
Cu/ZnO/ZrO ₂ /Al ₂ O ₃	B	0.04	48.41	5.86
	C	0.11	14.56	3.83
	D	0.18	47.22	6.29
	E	0.33	16.80	4.98
Cu/ZrO ₂ /Al ₂ O ₃	F	1.11	73.55	3.01

Average diameters of Cu particles are shown graphically in Figure 4.5 for all catalyst samples. It can be seen that there is a generally increasing trend in crystal diameter as Cu/Zr ratio increases from Sample A to F. The increase in copper particle size could be translated as significant amount of sintering which reduces amount of surface area available for reaction.

Sample F suffers from the largest particle diameter of 34.67 nm. Sample A has the lowest particle size and thus amount of surface area available and this translates to higher activity. All the samples have the particle size in the range of 10 – 45 nm suggesting formation of nano-crystals which are highly desirable on catalyst samples.

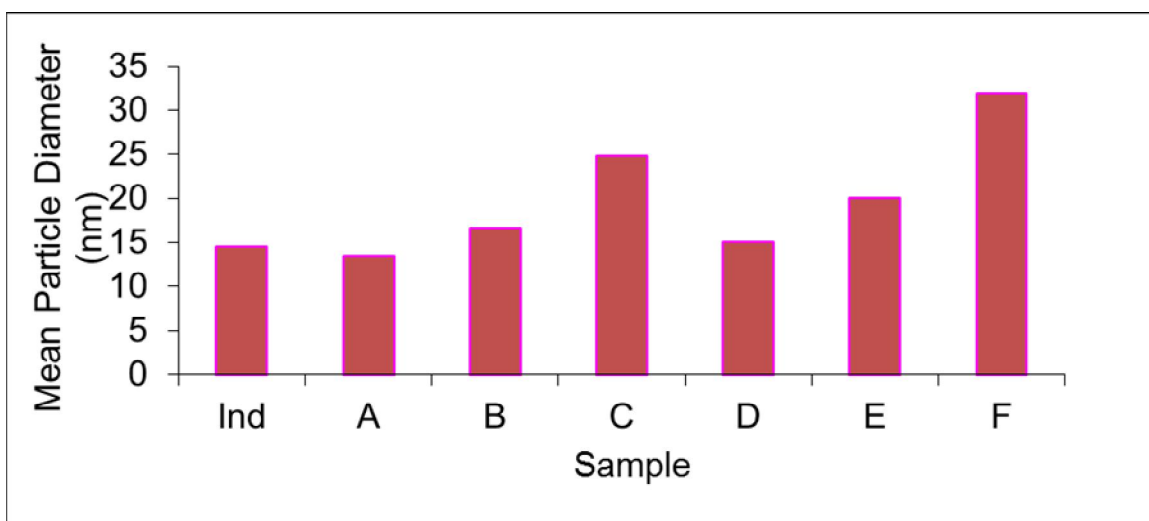


Figure 4.5: Mean particle diameters (Φ_{av}) in nm for all catalyst samples.

4.1.5 Thermal Decomposition Study by TGA

Thermal gravimetric analyses were conducted using the Pyris 1 TGA equipment developed by Perkin Elmer. Thermal gravimetric method (TGA) was conducted on dried and calcined sample C to study the effectiveness of calcination to remove salts. The graph of catalyst weight change (%) vs. Temperature was plotted and is shown in Figure 4.6.

From Figure 4.6, it can be clearly seen that thermal decomposition of metals nitrates into metal oxides in dried catalyst sample occurs at temperatures below 350 °C. At this temperature, it can be seen that the weight change of catalyst is the graph is at minimum and least amount of contaminates are present after this state. Thus this shows that calcination temperature at 350°C is suitable for removal of unoxidized salts.

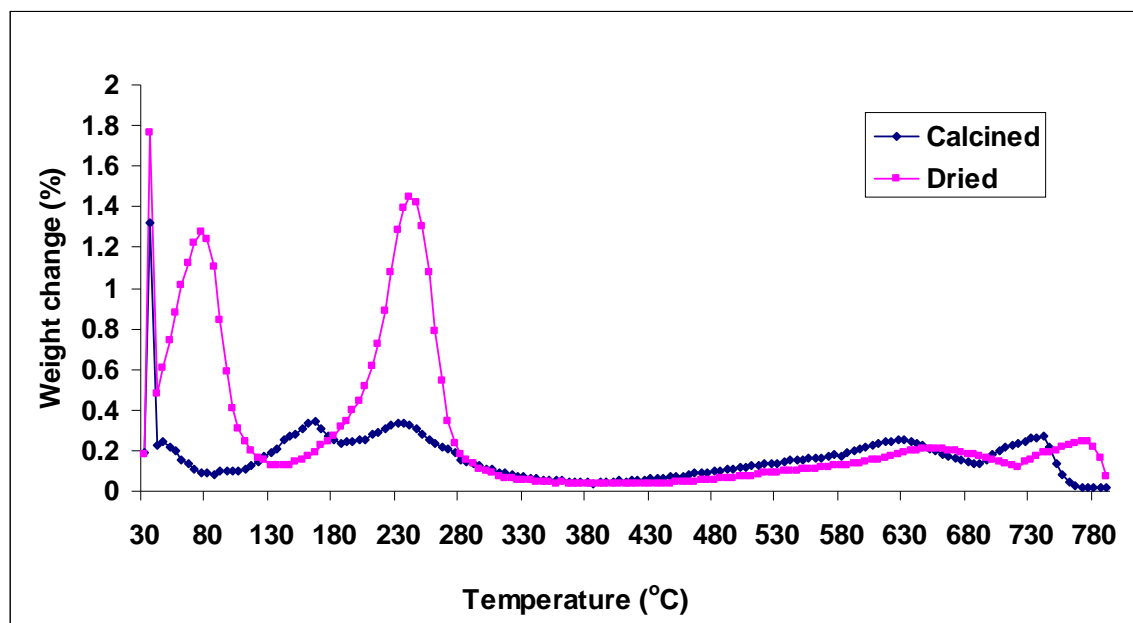


Figure 4.6: TGA graph of catalyst weight change (%) vs. Temperature for Dried and Calcined catalyst Sample C.

The temperature where decomposition occurs the most is at the range of 30 – 130°C and 170 – 280°C. This is consistent with the boiling point Temperature for copper nitrates (170°C), for zinc nitrate (105°C), for Aluminium nitrate (134°C) and finally zirconium nitrate (100°C) under atmospheric pressure [113]. This indicates all other nitrates are oxidized at the lower temperature range while copper nitrate is oxidized at the upper Temperature range.

A comparison of thermal stability between Sample A and commercial catalyst sample, both belonging to Cu/ZnO/Al₂O₃ series was also done by of thermal gravimetric method. This is to determine the thermal stability of prepared sample vs. commercial

sample under operating temperature of 250°C. The resultant graph is shown in Figure 4.7.

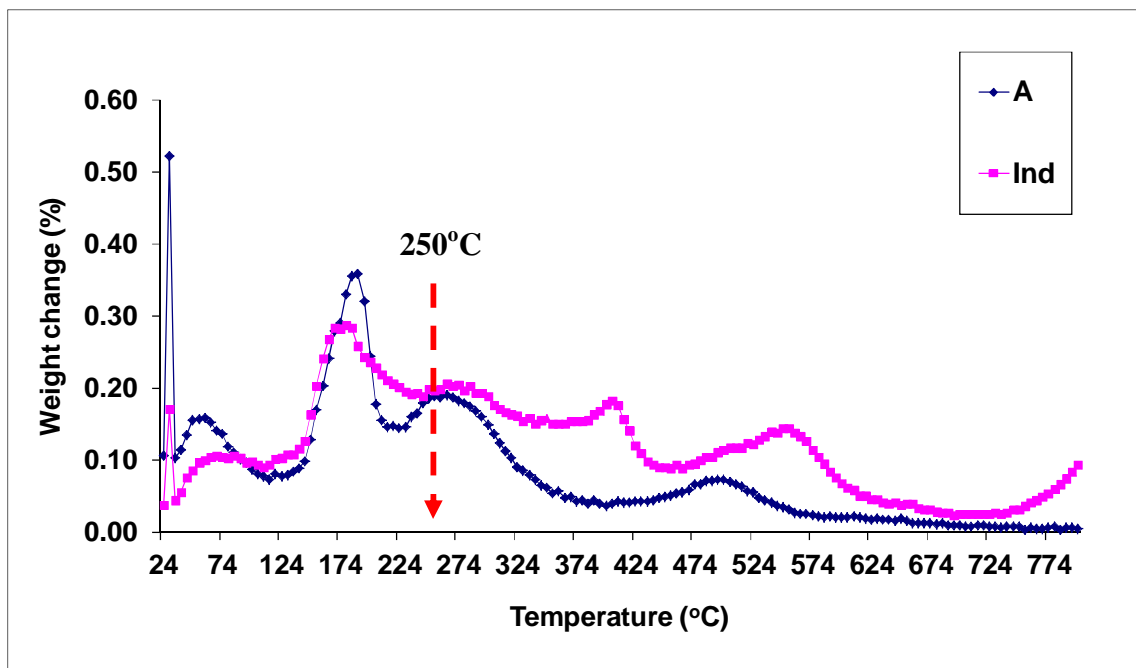


Figure 4.7: TGA graph of fresh commercial versus prepared catalyst A.

The dotted arrow on the graph indicate that at around the process operating temperature of 250 °C, the weight loss of commercial catalyst is higher than the prepared catalyst by difference of 0.0117%. This would suggest higher thermal stability of prepared catalyst as compared to commercial industrial catalyst at Industrial reaction conditions. Temperatures above 500 °C indicate almost total degradation of the oxide sites leaving mostly pure metal components only.

4.1.6 Reducibility and Temperature Optimization

Temperature Programmed Reduction (TPR) of all catalyst samples were conducted by means of the Thermo Finnigan TPDRO 1100 equipment. All samples were pretreated with nitrogen to remove volatile impurities (Section 3.3.2), cooled and then the reduction process was initiated from room temperature to 600°C. The resulting

Signal peaks (mV) vs. reduction temperature are plotted for all catalyst samples and for comparison are grouped together in Figure 4.8. The Signal (mV) here represents the amount of H₂ adsorbed at each Temperature. The area under the curves of each sample is defined as the total amount of H₂ gas adsorbed in mV and the signal is converted to mmol of gas adsorbed by using a pre-calibrated factor of $1.06745307416578899 \times 10^{-7}$ mmol/mV. This adsorption value would be further corrected by taking into account the gas adsorbed by Cu metal alone through inclusion of metal Cu wt% area. The graph of total H₂ adsorbed for each sample is plotted and shown in Figure 4.9.

Figure 4.8 shows the graph of reduction temperature and their corresponding H₂ gas adsorbed as Signal (mV) in the TPR analysis.

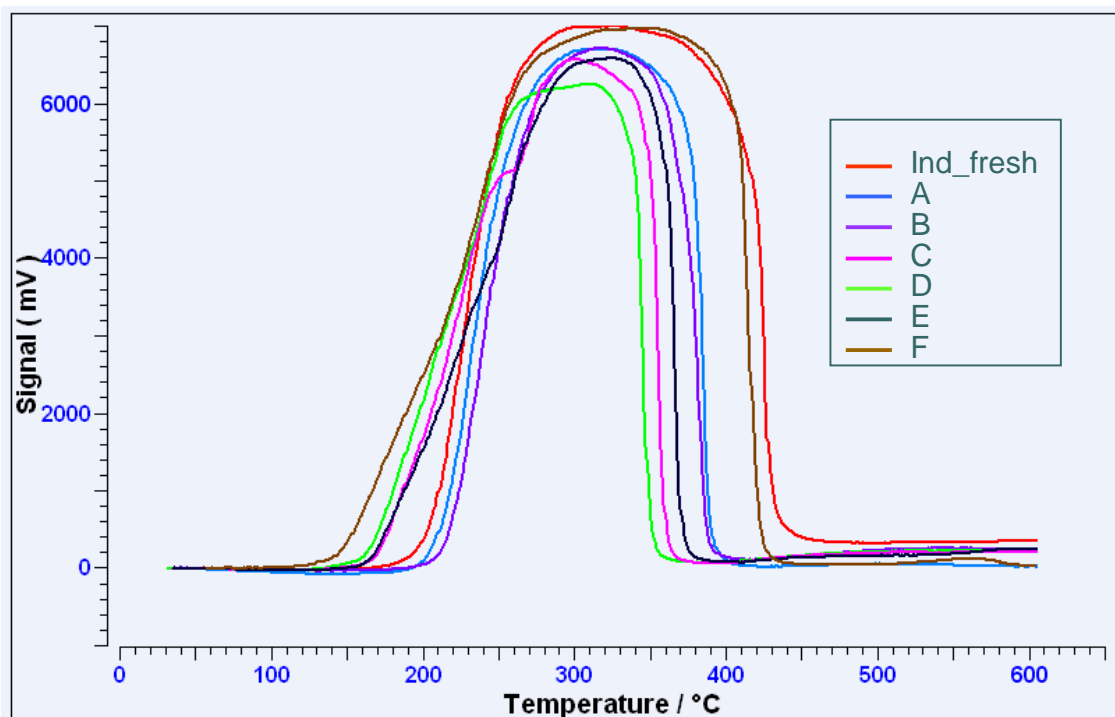


Figure 4.8: Graph of reduction temperature and their corresponding H₂ gas adsorbed as Signal (mV).

From Figure 4.8, it can be seen that for all catalyst samples, the H₂ adsorption or the reduction was zero until 110°C. At about 150 to 200°C H₂ adsorption steadily increased for all catalyst samples. H₂ adsorption peaked at 270°C and remained

constant until 350°C for all catalyst samples except for commercial sample Ind and Sample F. The latter samples remained at highest reduction peak until 380°C. After this maximum peak reduction period, H₂ adsorption dwindled and zeroed at 400°C for other catalyst samples except for Sample Ind and F which zeroed after 440°C.

Figure 4.8 shows that Sample F and Ind sample have a broader peak reduction temperature range as compared to other catalyst samples. The data for most optimum temperature for reduction is crucial for catalyst activation before activity is studied in the methanol synthesis process. For each sample it was determined as follows: Sample Ind, 325°C; Sample A, 315°C; Sample B 315°C; Sample C, 300°C; Sample D, 310°C; Sample E, 320°C; Sample F, 345°C. This temperature is in effect the highest peak obtained for each sample graphs in Figure 4.8 i.e. temperature with the highest signal is the temperature at which highest amount of H₂ adsorption takes place.

Figure 4.9 shows the amount of H₂ adsorbed by Cu metal crystals calculated from TPR analysis for the various catalyst samples.

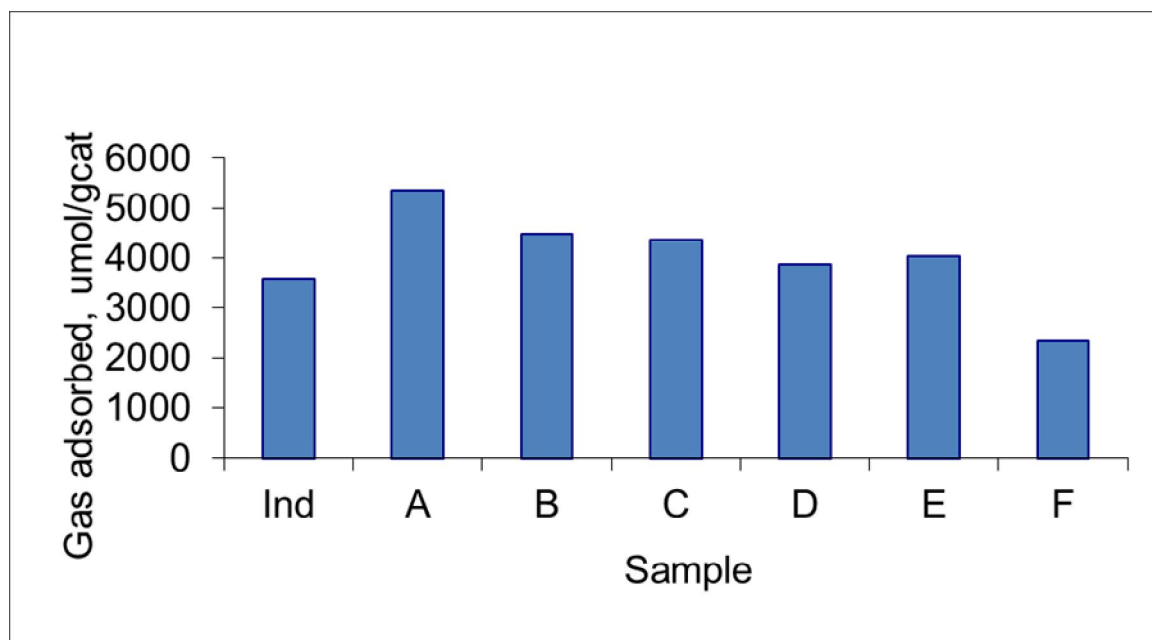


Figure 4.9: Total Hydrogen gas adsorbed by each catalyst sample in TPR analysis

Figure 4.9 qualitatively suggests the potential catalyst activity for Cu active sites. It has been established that greater amount of available Cu active sites is an indicator of higher activity. The results in Figure 4.9 are consistent with s-TPR results calculated for sum of Low and High peak adsorption as shown in Figure 4.3. From Section 4.4.3, it was noticed that Sample A has the greatest surface and bulk copper sites and thus potentially the highest activity for H₂ disassociation (bond breaking) on Cu sites is concerned. The hydrogenation of CO for methanol synthesis still depends heavily on amount of Zr and Zn active sites in catalyst samples [8].

4.2 Catalyst Structure and Morphology

4.2.1 Calcination and Phase Analysis by XRD

X-Ray Diffraction analysis was done at a scanning angle range of 2 - 80° and the scanning speed of 1.2°/min. The crystallite types present in the catalysts were identified by comparing the scanning angles and d-spacings of each peak in the resultant curves with the ones existing in the material library. The XRD analysis was conducted through the Bruker D8 Advanced Diffractometer instrument that uses CuK α radiation as its source.

Determining the optimum calcination temperature for catalysts is crucial to ensure the proper removal of salts from the catalysts phase and encourage oxidation on the catalyst surface. To determine the optimum temperature of catalysts oxidation, 4 dried samples of Sample C were calcined at 4 different temperatures, 200,300 350 and 400°C. After calcination these samples were analyzed by means of the XRD instrument to determine metal phases present in the catalyst sample. The resultant phase spectrum is shown in Figure 4.10.

In Figure 4.10, it can be seen that the Optimum Calcination Temperature for complete removal of nitrate and carbonate based salts is at 350°C. This is because a catalyst is not entirely oxidized at Temperatures of 200, 300 and 400°C. This can be

seen from the presence of unwanted peaks of copper azide, $\text{Cu}(\text{N}_3)_2$ at Bragg's angle of 12° . This copper azide peak however is not present for spectrum of catalyst calcined at 350°C .

Temperatures higher than 350°C are not suggested for calcination. This is because at higher temperatures the sintering of metal crystals on catalyst surface due to formation of larger aggregates causes the loss of active Cu metal surface area and hence reduced activity. Thus the optimum calcination Temperature for complete removal of salts and highest available surface area is at 350°C .

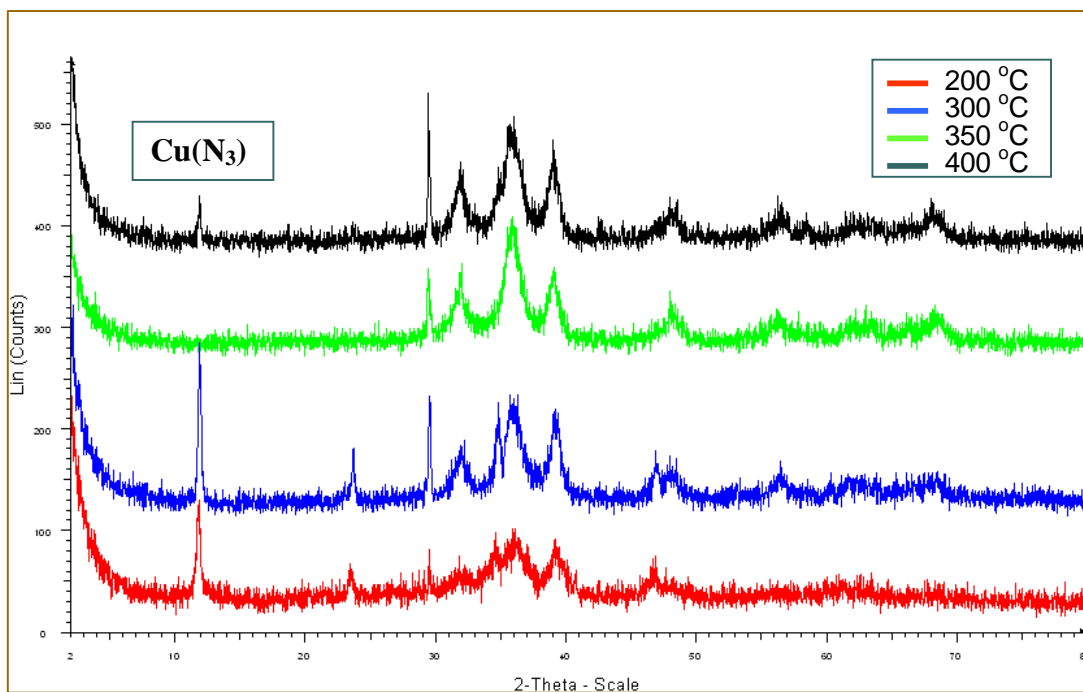


Figure 4.10: XRD Spectrum of 4 samples from Trial C at different calcined Temperatures.

A separate analysis using the XRD was done to study the effect of reactants in formation of the oxide phase in the catalyst. 2 separate sample of catalyst were prepared with the same metal ratio as sample C. One was prepared from ZnO and ZrO₂ as reactants while the other was prepared using $\text{Zn}(\text{NO}_3)_2 \cdot 6\text{H}_2\text{O}$ and $\text{N}_2\text{O}_7\text{Zr} \cdot x\text{H}_2\text{O}$ as reactants. Figure 4.11 of both spectrums after XRD analysis shows that there is no

significant difference in the metal oxide phase formed or its intensity of peaks due to the choice of reactants.

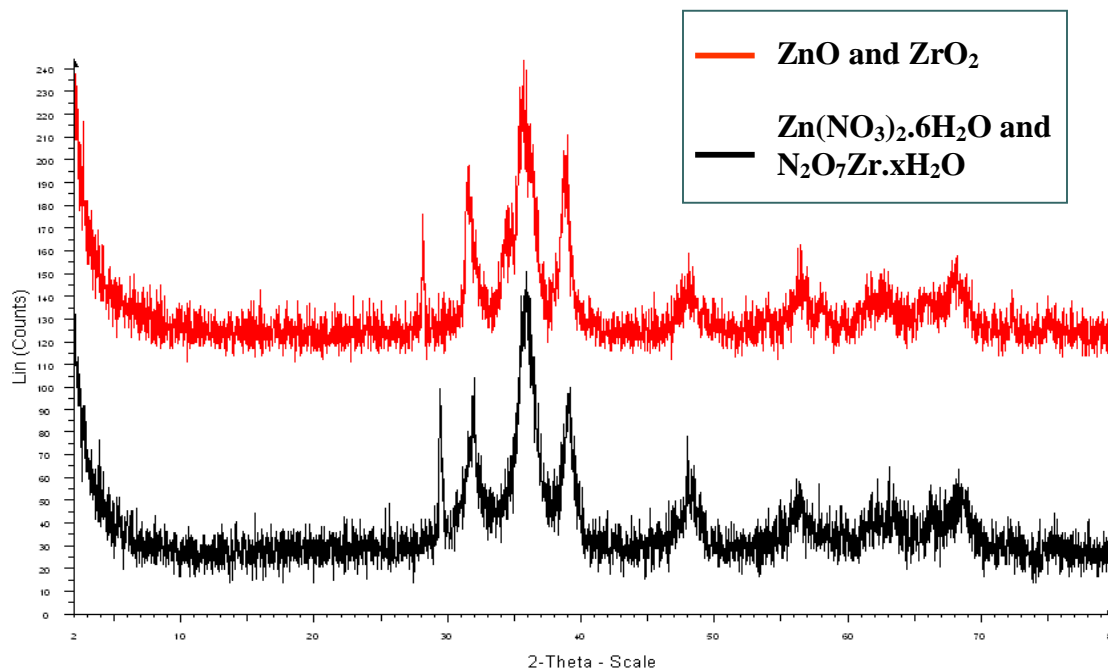


Figure 4.11: XRD spectrum for sample C prepared from two different reactant phases.

Finally, XRD analysis was done on all samples, commercial and prepared to investigate the metal oxide phases and their intensity as corresponding to their compositions. Figure 4.12 shows the spectrum of metal oxides phases formed in each catalyst sample. The actual phase of metal oxide formed is listed in Table 4.3.

In Figure 4.12, the Bragg's angle (2θ) for copper oxide phase is shown at 35.44° and 38.66° , for zinc oxide at 34.33° , for alumina at 32° and finally for zirconium oxide at 25° , 28.5° , 48° , 57° , 67° . Peak heights for all other metal oxides are almost the same except for zirconium oxide at 28.5° . This peak is characteristic for zirconia and as can be seen in Figure 4.12, the height of this peak increases from sample B to F as the amount of Zr in the sample increases.

In Figure 4.12, the used sample is the spent commercial catalysts sample(3 years on line), while fresh sample is an unused catalysts sample. The spectrum in spent sample

is broad and small in comparison to fresh commercial sample. This means the amount of metal phases on surface has reduced after 3 years of catalyst operation. This is probably due to bleeding of metals from catalyst surface into gas stream.

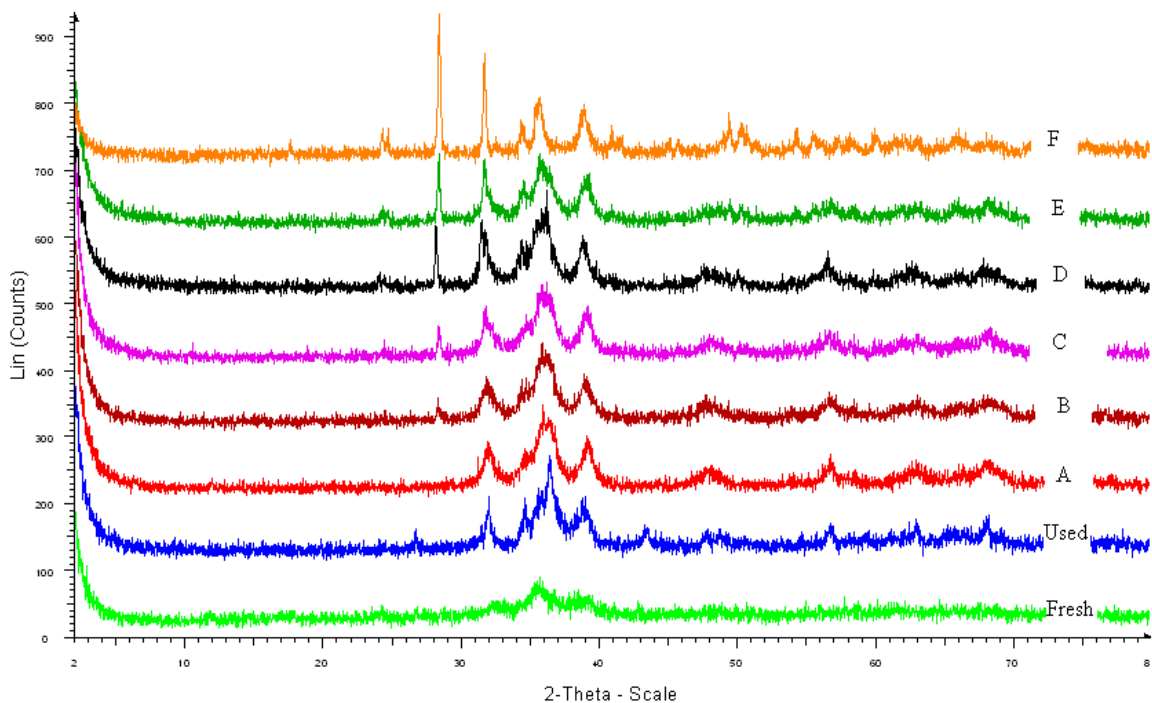


Figure 4.12: Spectrum of metal oxides phases formed in each catalyst sample

Table 4.3 shows the metal oxides phase formed for each catalyst sample in the XRD analysis. As can be seen in Table 4.3, the phase of oxide formed for copper oxide is monoclinic Tenorite and for zinc oxide is hexagonal Zincite. This is true for all catalyst samples containing Cu and Zn. Zirconium oxide phases however differ for different catalyst samples. For Zr containing samples, only sample D and F has monoclinic phases. The rest of the samples have formed hexagonal zirconia. Rhodes *et al* [114] report that formation of monoclinic zirconia is 5 times more active than other forms of zirconia due to increase in CO and CO₂ adsorption capacity. The increase in CO adsorption capacity could mean higher activity influenced by the Zr phase alone. The Zinc phase also has the ability of CO adsorption to produce methanol. Zr and Zn are the sites for hydrogen atoms spillover favorable for the formation of methanol [8].

Table 4.3: Phases of metal oxides formed for each catalyst sample.

Catalyst Series	Sample	Copper Oxide	Zinc Oxide	Alumina	Zirconium Oxide
Cu/ZnO/Al ₂ O ₃	Ind	Tenorite-Monoclinic	Zincite - Hexagonal	α -hexagonal	-
	A	Tenorite-Monoclinic	Zincite - Hexagonal	θ -monoclinic	-
Cu/ZnO/ZrO ₂ /Al ₂ O ₃	B	Tenorite-Monoclinic	Zincite - Hexagonal	θ -monoclinic	hexagonal
	C	Tenorite-Monoclinic	Zincite - Hexagonal	θ -monoclinic	hexagonal
	D	Tenorite-Monoclinic	Zincite - Hexagonal	θ -monoclinic	Baddeleyite-Monoclinic
	E	Tenorite-Monoclinic	Zincite - Hexagonal	θ -monoclinic	hexagonal
Cu/ZrO ₂ /Al ₂ O ₃	F	Tenorite-Monoclinic	-	γ -cubic	monoclinic

In methanol synthesis process, the high Al₂O₃ acidity causes the formation of dimethyl ether as a byproduct. This is because the large Bronstead Acid sites (Al-OH) where hydroxyl sites reside catalyzes methanol to dimethyl ether [82]. Thus, the need for a support which has low acidity and high inertness is very crucial. γ -alumina has high surface area but medium Bronstead acidity. θ -alumina has low acidity and high inertness despite its lower surface area. α -alumina has the lowest surface area and lowest acidity.

Among all of the alumina phases formed in the samples, sample F has the least preferred alumina type as it would increase formation of dimethyl ether as a byproduct. Commercial sample, Ind has the most preferred form of alumina, α -alumina, which is highly stable and least acidic and thus less byproduct such as dimethyl ether (DME) would be formed. All other samples form θ -alumina, which is optimum as it less acidic and has a high surface area for active site anchoring.

4.2.2 Surface Imaging

Field Emission Scanning Electron Microscopy (FeSEM) is a technology used to capture the image of the surface of a solid sample, determine its elemental composition as well determine the distribution of the elements on its surface. The model of the

FeSEM used for analysis was the SUPRA 55VP by Carl Zeiss. Two sets of images were obtained for each sample from the FeSEM detectors, SE1 and SE2. One is a Low resolution image from at 3000X to 5000X magnification while the other was a high resolution image at 20000X magnification. The Low resolution image for each catalyst sample is shown in Figure.4.12a to Figure 4.18a while the High resolution images are shown from Figure 4.12b to Figure 4.18b.

From our pervious particle size analysis in Section 4.14, it was determined that the article size for all catalyst samples was in the nm range i.e. Sample Ind, 14.51nm; Sample A, 13.91nm; Sample B, 17.80nm; Sample C, 27.27nm; Sample D, 16.60nm; Sample E, 20.95nm; Sample F, 34.67nm. The smallest particle size was obtained for catalyst sample A and Ind while the largest particle size was obtained for catalyst Sample F. This should be somewhat qualitatively confirmed through the observation of Low resolution FeSEM images which have a image width range of as low as 200nm.

It can be seen in Figure 4.12a and 4.13a that at Low resolutions the above claim on particle size analyses is justified. Indeed, sample A and Ind have smaller crystal sizes compared to a large agglomerant observed in Figure 4.18a for catalyst sample F. This would very well suggest that activity of Sample A and Ind is higher and thus Cu/ZnO/Al₂O₃ catalyst types has higher activity as far as particle size is concerned is much higher than the Cu/ZrO₂/Al₂O₃.

At Low resolution Images however, there can be clearly seen a set of 2 different particle sizes. One set of particles perhaps as small as 1nm are clearly distributed throughout the surface as shown in Figure 4.12b to 4.17b. The larger particles sizes in those Figures however are as large as a few μm . This shows that the particle sizes calculated from the s-TPR analysis in Section 4.14 are an average of those two particle size extremes. For Sample F however it can be seen in Figure 4.18b that the smaller crystal particles are not available and would explain the large average particle size obtained fro Sample F in Section 4.14. Also, the fractal-cylindrical-like structures seen in the top left of Figure 4.18b suggests the particle types in that Cu/ZrO₂/Al₂O₃ sample is cylindrical compared to the spherical-like structures obtained in all another catalysts samples.

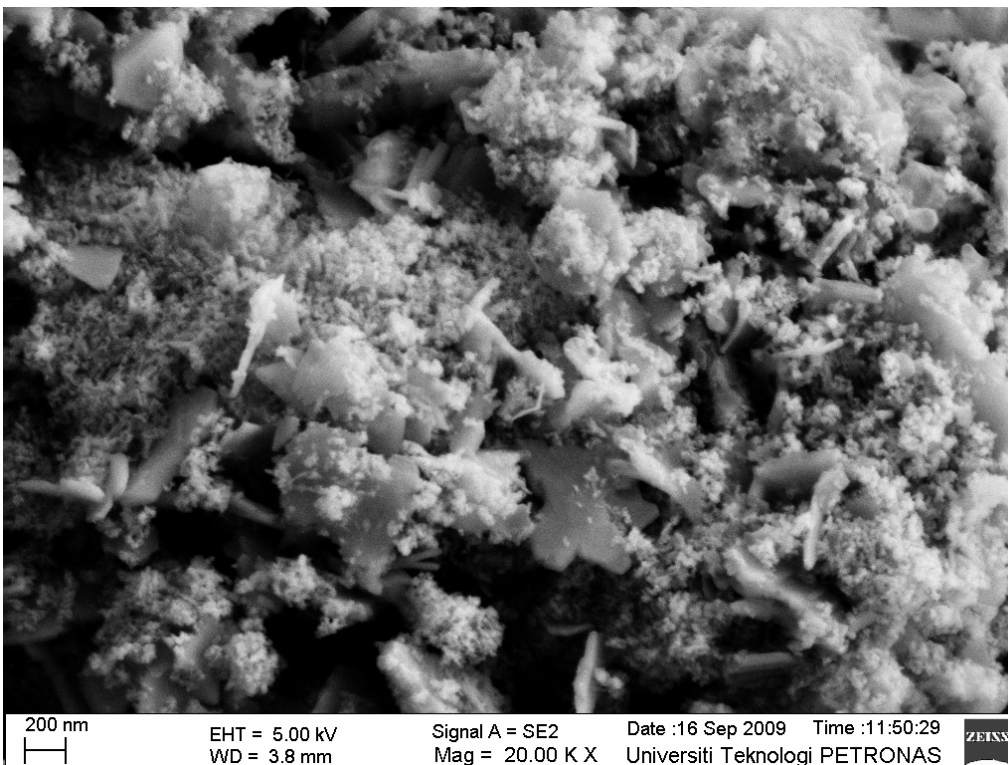
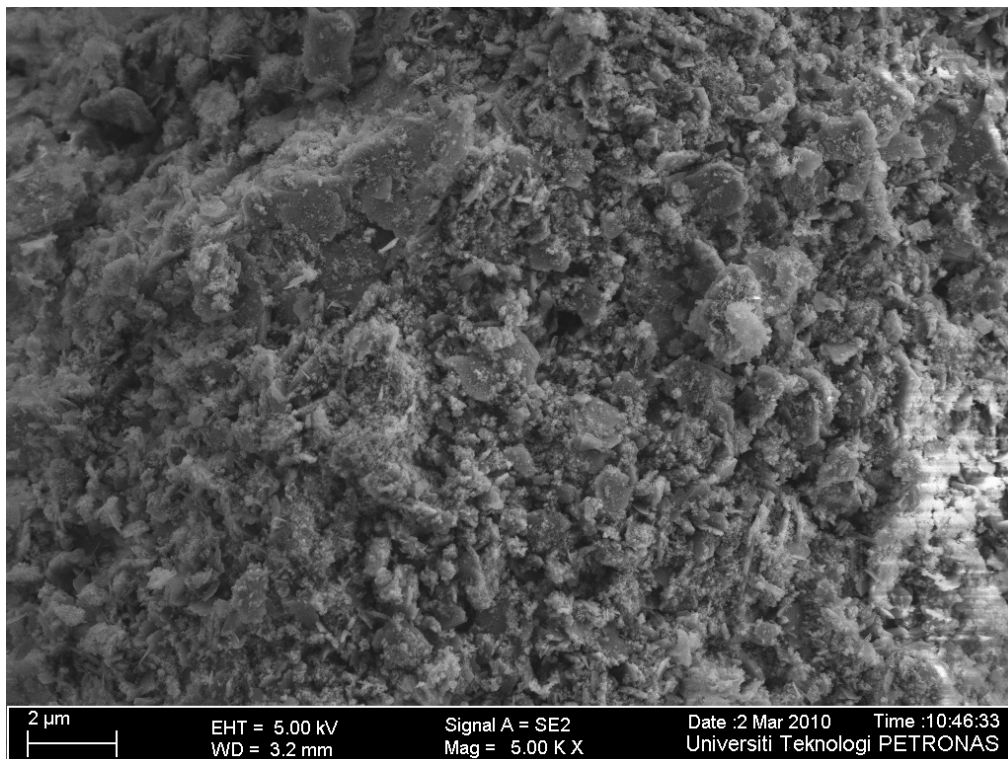


Figure 4.12a and b: (a) (TOP) Low resolution Image at 3KX of commercial catalyst sample, Ind.
 (b) (BOTTOM) High resolution Image at 20KX of commercial catalyst sample, Ind.

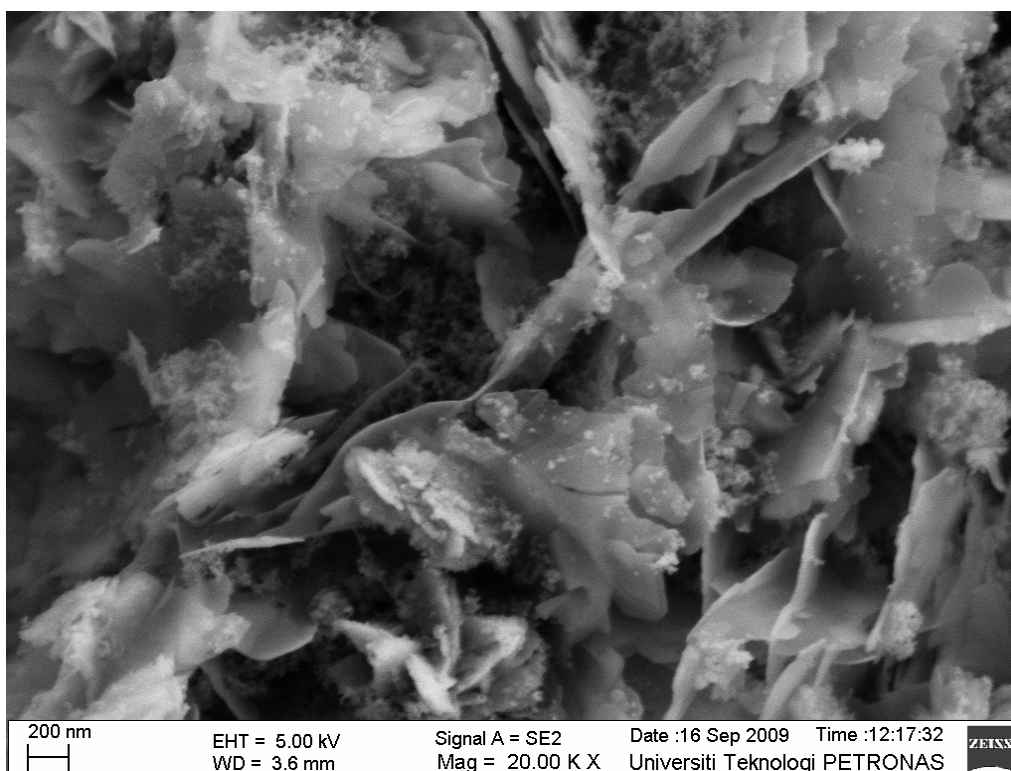
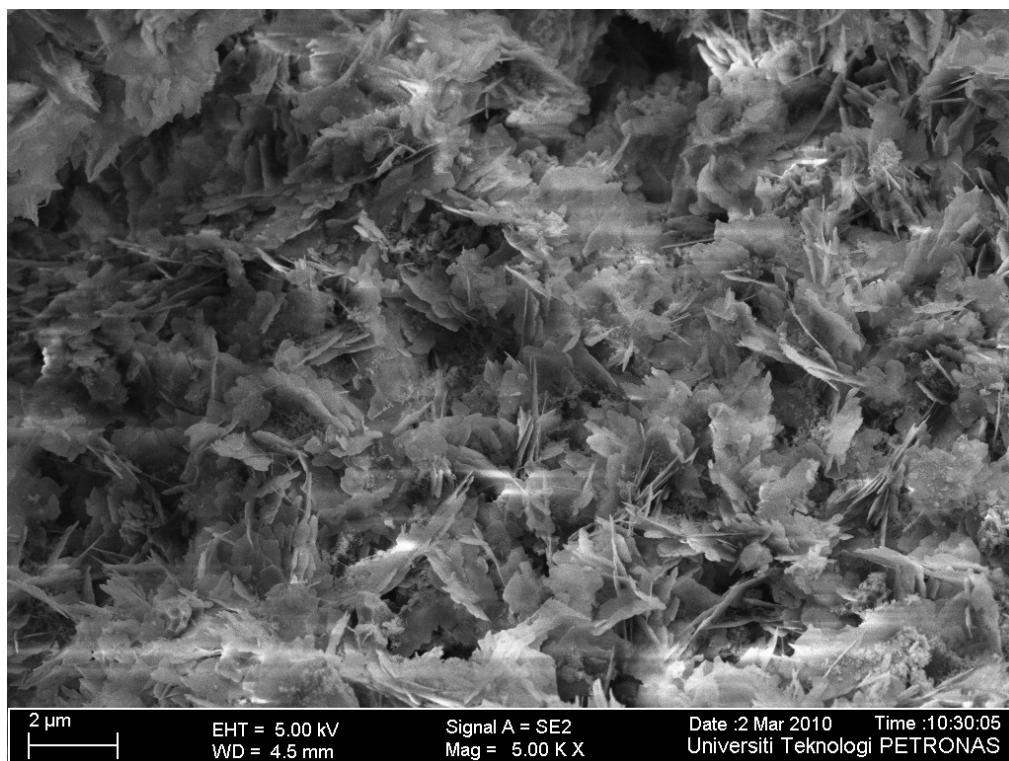


Figure 4.13a and b: (a) (TOP) Low resolution Image at 5KX of prepared catalyst sample A.
(b) (BOTTOM) High resolution Image at 20KX of prepared catalyst sample A.

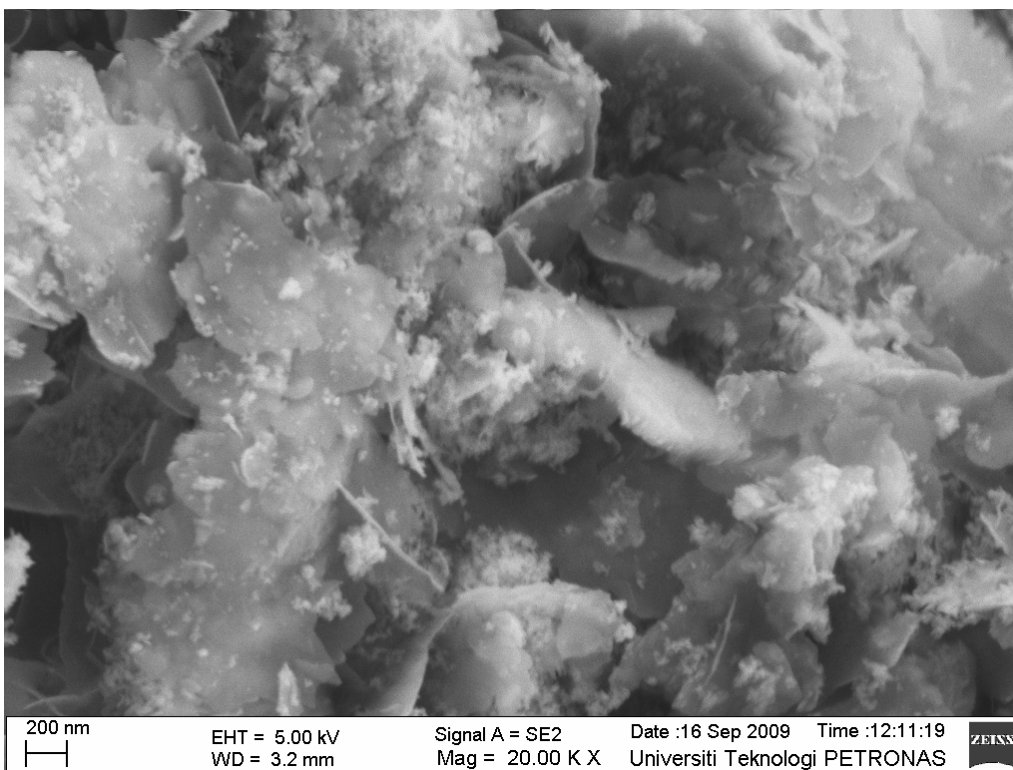
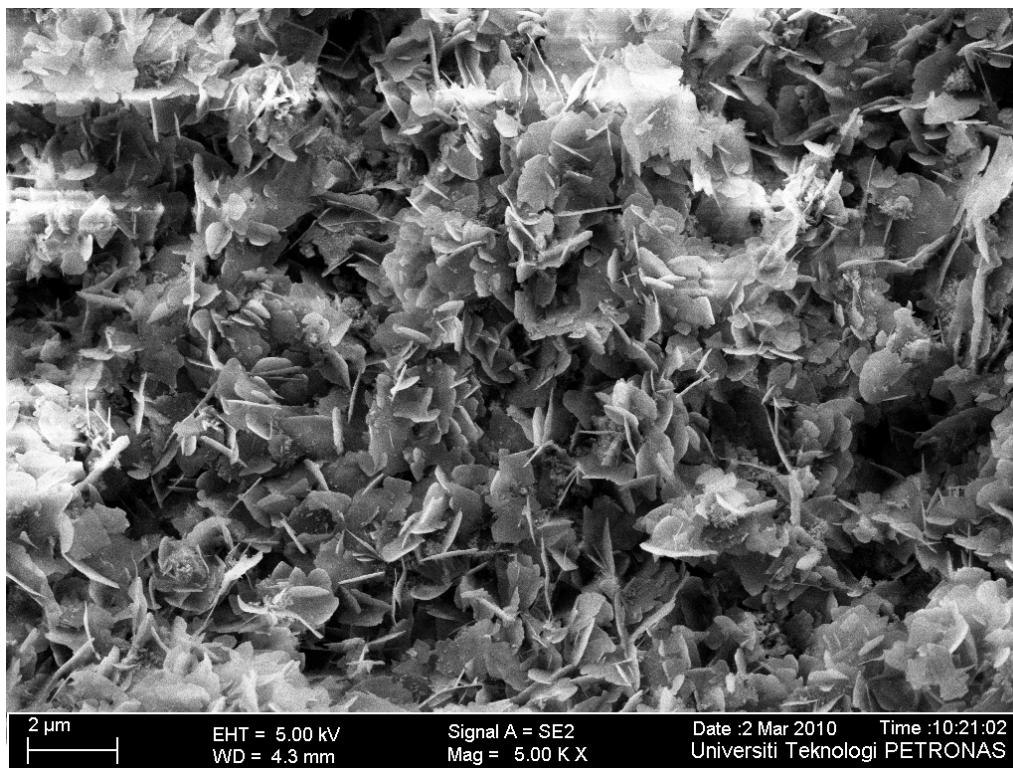


Figure 4.14a and b: (a) (TOP) Low resolution Image at 5KX of prepared catalyst sample B.
(b) (BOTTOM) High resolution Image at 20KX of prepared catalyst sample B.

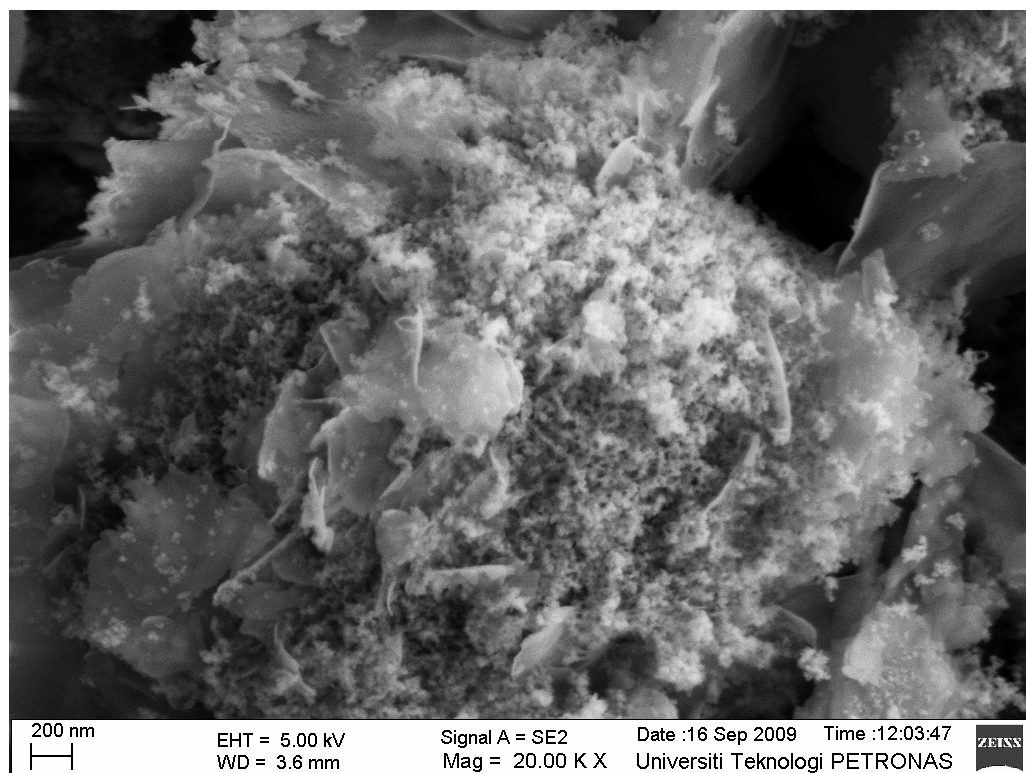
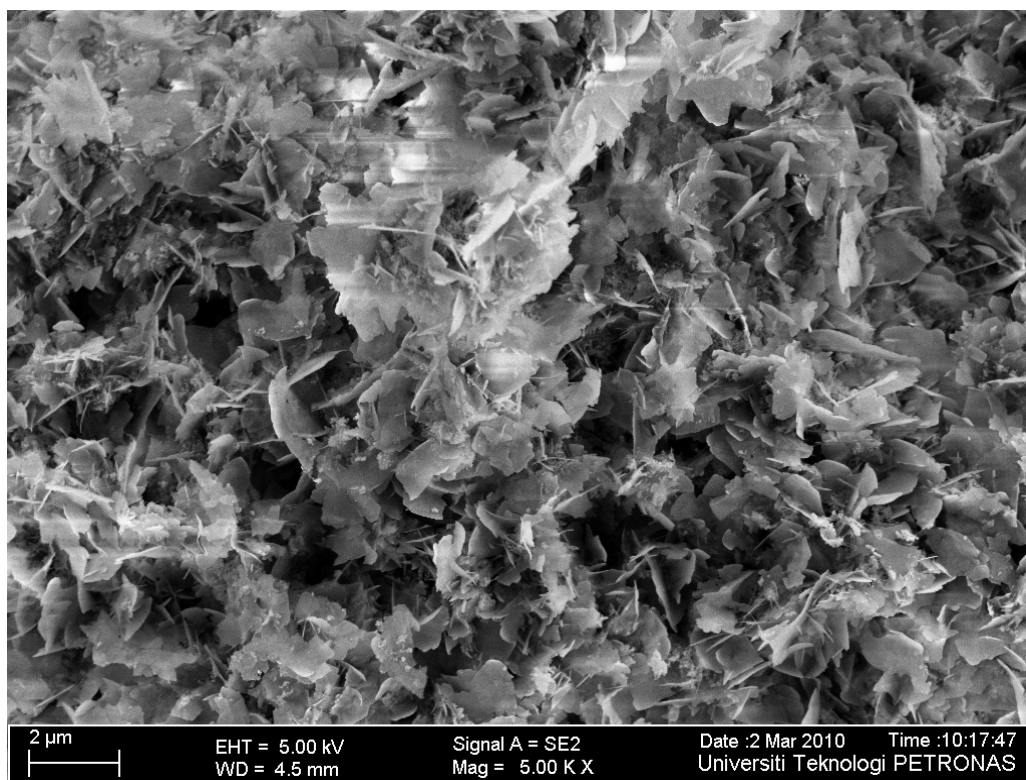


Figure 4.15a and b: (a) (TOP) Low resolution Image at 5KX of prepared catalyst sample C.
(b) (BOTTOM) High resolution Image at 20KX of prepared catalyst sample C.

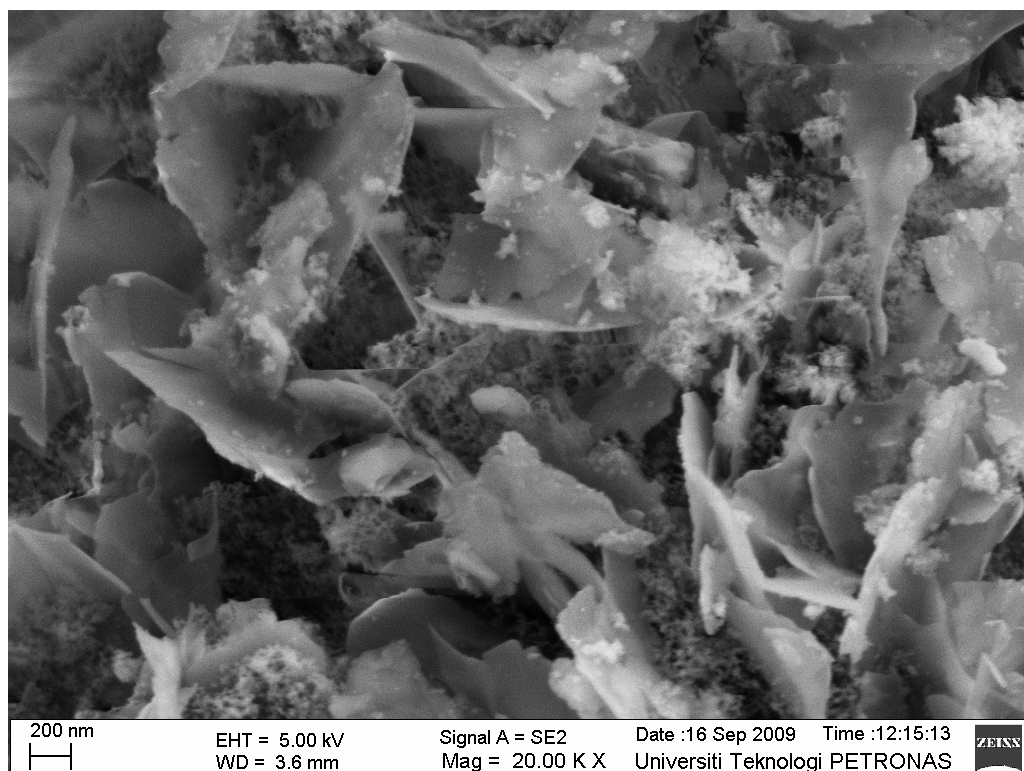
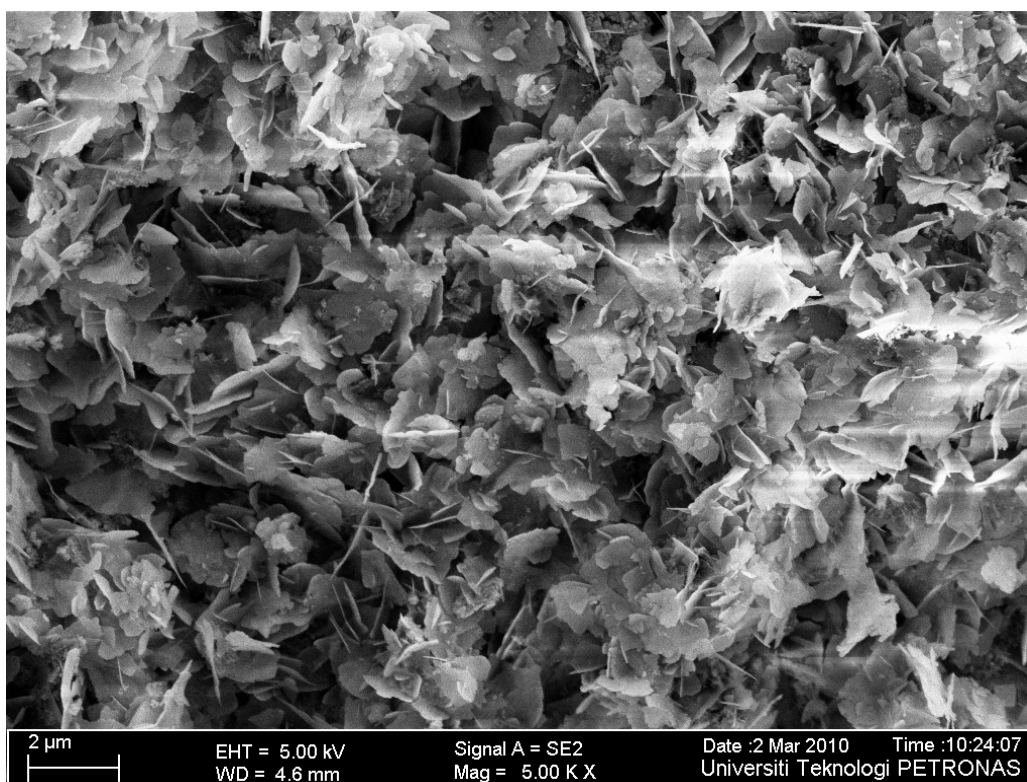


Figure 4.16a and b: (a) (TOP) Low resolution Image at 5KX of prepared catalyst sample D.
(b) (BOTTOM) High resolution Image at 20KX of prepared catalyst sample D.

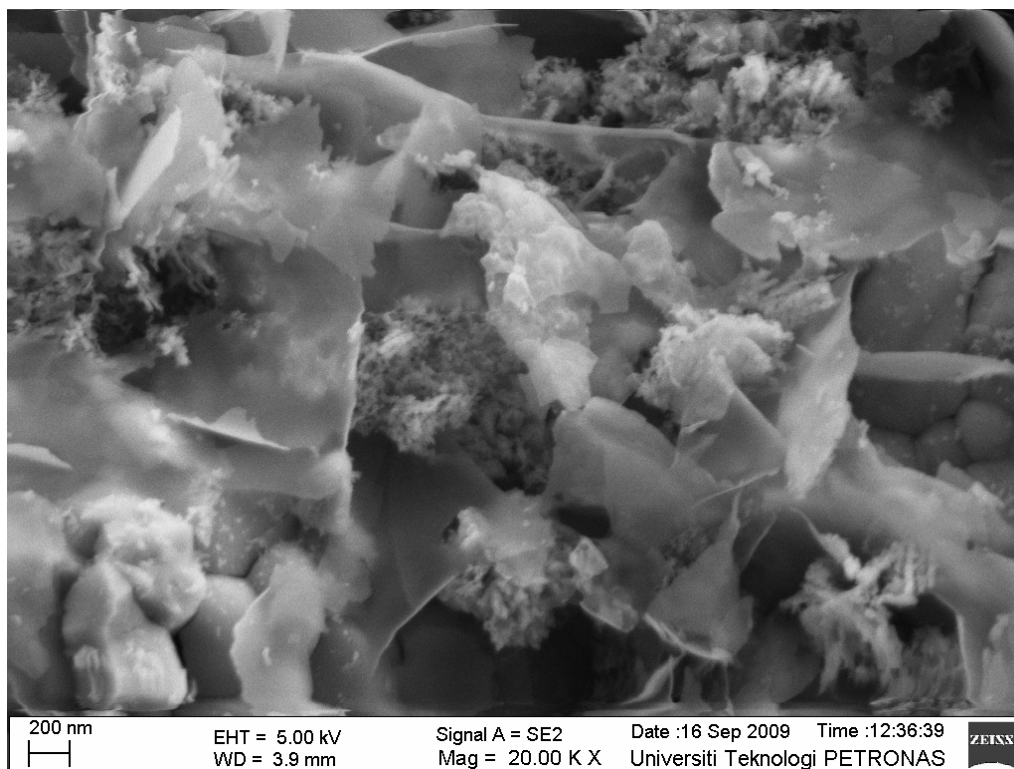
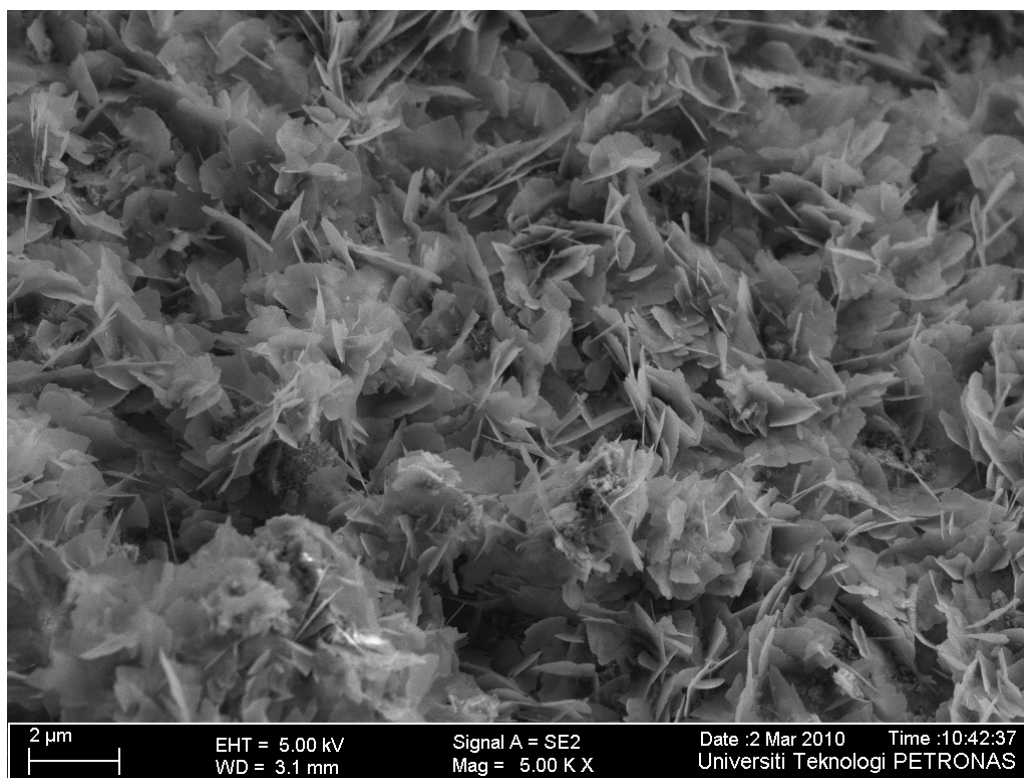


Figure 4.17a and b: (a) (TOP) Low resolution Image at 5KX of prepared catalyst sample E.
(b) (BOTTOM) High resolution Image at 20KX of prepared catalyst sample E.

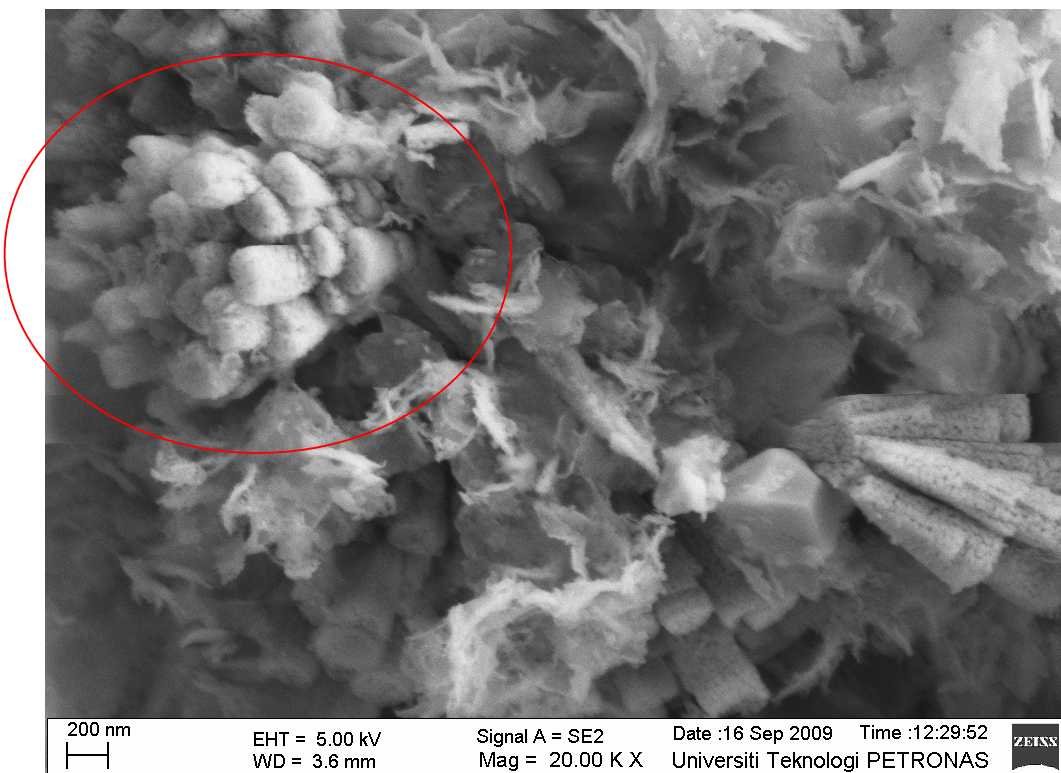
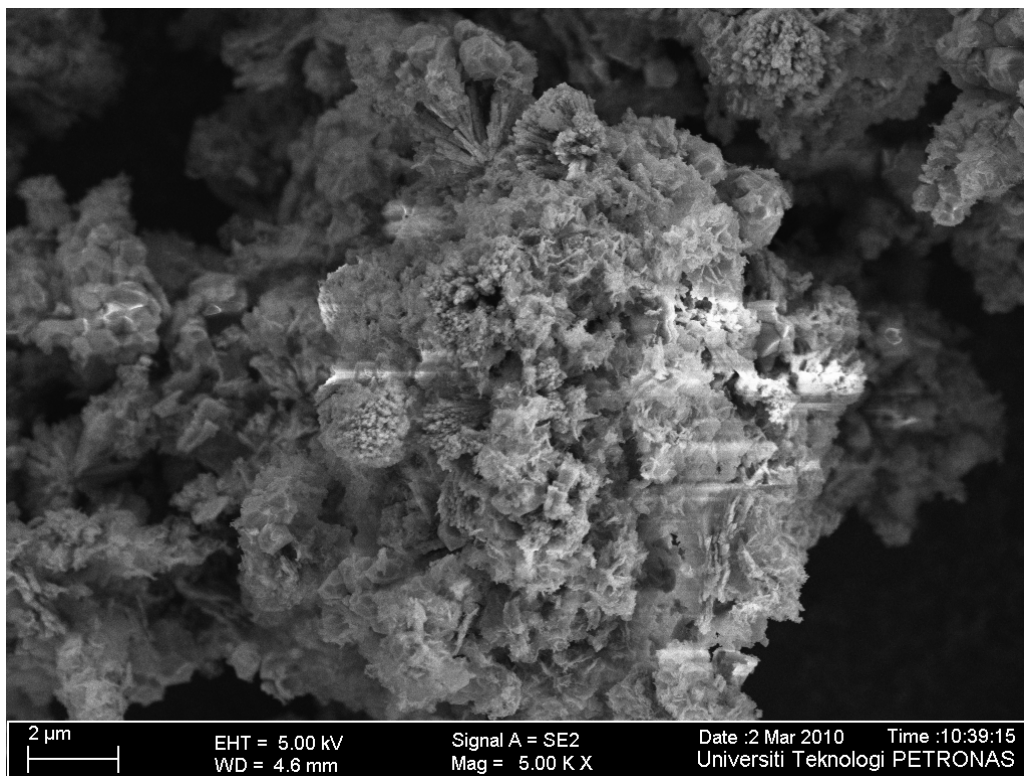


Figure 4.18a and b: (a) (TOP) Low resolution Image at 5KX of prepared catalyst sample F.
(b) (BOTTOM) High resolution Image at 20KX of prepared catalyst sample F.

4.2.3 Elemental Composition Analysis by EDX

Elemental composition of the sample at its surface is obtained by X-Ray Energy Dispersive Analysis (EDX) analysis. X-rays are released by the sample surface after electron bombardment and each element releases x-rays of a particular energy (keV). EDX was conducted on an image of width 6 μ m. Table 4.4 shows the calculated metal atomic compositions as well as Calculated and SEM-EDX metal ratios of commercial and prepared catalyst samples.

Table 4.4: Calculated metal atomic compositions & Calculated and SEM-EDX metal ratios of commercial and prepared catalyst samples.

Sample	Calculated Atomic Composition (%)				Atomic Ratios			
					Calculated		FESEM-EDX	
	Cu	Zn	Al	Zr	Zn/Cu	Zr/Cu	Zn/Cu	Zr/Cu
Ind ^a	52.66	34.37	12.98	0	-	-	0.65	0
A	42.86	47.62	9.52	0	1.11	0	1.21	0
B	42.06	46.73	9.35	1.87	1.11	0.04	1.25	0
C	40.91	45.45	9.09	4.55	1.11	0.11	1.1	0.14
D	39.82	44.25	8.85	7.08	1.11	0.18	1.23	0.14
E	40.91	36.36	9.09	13.64	0.89	0.33	1	0.23
F	42.86	0	9.52	47.62	0	1.11	0	0.47

^a Composition of Fresh and Spent Industrial Catalyst from SEM-EDX analysis.

Only metal compositions are taken into account during theoretical calculations while oxygen, carbon and nitrogen are considered together with metals in an EDX detected composition. Thus, Zn/Cu and Zr/Cu metal ratios are used to compare calculated and experimental properties. Table 4.4 shows the calculated atomic ratios as well as the comparison between calculated and experimental EDX atomic Zn/Cu and Zr/Cu metal ratios for all catalyst samples. It can be seen in the Atomic Ratio columns

that the ratios of Zn/Cu and Zr/Cu, both theoretical and experimental are in good agreement. For commercial catalyst sample, Ind, only EDX metal ratios are available.

From Table 4.4, it can be seen that the atomic metal ratios obtained from EDX analysis are greater than the calculated atomic Zn/Cu ratios. Since EDX gives a composition of metals on catalyst surface only, it very well means that more Zn is present on catalyst surface than on the subsurface of the catalyst samples. However, the case is reversed for Zr. It seems that the calculated Zr/Cu ratio is higher than the EDX values. This means that less Zr is present on catalyst sample than below it.

4.3 Catalyst Activity Study

Catalyst activity was studied in a catalytic micro tubular reactor as described in Section 3.4 and 3.5. The 30% CO/70% H₂ mix gas was flowed from the top of the reactor through the catalyst bed and the effluent gas was channeled into a Gas Chromatograph (GC) to analyze the composition of the reaction products. Two key properties are used as gauges for comparison of catalyst activity for all catalyst samples with variant metal compositions as displayed in Table 4.4. They are CO Conversion and Methanol Selectivity.

CO conversion X_{CO} , on the other hand was defined as change in CO concentration over initial CO concentration and catalyst mass at any given time during the reaction. Methanol selectivity S_{MeOH} was defined as concentration in mol% of methanol in the product gas over total concentration of all other products $\sum (n_x)^f$ in the product gas. The Selectivity, S_x of all other products was defined as mol% of product, n_x in the product gas over total concentration of all other products. Effluent gas concentrations were measured by the GC at every 15 minutes interval although Methanol Selectivity and CO conversion for each catalyst sample was calculated for every 30 minutes for a run time of 3.5 hours.

$$X_{CO} = \frac{(n_{CO})^i - (n_{CO})^f}{(n_{CO})^i \times g_{cat}} \times 100\% \quad 4.1$$

$$S_{MeOH} = \frac{(n_{MeOH})^f}{\sum (n_x)^f} \times 100\% \quad 4.2$$

$$S_x = \frac{(n_x)^f}{\sum (n_x)^f} \times 100\% \quad 4.3$$

The concentration of reactant gas was evaluated in the GC prior to the reaction for a number of times and the average concentration of the mixture gas was 29.98mol% CO and 70.1 mol% H₂. The gas mixture was flowed in to the reactor system at a flow rate of 210ml/min and catalyst bed temperature was maintained at 250°C and Pressure at 30 bars. In the reactor, catalysts mass for all samples was fixed at 1g.

4.3.1 Analysis of CO conversion

In the methanol synthesis reaction, CO conversion is a primary indicator of catalyst activity as CO is the limiting reactant. The amount of H₂ in syngas mixture is excess in industrial settings. This is because the conventional reaction to produce syngas from natural gas by steam reforming has a stoichiometric ratio of H₂ to CO of 3:1 as shown in equation 4.4. This syngas mixture is then directly injected into the methanol synthesis reactor for catalytic conversion to methanol.



CO conversion into methanol is defined by Equation 4.1. The CO conversion of catalyst samples are shown in Figure 4.19 and Figure 4.20. Table 4.4 lists the composition of metals (Cu, Zn, Zr, Al) in each catalyst sample. Figure 4.19 shows the

CO conversion comparison between 4 catalyst samples of type $\text{Cu/ZnO/ZrO}_2/\text{Al}_2\text{O}_3$ with varying composition of Zr and Zn at time interval of 30 minute over 3.5 hours of time on stream. Sample B, C and D has Zn/Cu ratio of 1.11 while sample E has Zn/Cu ratio of 0.89. As for Zr/Cu ratio, CO conversion increases from sample B to E .The Zr/Cu ratio is 0.04 for Sample B, 0.11 for Sample C, 0.18 for Sample D and 0.33 for Sample E.

It can be clearly seen from Figure 4.19 that the highest CO conversion among $\text{Cu/ZnO/ZrO}_2/\text{Al}_2\text{O}_3$ catalyst sample series is obtained for Sample D. Although the conversion rate changes throughout the period of study, it is still within the range of 2.5 to 3.5%. Sample B and C have extremely low CO conversion rates of 0.2 to 1.2 %.

This paints a very interesting point in the picture regarding the role of Zn and Zr in catalyst activity. It explores a unique combination of both Zn and Zr in the process of achieving maximum activity. Sample B and C have low Zr amount although high Zn but with low activity. Sample E however, has high Zr/Cu ratio of 0.33% but lower Zn/Cu ratio at 0.89%. Sample D has higher Zn/Cu ratio of 1.1% compared to sample E but with lower Zr/Cu ratio of 0.18%. Since Sample D has higher activity than Sample E, it shows that Zn has precedence over Zr in order of importance of metals that increase catalyst activity, i.e. facilitate the CO hydrogenation process on its surface.

Figure 4.20 on the other hand, shows the CO conversion at 30 minutes interval over a period of 3.5 hours of 3 different catalyst type representatives and Commercial catalyst as control. Commercial sample, Ind is of $\text{Cu/ZnO}/\text{Al}_2\text{O}_3$ type, Sample A is of $\text{Cu/ZnO}/\text{Al}_2\text{O}_3$ type, Sample D is of $\text{Cu/ZnO/ZrO}_2/\text{Al}_2\text{O}_3$ type and Sample F is of $\text{Cu/ZrO}_2/\text{Al}_2\text{O}_3$ type.

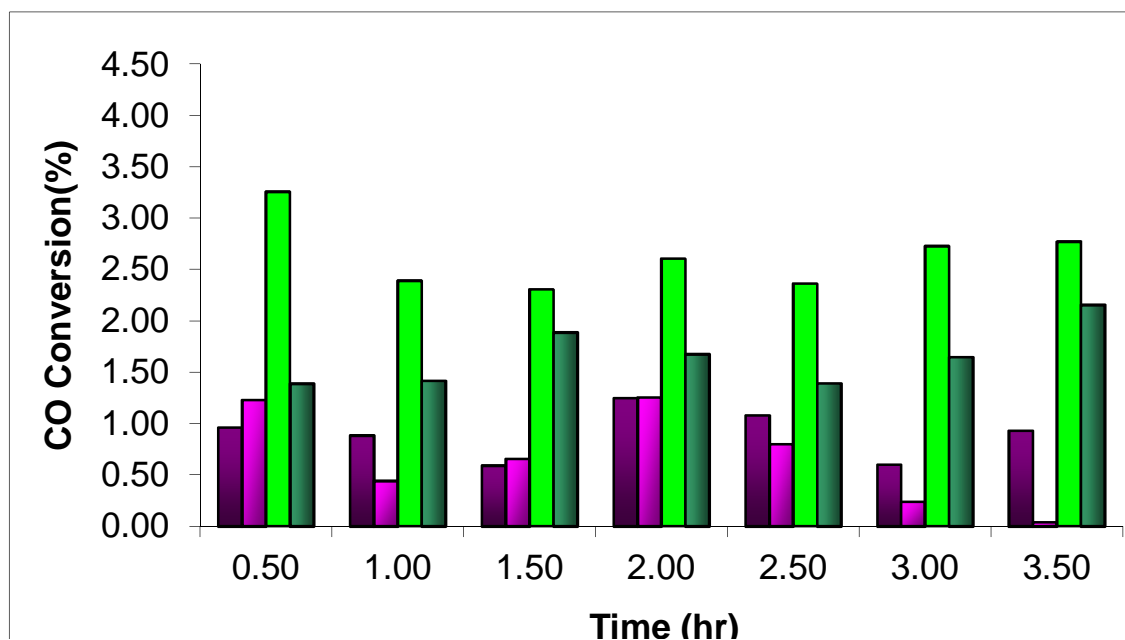


Figure 4.19: CO conversions in % for all Cu/ZnO/ZrO₂/Al₂O₃ type catalysts sample B, C, D and E.

From Figure 4.20 it can be seen that Sample A has the highest CO conversion up to 4% followed closely by Sample D up to 3.26%. Commercial Sample, Ind has very low CO conversion in the range of 0.3 to 0.75 % and Sample F which has no Zn in it has low activity as well in the range of 0.5 to 1.0%. For commercial sample Ind, its low activity is justified as it has very low Zn/Cu ratio of 0.65 as shown by the EDX study in Table 4.4. This low amount of Zn would most definitely limit the CO hydrogenation capacity of the catalyst.

Sample F contains a Zr/Cu ratio of 1.11 in contrast to Sample A which contains a Cu/Zn ratio of 1.11. However the low activity of Sample F and the very high activity of Sample A indicate strongly the previously stated notion of Zn being able to hydrogenate CO more effectively than Zr and hence increase metal activity.

Sample D and A however show a unique set of CO conversion rates at time on stream of 3.5 hours . For the first 2 hours the CO conversion of Sample D is much higher than Sample A, but after that, the CO conversion of Sample A increased

especially towards the last ½ hour of the study. This could be due to the effect of hysteresis in Sample D which is not so obvious in Sample A. Hysteresis happens when after a period of adsorptions of gas on catalyst surface and the formation of multilayer of adsorbed molecules on the catalyst surface occurs. This hinders the motion of the desorbed product gas away from the surface of the catalyst and thus impedes the reaction rate. This effect is more common on Zr surface than it is on Zn surface. This is because as the rate conversion of CO on catalyst Sample A increases steadily, the rate of conversion on the catalyst Sample D decreases until it reaches steady state.

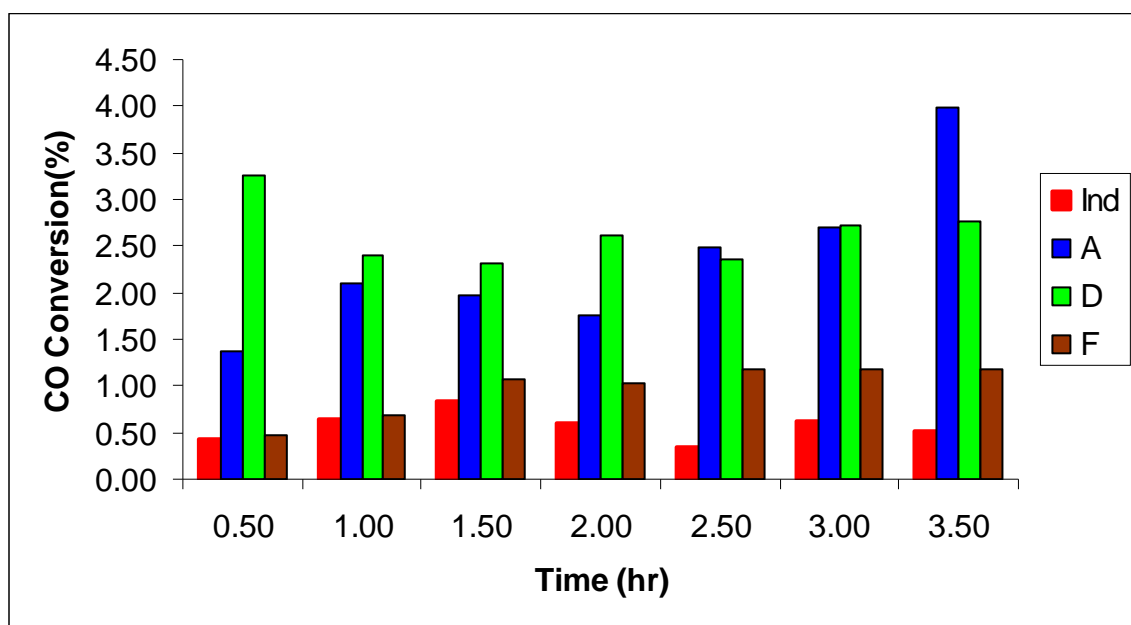


Figure 4.20: CO conversions in % for commercial catalyst samples Ind and prepared catalyst samples A, D and F.

The conversion rate per pass of CO in a methanol synthesis process has been reported to be around 0.8% for industrial type Cu/ZnO/Al₂O₃ catalysts at pressure 50 bar and temperature 224°C [21]. This is consistent with the CO conversion obtained which is in the range of 0.35%-0.84% for the Ind catalyst sample as shown in Figure 4.20 above. This highlights the low conversion rate per pass on current industrial scale and the potential of the prepared sample A and D to improve the methanol synthesis process.

4.3.2 Analysis of MeOH Yield

The Methanol synthesis process through syngas route is outlined in Equation 2.1 to 2.4 (Section 2.1.1). The reactant gas which contains only H₂/CO mixture hypothetically produces Methanol with the stoichiometric MeOH/CO ratio of 1:1 as shown in Equation 2.3. However, this is not the case generally observed. Klier et al proposed that the water gas shift (Equation 2.1) will occur in the forward direction for low CO₂ feed concentration to convert CO to CO₂ and thus encourage the hydrogenation of methanol as outlined in Equation 2.2 [13]. This reaction would also give a stoichiometric MeOH/CO ratio of 1:1. The stoichiometric ratio of CO /H₂ is 1:2 in either route. In our reaction, the molar ratio of CO/H₂ was set to 3:7. This was done so as to provide excess H₂ in the reaction. This precaution is crucial in order to discourage the Boudouard reaction (Equation 2.4) from occurring. This reaction involves the direct conversion of CO to CO₂ and C and is a major source of catalyst deactivation as carbon clogs the catalyst pore and reduces active metal surface area. The presence of excess H₂ would discourage the formation of carbon and encourage the route in Equation 2.1 for CO instead of Equation 2.4.

As the stoichiometric ratio for CO conversion is 1:19 (Equation 2.3), MeOH yield is thus defined as mol MeOH produced in effluent gas over mol CO in reactant gas as shown in Equation 4.5.

$$Y_{CH_3OH} = \frac{(n_{CH_3OH})^f}{(n_{CO})^i} \times 100\% \quad 4.5$$

Figure 4.21 is a plot of calculated MeOH yield (%) for commercial catalyst samples, Ind and prepared catalyst samples A to F at time interval of 30 minutes at time on stream of 3.5 hours. From Figure 4.21, it can be clearly seen that from the beginning of the reaction until 1.5 hours of study, MeOH yield by all catalyst samples increases until reaching steady state.

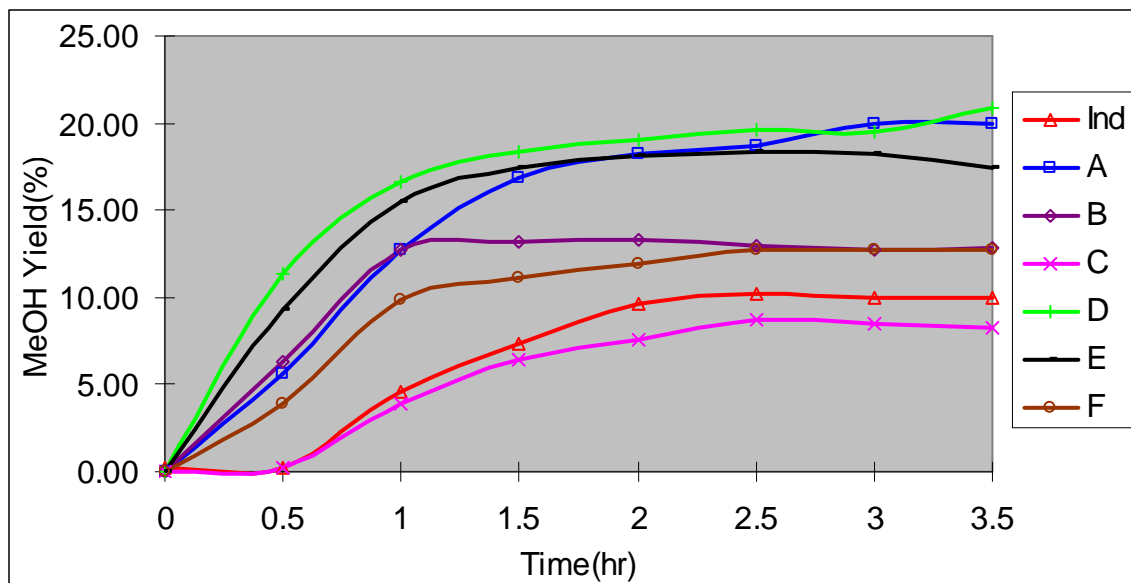


Figure 4.21: MeOH Yield in % for commercial catalyst samples, Ind and prepared catalyst samples A to F.

This phenomenon is explained as modification of metal oxide surfaces into a form of Cu/Zn and/or Cu/Zr metal alloy which work in tandem with each other to break the H₂ bond into H atoms and simultaneously hydrogenate hydrated CO into subsequent species before methanol is formed [115]. This surface modification usually requires time before an optimum metal-chemical structure is obtained and an equilibrium steady state MeOH yield is achieved.

Sample B, D and E reach steady state quickly at around 1 hr reaction time suggesting that the combination of Cu/Zn and Cu/Zr alloys evolve faster to reach equilibrium chemical state as compared to Cu/Zn species by itself in sample Ind and Cu/Zr alone in sample F which reach steady state MeOH yield at around 2.5 hours of reaction time.

Figure 4.22 shows the steady state MeOH Yield comparison between 4 catalyst samples (B, C, D, and E) of type Cu/ZnO/ZrO₂/Al₂O₃ series type with varying composition of Zr and Zn at hour 3.5 of time on stream. At this point, methanol yields

by all catalyst samples have somewhat stabilized. It can be seen clearly that the highest MeOH yield among this catalyst type is given by catalyst sample D followed closely by sample E and finally by sample B and C. This trend of MeOH yield complements the CO conversion given in Figure 4.19. This enforces the prior notion as in Section 4.3.1 that the catalyst activity is strongly dependent on both Zn and Zr composition. Zn composition has precedence over Zr in order of importance of metals that increase catalyst activity, i.e. Zn facilitate the CO hydrogenation process on its surface faster than Zr.

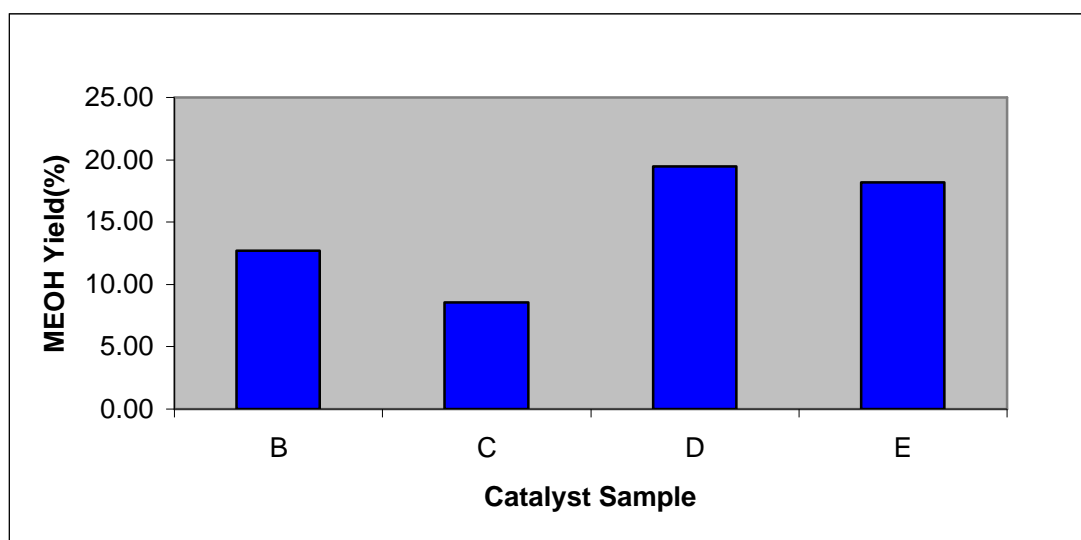


Figure 4.22: Steady state MeOH Yield in % for all Cu/ZnO/ZrO₂/Al₂O₃ type catalysts sample B, C, D and E.

The MeOH yield in Cu/ZnO/ZrO₂/Al₂O₃ series type catalyst samples can also be affected by the phase of metal Zr formed in the catalyst. As can be seen in Table 4.4, Sample D has formed the Zr of monoclinic type while sample B, C and E have formed tetragonal Zirconia. It has been reported that the CO and CO₂ adsorption capacity in monoclinic zirconia is greater leading to an activity 5 times greater than in other forms of zirconia [114]. This explains the high MeOH yield in Sample D and lower in other Cu/ZnO/ZrO₂/Al₂O₃ catalyst series types.

Figure 4.23 however, shows the steady state MeOH Yield at hour 3.5 time on stream for 3 different types of catalysts prepared. Commercial catalyst Ind functions as control. MeOH yield by given by catalyst sample A and D are much higher (20%) as compared to a lower yield given by sample F (12.78%) and finally the lowest yield given by commercial catalyst sample, Ind (10%). This trend is also similar in nature to the CO conversion trend by these samples given in Figure 4.20.

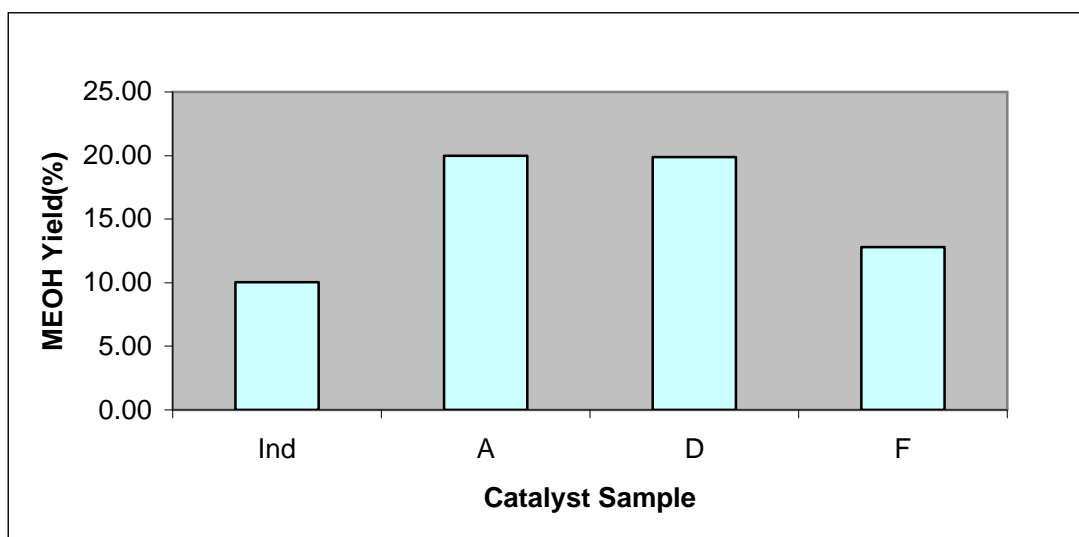


Figure 4.23: Steady state MeOH Yield in % for commercial catalyst samples Ind and prepared catalyst samples A, D and F.

4.3.3 Analysis of MeOH Selectivity

MeOH selectivity is a measure of the composition of methanol (in mol %) present in the product gas divided by the amount of all considered compounds (in mol %) in the product gas (Equation 4.2). Conventional byproducts of the methanol synthesis reaction by Cu/Zn and Cu/Zr based catalysts are higher alcohols, dimethyl ether, methyl formate, ketones, and aldehydes as well as various paraffinic hydrocarbons. However all these products are often present in small amounts especially hydrocarbons which are present in amounts of less than 5000 ppmwt. Water is also produced in a CO₂ free syngas feed but usually below the limits of detection of the Thermal Conductivity Detector (TCD) [116].

In the wake of limitations, the compounds in the product gas that were calibrated in the Gas Chromatograph (GC) and analyzed in this MeOH synthesis study were Methanol (CH₃OH), Ethanol (C₂H₅OH), Dimethyl Ether (CH₃OCH₃), Methyl Formate (HCOOCH₃), Methane (CH₄), Carbon Dioxide (CO₂), Water (H₂O) as well the unreacted Carbon Monoxide (CO) and Hydrogen (H₂). $\sum (n_x)^f$ in Equation 4.2 refers to the sum of all these compounds.

Figure 4.24 shows the MeOH Selectivity comparison between 4 catalyst samples (B, C, D, and E) of type Cu/ZnO/ZrO₂/Al₂O₃ with variant composition of Zr and Zn over a period of 3.5 hours of time on stream and 30 minutes of interval study. It can be seen that selectivity of MeOH is well above all other byproducts (95%) after 3.5 hours of time on stream for all samples of the Cu/ZnO/ZrO₂/Al₂O₃ type except for sample B as can be seen in Figure 4.24. For sample B, the MeOH selectivity which is extremely high in the beginning drops and finally reaches an optimum amount at 3.5 hours time on stream.

All samples of the Cu/ZnO/ZrO₂/Al₂O₃ type reach optimum selectivity of MeOH above 95% at hour 3.5 of time on stream. This is consistent with the MeOH Yield progress as shown in Figure 4.21 and most likely due to the surface modifications to form bimetal Cu-Zn and Cu-Zr alloy properties over time which produces the optimum amount of MeOH as discussed in Section 4.3.2.

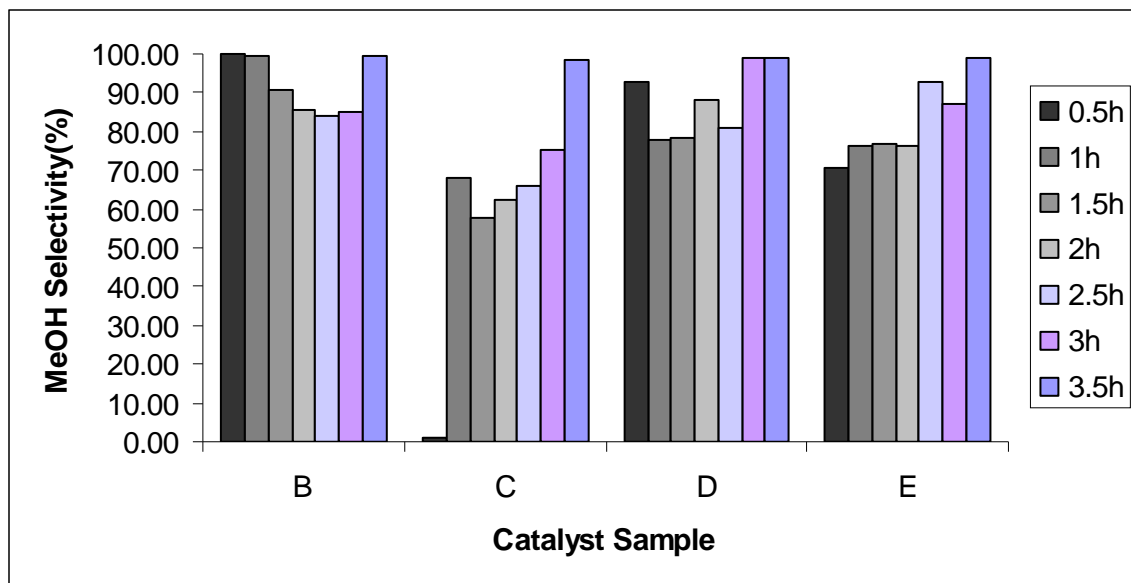


Figure 4.24: MeOH Selectivity in % for all Cu/ZnO/ZrO₂/Al₂O₃ type catalysts sample B, C, D and E.

Figure 4.25 however, shows the MeOH Selectivity comparison for 3.5 hours and 30 minutes interval for 3 different catalyst type representatives and Commercial catalyst as control, i.e. Commercial sample, Ind of Cu/ZnO/Al₂O₃ type, Sample A of Cu/ZnO/Al₂O₃ type, Sample D of Cu/ZnO/ZrO₂/Al₂O₃ series type and Sample F of Cu/ZrO₂/Al₂O₃ type. A similar trend of increasing MeOH selectivity can be seen over the period of 3.5 hour study in all catalyst types and is shown in Figure 4.25. Sample F however reaches optimum MeOH Selectivity at the first hour of the reaction study. The same reasons involving surface modifications of Cu-Zn and Cu-Zr are responsible for this methanol selectivity curve.

Figure 4.26 shows the steady state MeOH selectivity of all catalyst samples at end of 3.5 hours of time on stream. This is termed the optimum amount for selectivity of MeOH given by that particular catalyst sample and thus can be used to gauge individual performance. The types of products given by a catalyst sample are largely dependence on the composition of active metals as well as the morphology of the catalyst species. The Cu metal surface area and consequently the size of Cu aggregates have been stated

as a primary factor in dictating the activity and selectivity of the catalyst species [117-118]. It can be seen that the optimum MeOH selectivity trend as shown in Figure 4.24 is almost identical to the Total Cu Surface Area ($\text{m}^2/\text{g}_{\text{cat}}$) of the catalyst samples in Figure 4.4.

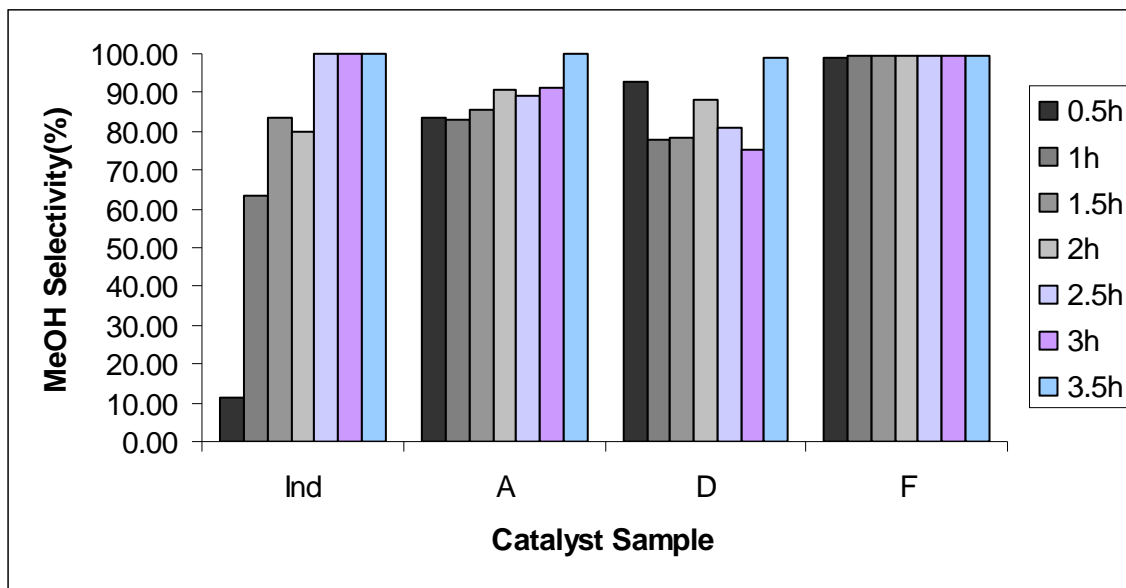


Figure 4.25: MeOH Selectivity in % for commercial catalyst samples Ind and prepared catalyst samples A, D and F.

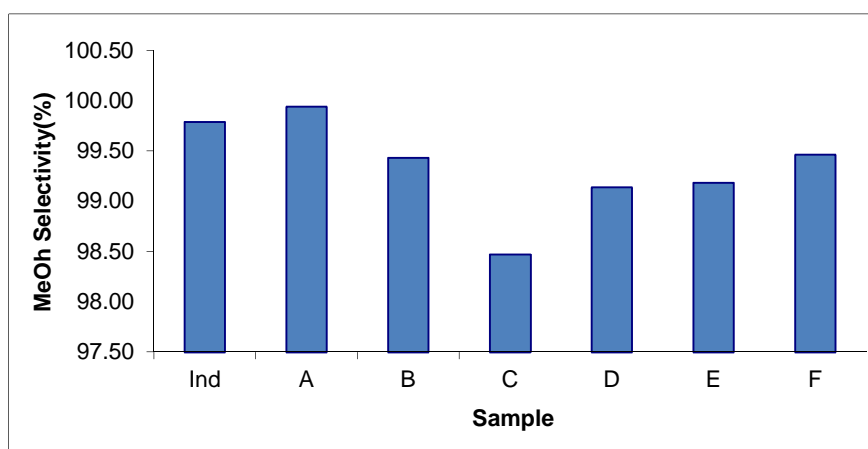


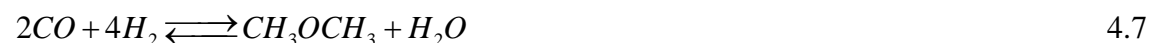
Figure 4.26: Steady State MeOH Selectivity at hour 3.5 in % for all catalyst samples.

Ind sample F, although has lower MeOH yield (Figure 4.2.3) and CO conversion (Figure 4.30) due to the lower Zn/Cu ratio, it still has high MeOH Selectivity. This could most likely be attributed metal oxide phase formed by its support which is the hexagonal α - alumina. This alumina type has been reported to have low amount of Bronstead acid sites (Al-OH). The hydroxyl sites are responsible for the formation of dimethyl ether (DME) due to the dehydration of MeOH that occurs on these sites [82].

Methanol Selectivity of up to 99.9% has been reported achieved from the Cu/ZnO/Al₂O₃ catalyst at Pressure 50 bars and Temperature 225°C [21]. In this study, most samples have achieved MeOH selectivity well above 98% at a Pressure of 30 bars and Temperature 250°C. Sample A has achieved the highest MeOH selectivity of 99.94%.

4.3.4 Analysis of DME Yield and Selectivity

Dimethyl Ether (DME) is an ether compound which is conventionally a byproduct in MeOH synthesis reactions. It is usually present in trace amounts when the Methanol synthesis process is catalyzed by the conventional Cu-ZnO based catalysts. The process which involves the formation of dimethyl ether is the dehydration of MeOH as shown in Equation 4.6. Methanol dehydration to DME is reported to occur on the surface of γ -Al₂O₃ and γ -Al₂O₃ modified with Phosphates or titanates [1].



DME yield is measure of amount of DME produced in the MeOH synthesis reaction. DME yield (%) is defined as 2 times the unit mols of DME detected in the product gas after the reaction over the amount of CO in the reactant gas. The 2 unit mol

of DME used is the result of the equilibrium stoichiometry of CO to DME which is 2:1 as shown in Equation 4.8. Thus the mol of CO has to be divided by 2 to gain normalized yield. Equation 4.8 is the net equation derived from the MeOH synthesis process (Equation 2.3) and MeOH dehydration to form DME (Equation 4.6).

$$Y_{DME} = \frac{2 \times (n_{DME})^f}{(n_{CO})^i} \times 100\% \quad 4.8$$

Figure 4.27 shows the DME yield in % for all catalyst samples at a 30 minutes interval in a 3.5 hour study. It can be seen that DME yield is extremely low in all catalyst samples, i.e. well below 0.015%. This suggests that DME production is a trivial process among the catalysts samples studied. However for some catalyst samples, the DME yield is more significant than others. For instance, it can be seen Figure 4.27 that the DME yield for Sample A, B, C, D and E is well below 0.01%. For sample F and the commercial sample Ind however, the amount of DME produced is greater and hence investigatiabale.

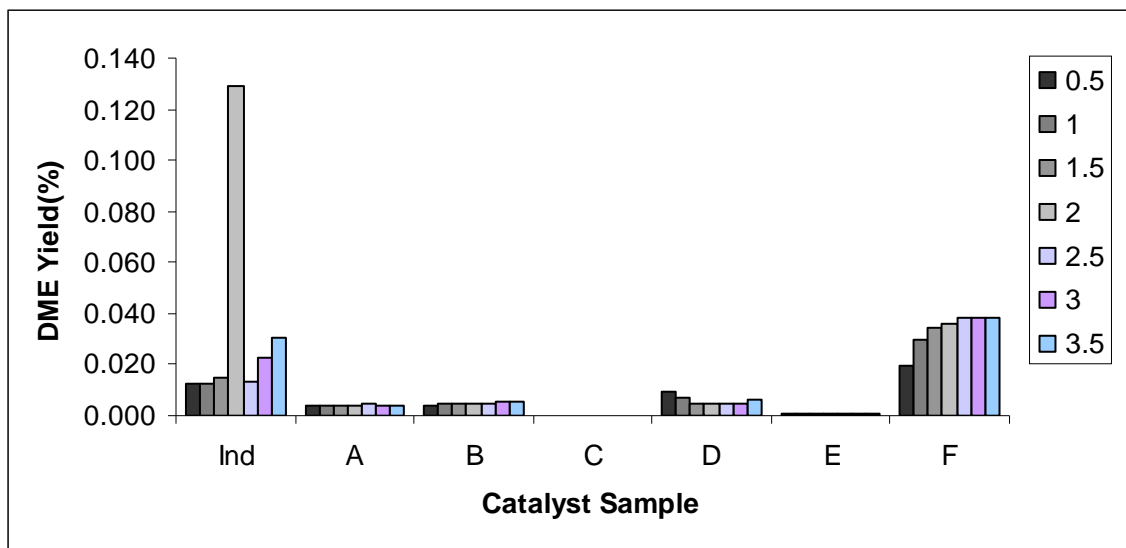


Figure 4.27: DME Yield in % for all catalyst samples in a 3.5 hour study

From previous EDX study it was established that the Zn/Cu ratio of commercial sample, Ind was 0.65. This ratio is far lower than other Zn containing samples A to E which have a Zn/Cu ratio above 1. It was outlined in previous sections that the MeOH synthesis process is a process that occurs on two regimes. Cu is the region where H₂ bond breaking occurs, while Zn and Zr is the region where CO and CO₂ hydrogenation to MeOH precursors and eventually MeOH occurs. It has been established by Askgaard *et al* [119] that the rate limiting step in the MeOH synthesis process is the formation of the methoxy species on the catalyst surface (H_3CO-M^a) as shown by equation 4.9 where M^a is the surface where hydrogenation of the H_2COO-* species occurs. M^a could either be Zn or Zr depending on the catalyst type.



For sample Ind this M_a species is Zn. This Zn site is extremely crucial as it is the rate limiting step (Equation 4.9) and could be impeded if this site was deactivated. For sample Ind, the low Zn/Cu ratio than other samples meant that the Zn sites are insufficient and there would be an excess of H atoms on the Cu surface from the H₂ bond breaking step. This would encourage the H atom spillover onto the Al₂O₃ support which would form highly acidic Al-OH Bronstead acid sites. These sites have been reported to be the prime location for DME formation [2]. This would provide explanation for the larger amount of DME Yield in sample Ind as compared to all other Zn containing samples.

A similar case is expected for sample F which is of the Cu/ZrO₂/Al₂O₃ series type. This is because it has no Zn present in its system and the Zr/Cu ratio is 0.47 obtained from EDX analysis. The M^a metal surface where the rate limiting step (Equation 4.9) occurs would be on this metal region. The DME produced in this sample however increases greatly than other samples as the reaction progresses. This could be due to the fact that the support type in this catalyst from XRD analysis was found to be the γ -Al₂O₃ type compared to the α -Al₂O₃ and θ -Al₂O₃ found in all other catalyst

samples. It was previously noted that the γ -Al₂O₃ is a prime location for DME formation as it has Al-OH species present that would dehydrate the MeOH formed [1].

DME selectivity is a gauge that determines the preference DME production has over all other products on a catalyst surface in the MeOH synthesis reaction. Equation 4.10 defines the DME Selectivity as the mol% of DME detected in the MeOH synthesis reaction from product gas over the amount of other product compounds (in mol %) detected in the product gas.

$$S_{DME} = \frac{(n_{DME})^f}{\sum (n_x)^f} \times 100\% \quad 4.10$$

Figure 4.28 plots the Selectivity of DME in % all catalyst samples, Ind as well as prepared samples A to F over a period of 3.5 hours of time on stream at a 30 minutes time interval. It can be seen that the results of DMEselectivity are consistent with previously discussed DME yield data. All samples except for commercial sample Ind and prepared Cu/ZrO₂/Al₂O₃ type sample F show DME yield below 0.1% throughout the period of study. Apart from having MeOH Yields close to 99.9%, these samples have DME as their 2nd largest product. Commercial sample, Ind while exhibiting high DME selectivity in the first half of the study, recede its DME selectivity to about 0.1% equilibrium. This is consistent with the MeOH Selectivity data for Ind sample (Figure 4.24) as it has low MeOH selectivity in the beginning but reaches very high stable MeOH selectivity at the 2nd half of the study. This was most likely due to the surface modification and the formation of Cu-Zn bimetal alloy as was discussed in Section 4.3.1.

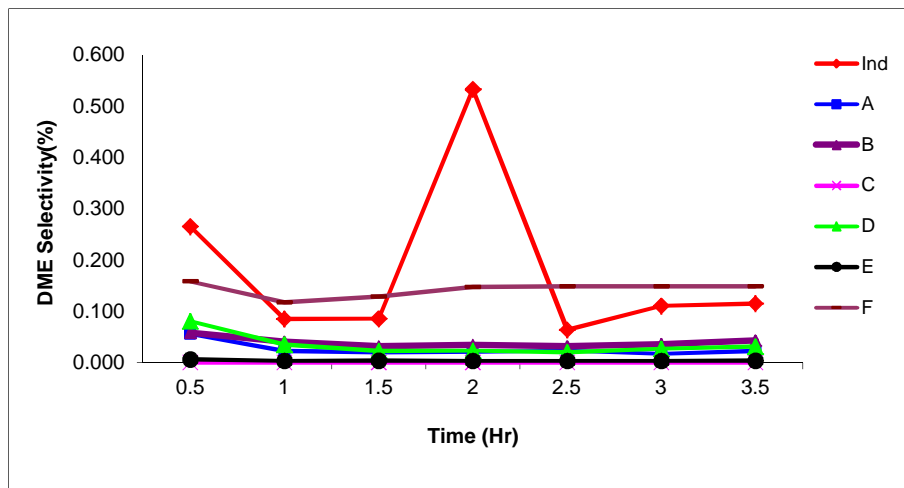


Figure 4.28: DME Selectivity in % for all catalyst samples in a 3.5 hours study.

Sample F has a different mechanism altogether as was displayed in both its MeOH Selectivity (Figure 4.25) and DME Selectivity (Figure 4.28) data. It can be seen in both images that sample F has very stable MeOH as well DME Selectivity throughout the 3.5 hour study. In the case of DME selectivity it is at around 0.15% for Sample F. Together with the 99.5% MeOH selectivity this is the total compounds produced by the syngas reaction. Sample F also the highest stable DME selectivity as compared to all other samples and this is namely due to its γ -Al₂O₃ sites as discussed earlier [2].

4.3.5 Analysis Ethanol of Yield and Selectivity

Higher alcohols (other than MeOH) are typical byproducts in the methanol synthesis process catalyzed by the Cu-ZnO catalysts type [1]. Although they are present in very low amounts in conventional MeOH products (typically 60ppm in Grade AA [120]), they still have been considered for discussion in the product gas. Equation 4.11 outlines a general stoichiometric equation for the equilibrium production of higher alcohols from syngas of CO and H₂ feed. Equation 4.12 on the other hand, outlines a more specific stoichiometric equation for the reaction of syngas to produce Ethanol and water.



Figure 4.29 shows the ethanol yield for all studied catalysts samples in a 3.5 hour time on stream study at a 30 minute time interval of analysis. It can be seen clearly that ethanol is only present as a product in the samples B, C, D and E as against samples Ind, A and F. This is highly suggestive as sample B, C, D and E are all Cu/ZnO/ZrO₂/Al₂O₃ type catalysts. The clear inference here would be that ethanol is only produced (in detectable amounts by TCD) in samples where both Zn and Zr are present as reactive sites as they are the variables in all catalyst compositions.



Industrially, ethanol is usually produced by hydration of ethylene in phosphoric acid acting as the catalyst (Equation 4.13) at 250°C and 60-70 bar [121]. This however is an easy procedure as the carbon-carbon bond is already established in the ethylene (C₂H₄) compound and the process only requires the reduction in activation energy of the water molecule(i.e. O-H bond breaking) by forming an intermediate species of ethylene and phosphoric acid compounds.

However, the process of ethanol synthesis directly from CO and H₂ requires the formation of carbon-carbon bond. This requires a reagent having nucleophilic carbon atom (C^{δ-}) and a reagent with an electrophilic carbon atom (C^{δ+}). These opposite polarities in carbon reacting species leads to the formation of a carbon-carbon bond [122]. The species of C-O has an electrophilic C site while a C-H species has a nucleophilic C site. These two sites could be instrumental in the formation of ethanol precursors and eventually ethanol as a byproduct in the catalysts.

An instance of an ethanol production process is the MeOH homologation with H₂ and CO as shown in Equation 4.14. Such reaction is reported to occur on Cobalt carbonyl (Co-CO) complex surfaces at temperature 290°C and pressure 18.4MPa as well as H₂/CO ratio of 1.05 [123]. The high pressures in these reactions are necessary as the reaction involves a C-C bond formation as described earlier. This process could explain the formation of ethanol as a byproduct albeit in small amount on the surface of Cu-Zn-Zr catalysts systems.

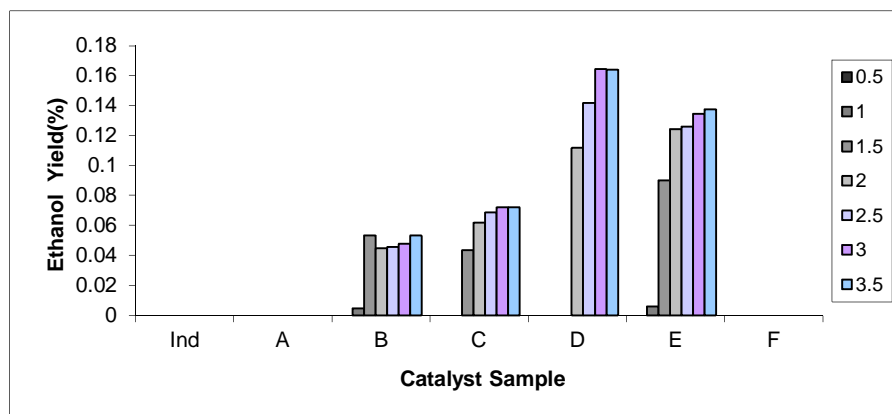


Figure 4.29: Ethanol Yield in % for all catalyst samples in a 3.5 hour study

It is evident in Figure 4.29 that the formation of ethanol is increasing from sample B, C and D but ensample E it is lower than sample D. It can be noted that the amount of Zr increases from sample B to E. However, the amount of Zn in sample E is lower than sample D. Thus the combination sites of Zn-Zr are the largest in sample D. This encourages the previous notion that the Zr-Zn sites encourage the formation of carbon-carbon bonds which evolve into ethanol. Also, it can be seen that the formation of methanol in all catalyst species containing Zn-Zr increases as shown in Figure 4.29. This suggests that as the surface evolves over the period of study due to adsorptions and desorption, more Zn-Zr sites are formed which enhance formation of ethanol.

The Ethanol selectivity trend in Figure 4.30 for sample B to E is also consistent with the Ethanol yield trends. It is clear that ethanol selectivity does increase over time but reaches optimum at below 1% for all catalysts sample.

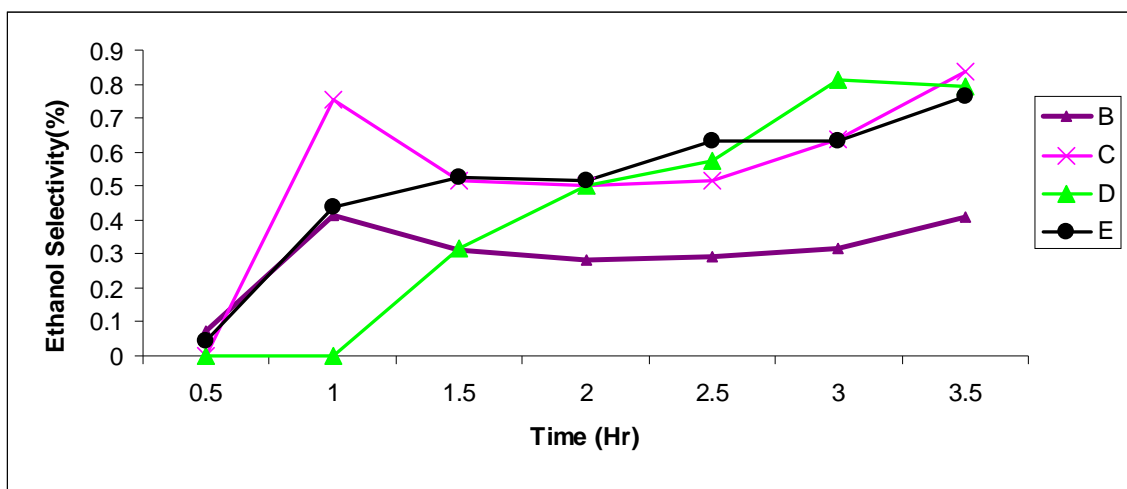


Figure 4.30: Ethanol Selectivity in % for all Cu/ZnO/ZrO₂/Al₂O₃ type catalyst samples in a 3.5 hours study.

4.3.6 Analysis of Methyl Formate Yield and Selectivity

Methyl formate ($HCOOCH_3$) has been a crucial chemical in industries predominantly in the production of formamide and dimethylformamide and latex coagulant. It is also a common byproduct in Cu-based MeOH synthesis reactions. It has been discovered that Methyl Formate has been predominantly produced from further reactions of MeOH and not directly from CO and H₂ in the Methanol synthesis reactions.

There are two main possible routes for production of Methyl formate from MeOH. They are the dehydrogenation of MeOH (Equation 4.15) and carbonylation of MeOH (Equation 4.16). MeOH dehydrogenation reaction usually occurs on transition metals such as Cu and Pd based catalysts. It has been reported that a conversion of 18%

and selectivity to Methyl formate of 94% from MeOH in a reaction conditions of 270°C and 10bar. These conditions are comparable to the ones studied in our reaction [124].

MeOH carbonylation however occurs conventionally on alkali metal catalysts such as sodium methoxide at pressure of 810MPa and Temperature 80°C [125]. This reaction Therefore is unlikely to be occurring in our study due to the high Pressure requirement as well as the need for Na based catalyst which is not present in our catalysts systems.

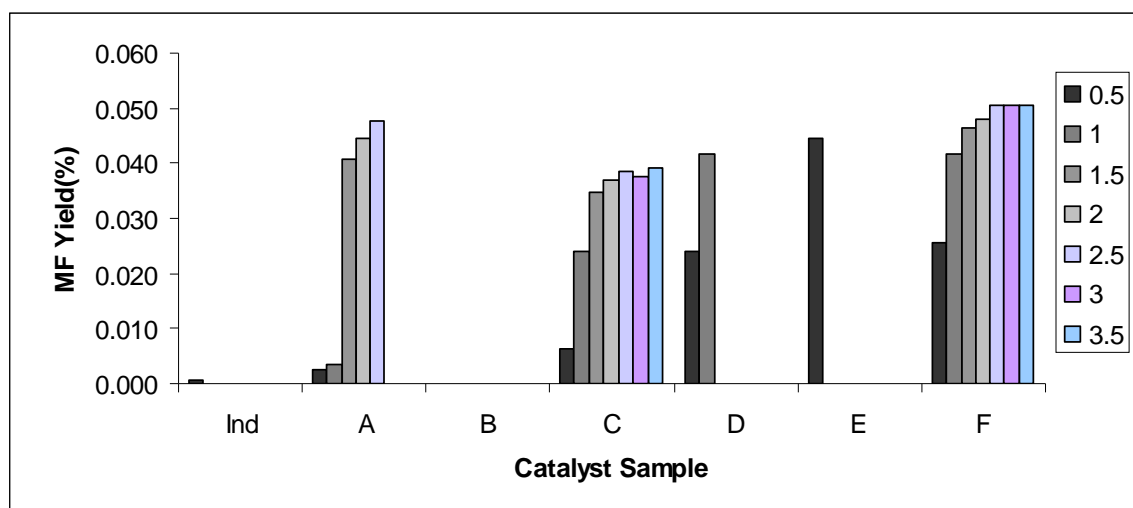


Figure 4.31: Methyl Formate (MF) Yield in % for all catalyst samples in a 3.5 hour study

Figure 4.31 shows the methyl formate yield (in %) for all catalysts sample over a period of 3.5 hour of time on stream. Overall methyl formate yield in catalysts samples is extremely low i.e. < 0.05%. It can be seen that mainly catalysts sample C and F has had active yield of Methyl formate throughout the period of study. Sample A on the other hand, had Methyl formate produced only at the middle of the study period and

none at the beginning and the end. $\gamma\text{-Al}_2\text{O}_3$ support has been observed to be the site of Methyl formate yield in Pd-ZnO catalysts at pressure 200°C and 10bars [124].

XRD phase analysis reveals that only sample F has had $\gamma\text{-Al}_2\text{O}_3$ phase formed in its support. That would explain the higher formation of methyl formate in Sample F. Sample C which has low Cu dispersion and hence lower Cu are could encourage the further adsorption of MeOH on due to low availability of H atoms from Cu sites and hence increase Methyl formate production. This is also supported by the fact that Sample C has the low overall MeOH production among the studied catalyst samples.

Figure 4.32 which shows the overall Methyl formate selectivity, shows the low selectivity of this product (<0.5%) compared to all other products the reaction. It is consistent with the Methyl formate Yield data on Figure 4.31 where only Sample C and F have active production of Methyl formate.

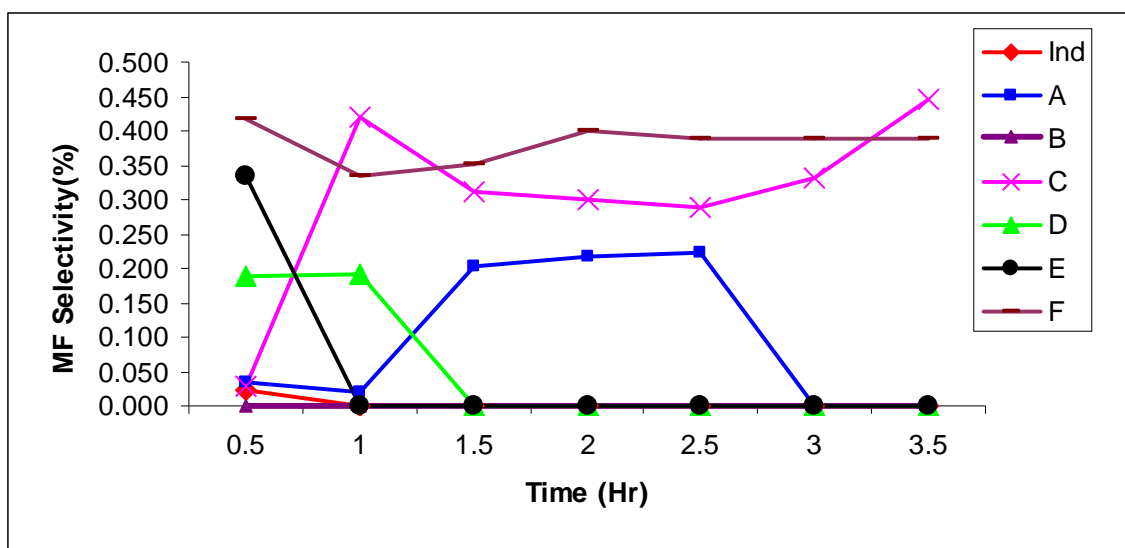
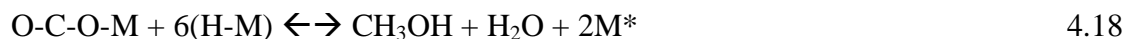


Figure 4.32: Methyl Formate (MF) Selectivity in % for all catalyst samples in a 3.5 hours study.

4.3.7 CO₂ formation study as an Intermediate species type

Carbon dioxide is a crucial intermediate in the MeOH synthesis process from a CO/H₂ feed system. It has been a favorable hypothesis that MeOH is produced mainly from the route of CO₂ hydrogenation on the surface of Zn and/or Zr (Zn or Zr site is represented as M*). A generic 4 step procedure for the production of MeOH in a gas feed system where no H₂O and CO₂ is present is outlined in Equation 4.17 to 4.20.



The first step (Equation 4.17) is the formation of CO₂ from CO in a H₂O-free feed mixture. It involves the adsorption of CO on the hydrogenation site M-O (Zn-O or Zr-O) and the consequent bonding of with the O on the M-O lattice to form an intermediate site of O-C-O -M . These intermediary sites are of significant consequence in the next step (Equation 4.18) where the spillover H atoms (Cu sites breaks the bond in H₂ molecule and H atoms are transferred unto the M sites) react with this intermediary O-C-O -M site to produce desorbed MeOH and H₂O as well 2 sites of M* (Zn²⁺ or Zr⁴⁺).

These positively charged sites M* are crucial in the readsorption of H₂O molecule and the formation of the H-O-M sites. These H-O-M sites are crucial for they have available excess O atoms which are necessary to continue the formation of the intermediary O-C-O-M sites (Equation 4.19). The formation of water as an intermediate O source (Equation 4.20) is thus the reason why it was not detected in the TCD signal as it was fully reutilized in the reaction process.

Figure 4.35 to Figure 4.41 shows the comparison between CO₂ production and MeOH Yield for each catalyst sample throughout a 3.5 hour time on stream at an interval of 30 minutes. It can be seen that a clear trend of CO₂ production which increases in the beginning of the reaction and reduces towards the end of the study period in contrast to the increasing MeOH yield. It Therefore can be deduced that the relationship between CO₂ detected and the stability of MeOH yield in the reaction is closely related.

The adsorption and oxidation of the CO species to become CO₂ also occurs on the same surface site as does the methoxy formation (Zn and/or Zr) as shown in Figure 4.33. This site is also crucial for all other stages of hydrogenation and oxidation processes until the desired MeOH product is achieved and desorbed from this surface. Thus a system of series mechanisms has to be established in order to allow for each step to take place and complete before the next step can proceed. This process would take place on each site (Zn and/or Zr) available on the catalyst surface. This procedure can be witnessed in Figure 4.34.

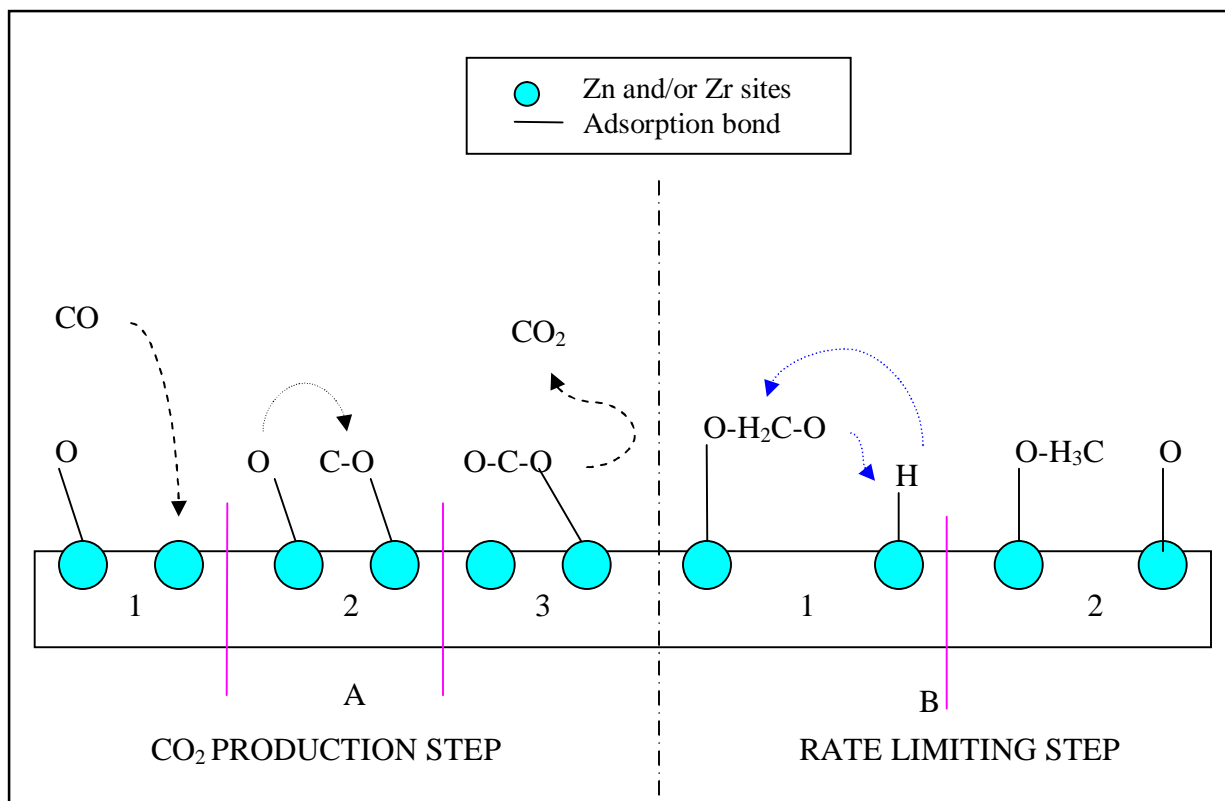


Figure 4.33: Visualization of the CO₂ production step (A) and the rate limiting methoxy formation step (B).

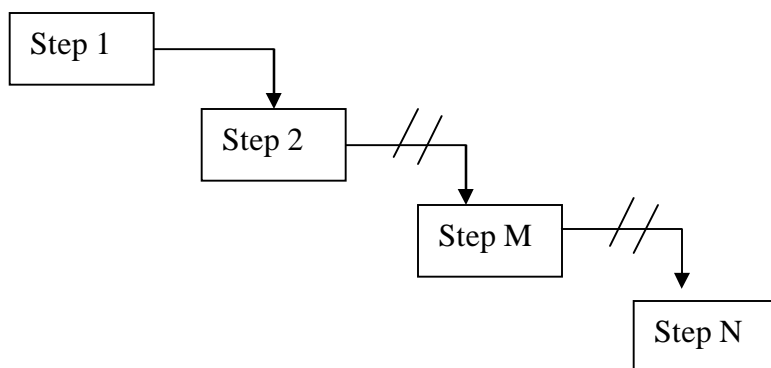


Figure 4.34: Step wise series procedure to formation of each intermediate before final product can be formed.

However, since the Methoxy production step is rate limiting it is conceivable that the effect would be rippled off all the way back until the initial Step 1 (Equation

4.17) of CO oxidation to CO₂ would be as well affected. The bond of Metal-Oxygen in H₂COO-M is stronger than the bond of Metal –Oxygen in O-C-O-M. The Zn-O bond of H₂COO-Zn has a bond disassociation energy of 133.9kJ/mol while the Zn-O bond in O-C-O-Zn has a bond disassociation energy of 43.6 kJ/mol [126]. Bond disassociation energy (BDE) is the amount of energy required to break a particular bond.

It is evident that the weaker bond (O-C-O-M) would be broken prematurely by the excess of formation of the stronger bonds (H₂COO-M) and lead to the formation of free CO₂ gas in all catalyst samples which would be detectable in all samples as evident from the data in Figure 4.35-4.41.

This scenario however does not continue throughout the process as it can be seen in Figure 4.35 -4.41 that the amount of CO₂ drops to zeros after a period of 2-3 hours of reaction. This would suggest a change in CO adsorption capacity on the surface to account limited surface sites as major amount of M* sites are still engaged in the methoxy formation process (Equation 4.9). The amount of CO adsorbed would naturally decrease due to the limited sites available at any given moment and thus the amount of prematurely desorbing CO₂ too will decrease until none is seen. Equilibrium between adsorption of CO and the rate limiting step would be reached and from there onwards the MeOH yield should reach stability. This can be seen clearly in all catalyst samples from Figure 4.35-4.41.

Another factor to be considered would be the period before stability of Yield and zero CO₂ byproduct is reached. As a rule of thumb, lower Zn/Zr sites would lead to quicker halt of CO₂ formation as less time would be required for the ripple effect of CO₂ desorption and hysteresis on Zn/Zr surface to cease. Less total sites would mean less initial amount of CO adsorbed (and oxidized to CO₂) and therefore less forced desorption of CO₂. That would explain why commercial sample Ind reaches zero-CO₂ state quicker as shown in Figure 4.35. This is because it has less Zn sites (Zn/Zr ratio 0.65) in comparison to other Zn containing catalyst samples.

Sample F which reaches zero-CO₂ state even more quickly suggests that there is a large portion of inactive Zr sites (ZrO₂ phase) while releases CO₂ much more easily. For instance Zr-CO has a BDE (bond dissociation energy) of 627 kJ/mol while ZrO₂-CO has a BDE of only 60 kJ/mol [126]. All other catalyst sample reaches zero-CO₂ state at around 3- 3.5 hours suggesting optimum catalyst activity after that period of study.

Another evidence of this theory that number of Zn/Zr sites available dictates the speed at which a zero-CO₂ free state is reached is the initial conversion of CO for all catalysts samples. The higher conversion of CO simply means that less CO is detected by TCD in the product gas. Therefore, if less CO is detected in product gas more is adsorbed on the catalyst surface. This observation is consistent with the evolution of CO conversion for commercial catalyst sample, Ind in Figure 4.20. It is evident that the amount of CO adsorbed increases in the beginning of the reaction before reducing at 2 hour of study.

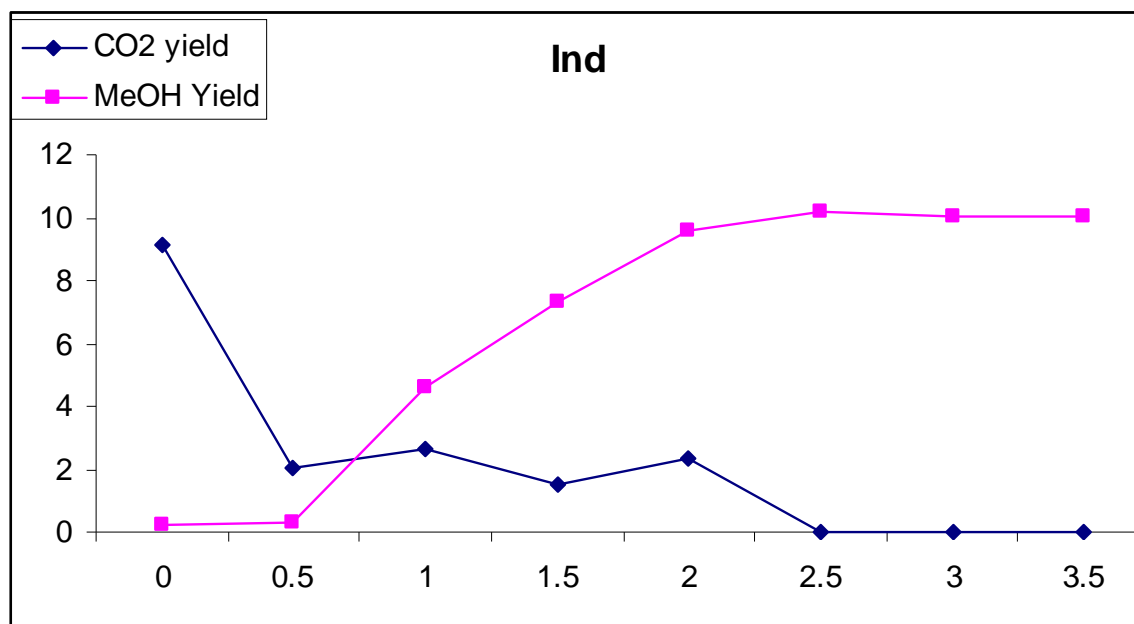


Figure 4.35: Comparison of CO₂ and MeOH yield for commercial catalyst sample, Ind

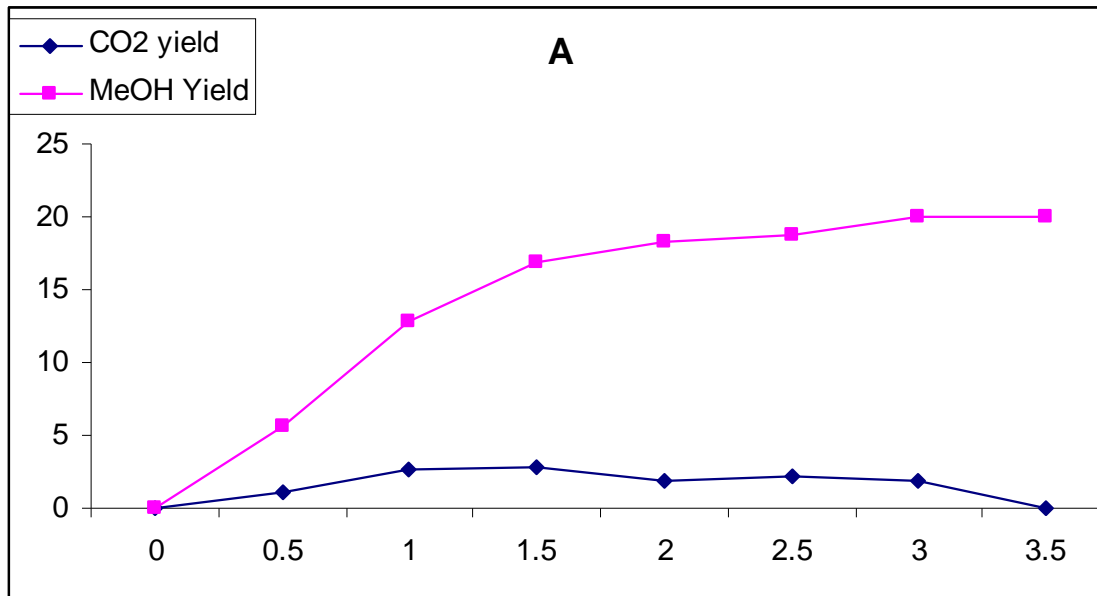


Figure 4.36: Comparison of CO₂ and MeOH yield for catalyst sample A

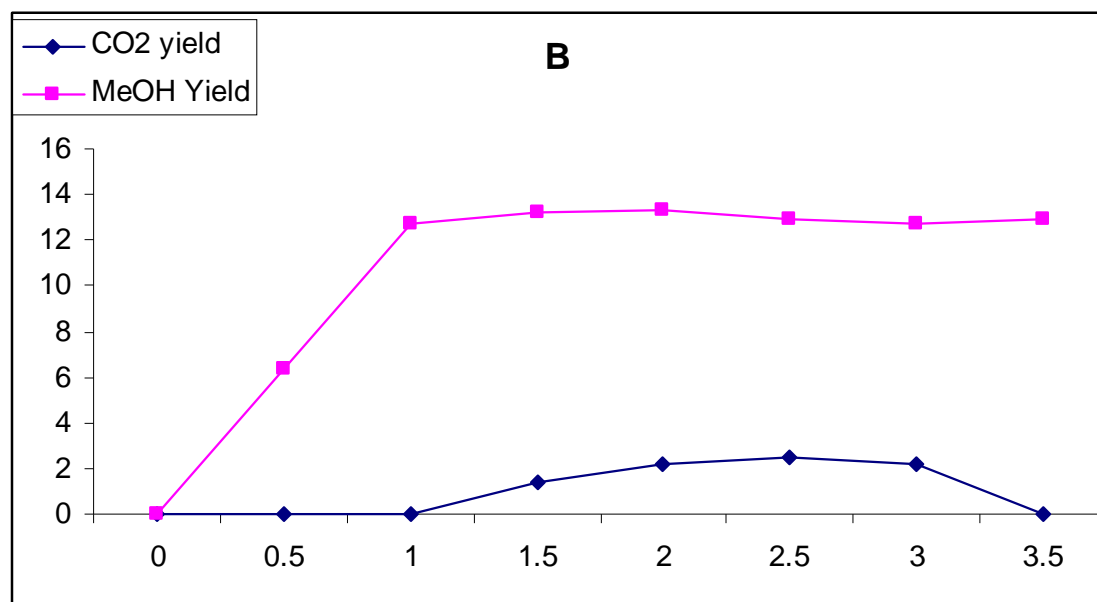


Figure 4.37: Comparison of CO₂ and MeOH yield for catalyst sample B

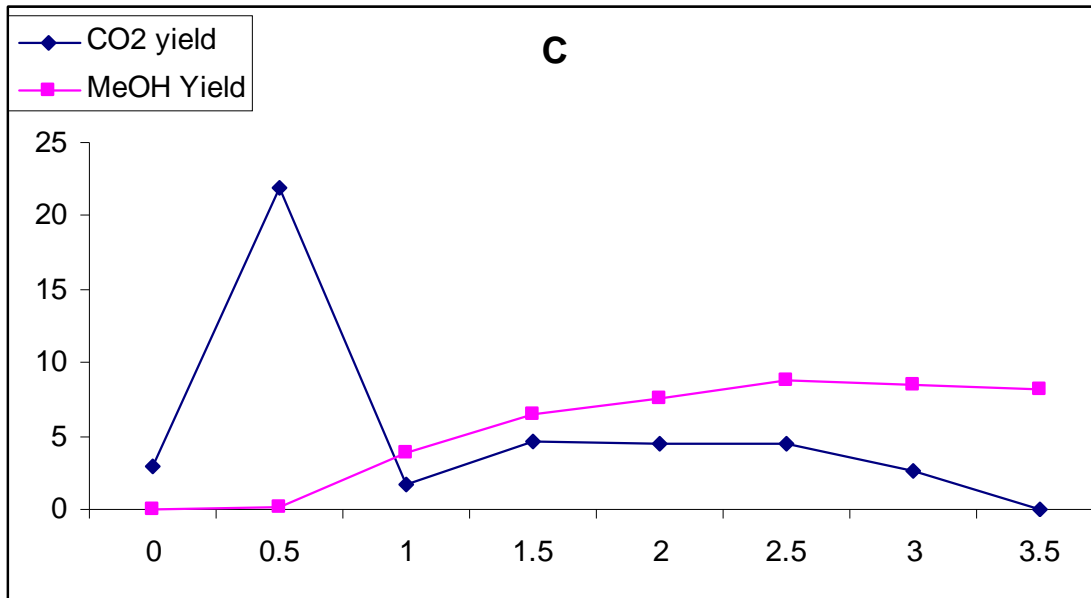


Figure 4.38: Comparison of CO₂ and MeOH yield for catalyst sample C

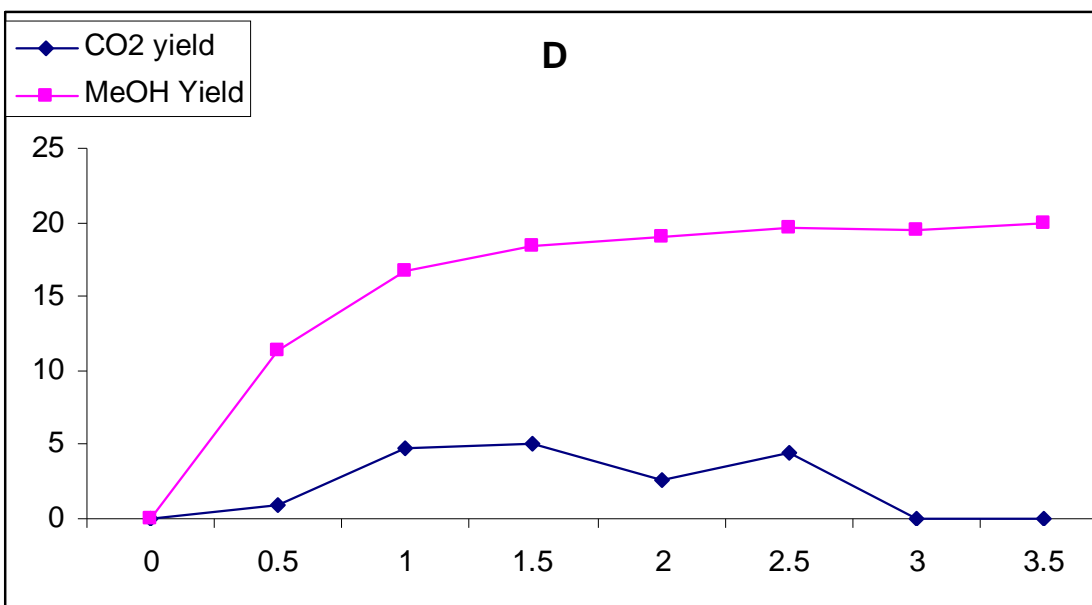


Figure 4.39: Comparison of CO₂ and MeOH yield for catalyst sample D

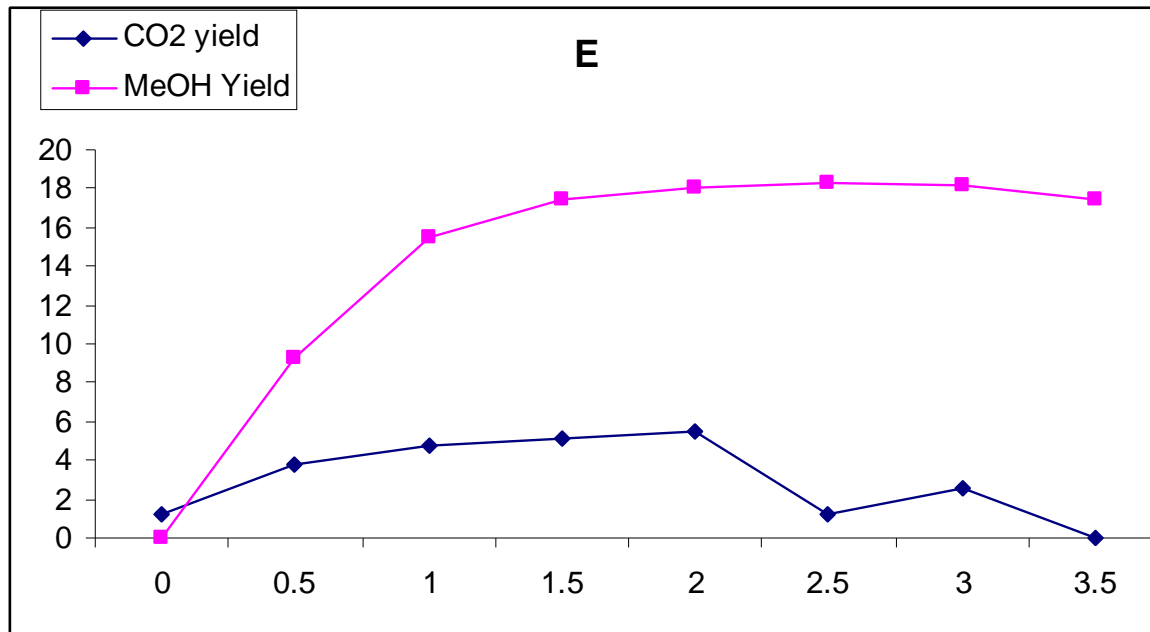


Figure 4.40: Comparison of CO₂ and MeOH yield for catalyst sample E

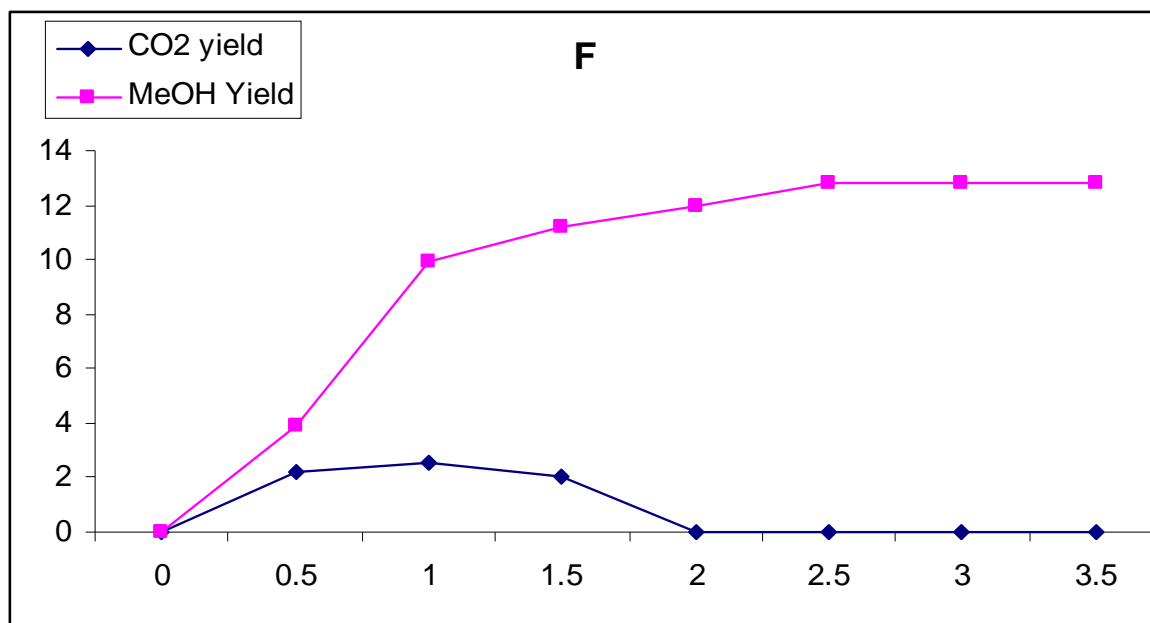


Figure 4.41: Comparison of CO₂ and MeOH yield for catalyst sample F

4.3.8 CH₄ formation and carbon formation study

After Cu site sintering, coke deposition or formation of inactive carbon on catalyst active sites has been the main source of catalyst deactivation in industrial catalytic history. Inactive carbon (or coke) has the ability to block the active sites by forming stable Metal-Carbon bonds or by blocking the catalytic pores causing the inaccessibility of reactant gas to active sites. Inactive carbon, C(s) may be formed on supported metal catalysts surface via CH₄ decomposition or by CO disproportionation (Boudouard reaction) as shown in Equation 4.21 - 4.22 [127].



Figure 4.42 shows the CH₄ yield for the period of 3.5 hour of time on stream study at a 30 minutes time interval for all catalyst samples. The formation of methane follows an opposite trend to that of MeOH synthesis. It is conceivable that the formation of methane would be a direct alternative process to MeOH synthesis as both processes would have to compete for CO and H₂ available in the reactant gas.

Even more interesting is the consistent trend of CH₄ yield and carbon weight formation of every sample. The carbon weight formed for all catalysts samples was quantified by use of the LECO CHNS-932 equipment and is shown in Figure 4.43 and Table 4.5. It would be fair to deduce that the Equation 4.11 would be a dominant route in the formation of inactive carbon as the trend of both CH₄ yield and C(s) weight in catalyst samples is consistent with one another except for commercial sample, Ind. For the commercial sample, the C(s) weight quantified by the CHNS equipment is much higher than other catalysts samples. This is because the commercial sample, Ind had already included some amount of (4.21 wt %) graphitic carbon in its fresh catalyst sample as revealed by the EDX analysis study. But this graphitic carbon was introduced

as a binding agent and only included in the catalyst sample industrially during the pelletization process. Hence it's not chemically bonded with the catalysts sample and would thus have been lost quite easily during the sample crushing process before activity study or during spent catalyst retrieval.

Sample F has a peculiar property as it formed no methane and the least amount of inactive carbon. This suggests a unique property of Zr based catalysts which impedes catalyst deactivation by discouraging methane formation and hence its decomposition into inactive carbon. Sample C which has recorded the least activity in MeOH synthesis and CO conversion has shown the highest steady methane formation as well as high C(s) formation.

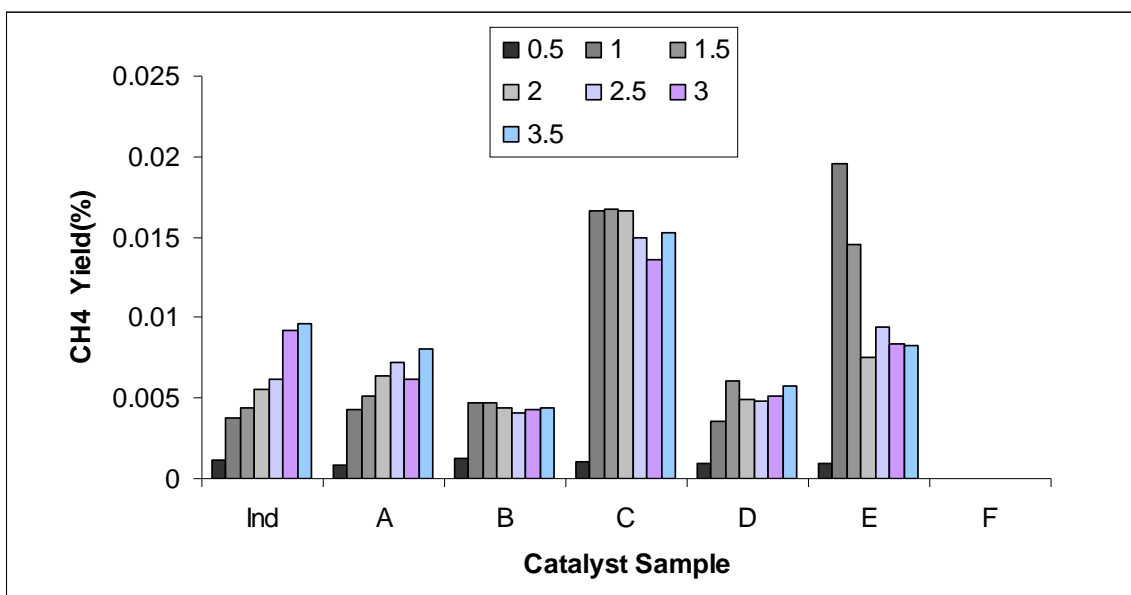


Figure 4.42: CH₄ Yield in % for all catalyst samples in a 3.5 hours study.

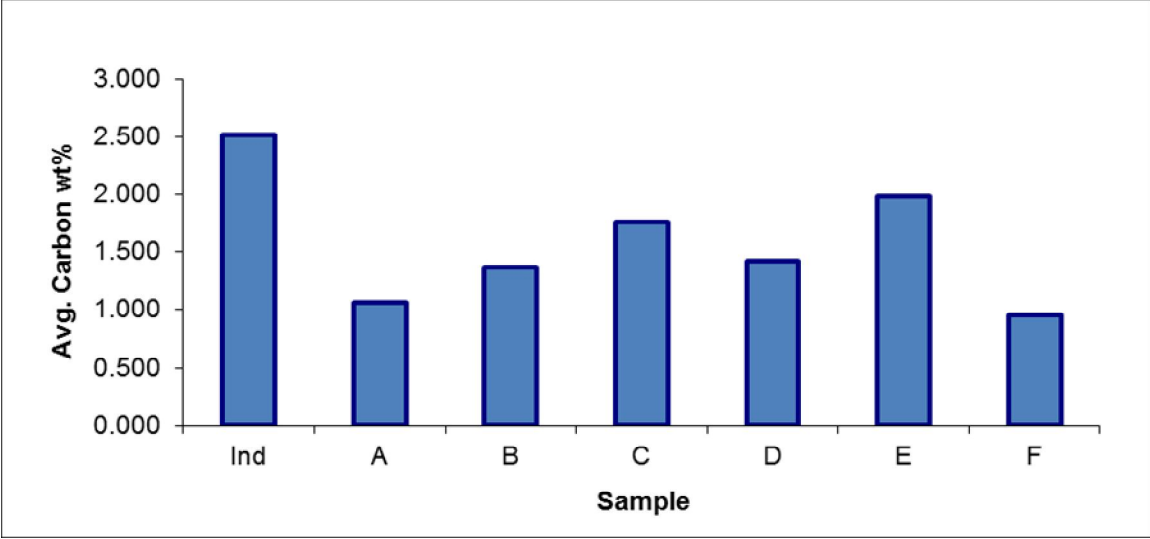


Figure 4.43: Carbon weight formed in wt% for all catalysts samples

Table 4.5 is a collection of the quantified carbon amount formed in all catalysts samples with an average of 3 readings per sample.

Table 4.5: Carbon formation for all catalysts samples

Catalyst sample	Run	Sample Weight (mg)	Carbon (wt %)	Average Carbon (wt %)	Standard Deviation (wt %)
Ind	1	1.701	2.510	2.510	0.001
	2	1.508	2.509		
A	1	1.556	1.041	1.060	0.026
	2	1.682	1.078		
B	1	1.368	1.364	1.364	0.000
	2	1.444	1.364		
C	1	1.559	1.752	1.752	0.000
	2	1.724	1.752		
D	1	1.555	1.440	1.419	0.030
	2	1.975	1.397		
E	1	1.345	1.995	1.987	0.011
	2	1.628	1.979		
F	1	1.729	0.962	0.956	0.008
	2	1.722	0.950		
SulfaMethazine standard	1	1.50	50.65	50.780	0.184
	2	1.50	50.91		

4.4. Catalytic Kinetic Analysis

4.4.1 Elementary Reactions Kinetics: 2 site study (Cu and Zr/Zn)

The reduction of metal oxide sites to available metal sites is crucial to encourage reactant gas adsorption on catalysts surface. However, in catalysts samples where no CO₂ and H₂O were present, the main source for O atoms in the initial reaction is the metal oxides surfaces. Thus in order to determine the optimum coverage of O sites, (θ_O) on Zn/Zr sites where methanol synthesis occurs, this analytical kinetic study has been conducted. Two major constraints have been set in line with the operating parameters in our prior experimental study:

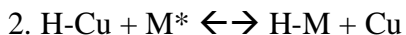
- I. Only CO and H₂ gas is present in the reactant gas without H₂O or CO₂ is present in the reactant gas and no other O atoms source.
- II. Two distinct sites are present on catalysts surface, i.e.
 - Cu for H₂ bond breaking to form H atom supply
 - Zn/Zr sites where hydrogenation of CO occurs to finally form MeOH

This study is the extension of the analytical kinetic study by Askgaard et al. [119] with the reactant gas CO₂ and H₂ and a Cu only surface site present for all interactions. The elementary kinetic reactions are shown below. Reaction 7 (CH₃O-M formation) is the rate determining step (RDS) as it is the slowest reaction and would determine the overall reaction rate in the methanol synthesis study [119]. H₂ disassociation happens on Cu surface and H atoms spillover to Zn/Zr (M*) and further react with CO to form MeOH.

A. Cu site disassociation



B. H atom spillover from Cu to M(Zn and/or Zr sites)



C. Zn and/or Zr site activity

3. $\text{CO}(\text{G}) + \text{M}^* \leftrightarrow \text{CO-M}$
4. $\text{CO-M} + \text{O-M} \leftrightarrow \text{O-C-O} + \text{M}^*$
5. $\text{O-C-O-M} + \text{H-M} \leftrightarrow \text{O-C(H)-O-M} + \text{M}^*$
6. $\text{O-C(H)-O-M} + \text{H-M} \leftrightarrow \text{O-C(H,H)-O} + \text{M}^*$
7. $\text{O-C(H,H)-O-M} + \text{H-M} \leftrightarrow \text{H-C(H,H)-O(H)-M} + \text{M}^*$ (RDS)
8. $\text{H-C(H,H)-O(H)-M} + \text{H-M} \leftrightarrow \text{H-C(H,H)-O(H)-M} + \text{M}^*$
9. $\text{H-C(H,H)-O(H)-M} \leftrightarrow \text{H-C(H,H)-O(H)} + \text{M}^*$

4.4.2 Elementary Reaction Rate Equations

The total elementary reactions rates and their algebraic rearrangements are shown below. All other reactions except for Equation 7 are assumed to be in near equilibrium [119]. The description of symbols is:

θ_x – coverage of adsorbate x on metal surface (V means vacant, Cu means Cu sites and M means Zn and/or Zr sites)

k_i – forward reaction rate constant for reaction i. If k_{-i} , for backward reaction rate constant for the reaction i.

K_i - Equilibrium reaction rate constant. $K_i = k_i/k_{-i}$

P_A – Pressure of gas A in the system ($P_A = P_A/P^0$). P^0 is the reference pressure at STP.

r_i – Rate of Reaction for reaction i. ($r_i = r_{+i} - r_{-i}$) . If forward reaction rate is equal to backward reaction rate, ($r_{+i} = r_{-i}$) then overall reaction i is at equilibrium.

$$1. k_1 P_{H_2} \theta_{\theta_{VCu}}^2 = k_{-1} \theta_{HCU}^2$$

$$\frac{\theta_{HCU}}{\theta_{\theta_{VCu}}} = \sqrt{K_1 P_{H_2}}$$

$$2. k_2 P_{CO} \theta_{VM} = \theta_{CO} k_{-2}$$

$$\theta_{CO} = K_2 P_{CO} \theta_{VM}$$

$$3. k_3 \theta_{HCU} \theta_{VM} = k_{-3} \theta_{HM} \theta_{VCu}$$

$$\frac{\theta_{HM}}{K_3 \theta_{VM}} = \frac{\theta_{HCU}}{\theta_{VCu}}$$

$$\frac{\theta_{HM}}{K_3 \theta_{VM}} = \sqrt{K_1 P_{H_2}}$$

$$\frac{\theta_{HM}}{\theta_{VM}} = K_3 \sqrt{K_1 P_{H_2}}$$

$$4. k_4 \theta_{CO} \theta_O = k_{-4} \theta_{OCO} \theta_{VM}$$

$$\theta_{OCO} = \frac{K_4 \theta_{CO} \theta_O}{\theta_{VM}}$$

$$\theta_{OCO} = \frac{K_4 (K_2 P_{CO} \theta_{VM}) \theta_O}{\theta_{VM}}$$

$$\theta_{OCO} = K_2 K_4 P_{CO} \theta_O$$

$$5. k_5 \theta_{OCO} \theta_{HM} = k_{-5} \theta_{CHOO} \theta_{VM}$$

$$\theta_{CHOO} = K_5 (\theta_{OCO}) \left(\frac{\theta_{HM}}{\theta_{VM}} \right)$$

$$\theta_{CHOO} = K_5 (K_2 K_4 P_{CO} \theta_O) (K_3 \sqrt{K_1 P_{H_2}})$$

$$\theta_{CHOO} = (K_1)^{1/2} K_2 K_3 K_4 K_5 \sqrt{P_{H_2}} P_{CO} \theta_O$$

$$6. k_6 \theta_{CH_2OO} \theta_{HM} = k_{-6} \theta_{CH_2OO} \theta_{VM}$$

$$\theta_{CH_2OO} = K_6 (\theta_{CH_2OO}) \left(\frac{\theta_{HM}}{\theta_{VM}} \right)$$

$$\theta_{CH_2OO} = K_6 \left((K_1)^{1/2} K_2 K_3 K_4 K_5 \sqrt{P_{H_2}} P_{CO} \theta_O \right) \left(K_3 \sqrt{K_1 P_{H_2}} \right)$$

$$\theta_{CH_2OO} = K_1 K_2 (K_3)^2 K_4 K_5 K_6 P_{H_2} P_{CO} \theta_O$$

$$8. k_8 \theta_{CH_3O} \theta_{HM} = k_{-8} \theta_{CH_3O} \theta_{VM}$$

$$\theta_{CH_3OH} = K_8 \theta_{CH_3O} \left(\frac{\theta_{HM}}{\theta_{VM}} \right)$$

$$\theta_{CH_3OH} = K_8 \theta_{CH_3O} \left(K_3 \sqrt{K_1 P_{H_2}} \right)$$

$$\theta_{CH_3OH} = (K_1)^{1/2} K_3 K_8 \sqrt{P_{H_2}} \theta_{CH_3O}$$

$$9. k_9 \theta_{CH_3OH} = k_{-9} P_{CH_3OH} \theta_{VM}$$

$$\theta_{CH_3OH} = K_9 P_{CH_3OH} \theta_{VM}$$

From Eq. 8 & 9

$$(K_1)^{1/2} K_3 K_8 \sqrt{P_{H_2}} \theta_{CH_3O} = K_9 P_{CH_3OH} \theta_{VM}$$

$$\theta_{CH_3O} = \frac{K_9 P_{CH_3OH} \theta_{VM}}{(K_1)^{1/2} K_3 K_8 \sqrt{P_{H_2}}}$$

Thus the RDS (r_7):

$$r_7 = \text{RDS} = r_{+7} - r_{-7}$$

$$r_7 = k_7 [\theta_{CH_2OO}] [\theta_{HM}] - \frac{k_7}{K_7} [\theta_{CH_3O}] \theta_O$$

$$r_7 = k_7 \left[K_1 K_2 (K_3)^2 K_4 K_5 K_6 P_{H_2} P_{CO} \theta_O \right] \left[K_3 \sqrt{K_1 P_{H_2}} \theta_{VM} \right] - \frac{k_7}{K_7} \left[\frac{K_9 P_{CH_3OH} \theta_{VM}}{(K_1)^{1/2} K_3 K_8 \sqrt{P_{H_2}}} \right] \theta_O$$

$$r_7 = k_7 \theta_{VM} \theta_O \left[(K_1)^{3/2} K_2 (K_3)^3 K_4 K_5 K_6 P_{CO} (P_{H_2})^{3/2} - \frac{K_9 P_{CH_3OH}}{(K_1)^{1/2} K_3 K_7 K_8 \sqrt{P_{H_2}}} \right]$$

4.4.3 Optimization of θ_O on rate of reaction

To determine the effect of θ_O in the overall reaction rate, all constants K_i and k_i are set to 1. Now the equation, r_7 is just the function of gas pressures and coverage of vacant sites as well as oxide sites.

In the beginning of the reaction, (after catalyst reduction) the available surface metal sites can be divided into two only, vacant and O atom covered. The sum of the coverage of O and vacant sites is:

$$\theta_O + \theta_{VM} = 1$$

Now, the final reaction rate equation is:

$$r_7 = (\theta_O)(1 - \theta_O) \left[P_{CO} (P_{H_2})^{3/2} - \frac{P_{CH_3OH}}{\sqrt{P_{H_2}}} \right]$$

To determine the θ_O that maximizes the reaction overall reaction rate (r_7), differentiate r_7 with respect to θ_O and set the derivate equal to 0.

$$\frac{\partial r_7}{\partial \theta_O} = 0;$$

$$\frac{\partial r_7}{\partial \theta_O} = 0 = (1 - 2\theta_O) \left[P_{CO} (P_{H_2})^{3/2} - \frac{P_{CH_3OH}}{\sqrt{P_{H_2}}} \right]$$

$$\text{Since } \left[P_{CO} (P_{H_2})^{3/2} - \frac{P_{CH_3OH}}{\sqrt{P_{H_2}}} \right] \neq 0;$$

$$0 = (1 - 2\theta_O)$$

$$\theta_O = 0.5$$

Thus reaction rate is highest when the coverage of O atoms (on the available, Zn and/or Zr) is half and the other half is vacant sites. This would suggest a study of reduction of catalysts samples in order to optimize the surface coverage of O sites to 05.

Plainly, this means that in the absence of H₂O and CO₂ in the feed gas, the reduction of catalyst surface has to be controlled. That is, half of the surface Zn or Zr sites have to be oxidized and the other half reduced. This would allow maximum initial reaction activity as the Zn or Zr surface would be the source of O atoms required in the oxidation process.

CHAPTER V

CONCLUSIONS AND RECOMMENDATIONS

5.1 Conclusions

The objective of preparing a Cu based catalyst and to study the effect of Zr and Zn presence in the catalyst samples were met. Also the role of alumina support was thoroughly explored in this thesis.

The characterization of the prepared catalyst of various compositions and support types was done together with the Industrial fresh and used catalyst successfully in this first part of the study.

The type of Zirconia compound formed in the catalyst was monoclinic Zirconia which has higher reported activity than the variant tetragonal Zirconia.

Also, a range of 300 to 345°C of reduction Temperature was determined. The thermal stability of prepared catalyst was also higher than industrial catalyst at the industrial operating Temperature of 250 °C. Catalyst A also has the highest Low Temperature peak among all prepared catalysts as well has highest dispersion and metal surface area than the industrial catalyst. This is a strong indicator of high activity.

As predicted by s-TPR analysis of Low and High Cu surface area, sample A has the highest CO conversion as well as MeOH selectivity. However this alone was not the

gauge for activity as the Zn/Cu and/or Zr/Cu ratio too played a major role. Zn/Cu ratio below 1 reduced catalysts activity as seen in the case of commercial sample, Ind.

5.2 Recommendations

On the experimental site, the catalyst samples should be studied in a pilot scale reactor to include the effect of packing and pelletization on catalyst activity. Also further in-situ analysis of surface changes can be explored by in-situ XRD or in-situ FeSEM.

For the kinetic studies, a future theoretical framework using partition functions should be employed. This is to further describe the kinetics of methanol synthesis process with the changes of Temperature and Pressure and its effects on rate of reaction.

REFERENCES

- [1] H.H Kung, Methanol production and Use, pg 2-3, CRC Press, 1994
- [2] C.H.Bartholomeow, R.J Farrauto, Chapter 5 & 6: Fundamentals of Industrial Catalytic, Wiley-Interscience, 2007.
- [3] Presentation, Methanol by Lurgi Technology, Market for Methanol, 2003
- [4] <http://www.petronas.com.my/internet/Directory.nsf/>
- [5] <http://www.statistics.gov.my>
- [6] Yin Y Q, Xiao T C, Su J X, Wang H T, Lu Y L, Li Sh B. *J MolCatal (China)*, 2000, 14(5): 373
- [7] Guo H G, Han W F, Shen J L, Liu H Zh. *Ind Catal*, 2003, 11(3):39
- [8] F.Arena, G. Italiano , K. Barbera, S. Bordiga, G. Bonura ,L. Spadaro , F.Frusteri , Solid-state interactions, adsorption sites and functionality of Cu-ZnO/ZrO₂ catalysts in the CO₂ hydrogenation to CH₃OH, *Applied Catalysis A: General* 350 (2008) 16–23
- [9] PETRONAS Methanol Labuan (PMLSB) Presentation, *New Method: Unloading Catalyst under Inert Condition.*
- [10] CEN Yaqing, LI Xiaonian, LIU Huazhang, Preparation of Copper-Based Catalysts for MethanolSynthesis by Acid–Alkali-Based Alternate Precipitation Method, *Chin J Catal*, 2006, 27(3): 210–216.
- [11] *Applied Catalysis A: General* 281 (2005), 199-205
- [12] <http://en.wikipedia.org/wiki/Methanol>
- [13] Klier K., 1982, *Adv. Catal.*, 31:243
- [14] S. Lee, V.R. Parameswaran, I. Wender, C.J. Kulik, *Fuel Sci. Techol. Int.*, Marcel Dekker, New York
- [15] T.M.L. Wigley, The Climate Change Commitment, *Science* 307 (5716), pp. 1766-1769. (2005).

- [16] M. Jia, W. Li, H. Xu, S. Hou, Q. Ge, An integrated air–POM syngas/dimethyl ether process from natural gas, *Appl. Catal. A: Gen.*, Vol. 233, pp. 7. 2002.
- [17] (a) M. Xu, J. H. Lunsford, D. W. Goodman, Synthesis of dimethyl ether (DME) from methanol over solid-acid catalysts, *Appl. Catal. A: Gen.*, Vol. 149, pp. 289. 1997. (b) K. W. Jun, H. S. Lee, H. S. Roh, S. E. Park, Highly Water-Enhanced H-ZSM-5 Catalysts for Dehydration of Methanol to Dimethyl Ether *Bull. Korean Chem. Soc.*, Vol. 24, pp. 106. 2004.
- [18] R. Rauch. (2002). “Biomass Gasification to produce Synthesis Gas for Fuel Cell, Liquid Fuels and Chemicals”. IEA Bioenergy Agreement, Task 33: Thermal Gasification Biomass (2001-2003), p4-p8.
- [19] M. Xu, D. W. Goodman, Catalytic dehydration of methanol to dimethyl ether (DME) over Pd/Cab-O-Sil catalysts, *Appl. Catal. A: Gen.*, Vol. 149, pp. 303. 1997.
- [20] S. Lee, *Methanol Synthesis Technology*, CRC Press, 1990
- [21] J.B. Hansen, *Handbook of Heterogeneous Catalysis*, Weinham Germany, 1997
- [22] J. Skrzypek, J. Sloczynski, J. and S. Ledakowicz, *Methanol Synthesis Science and Engineering*, Polish Scientific Publishers, 1994
- [23] Y. Nitta, T. Fujimatsu, Y. Okamoto, T. Imanaka, Effect of starting salt on catalytic behaviour of Cu-ZrO₂ catalysts in methanol synthesis from carbon dioxide, *Catal. Lett.*, Vol. 17, pp. 157. 1993.
- [24] T. Takegawa, G. Pleizier, Y. Amenomiya, Methanol synthesis from CO₂ + H₂ : Characterization of catalysts by TPD, *Appl. Catal.*, Vol. 18, pp. 285. 1985.
- [25] A. P. Walker, R. M. Lambert, R. M. Nix, J. R. Jennings, Methanol synthesis over catalysts derived from CeCu₂: Transient studies with isotopically labelled reactants, *J. Catal.*, Vol. 138, pp. 694. 1992.
- [26] N. Kanoun, M. P. Astier, G. M. Pajonk, Catalytic properties of new Cu based catalysts containing Zr and/or V for methanol synthesis from a carbon dioxide and hydrogen mixture, *Catal. Lett.*, Vol. 15(3), pp. 231-235. 1992.
- [27] J. Barrault, Z. Rassoul, M. M. Bettahar, Promoting effects on catalytic properties of Cu/TiO₂ in carbon oxides conversion, *Stud. Surf. Sci. Catal.*, Vol. 61, pp. 367. 1991.

- [28] H. Arakawa, K. Sayama, K. Okabe, A. Murakami, Promoting Effect of TiO₂ Addition to CuO-ZnO Catalyst on Methanol Synthesis by Catalytic Hydrogenation of CO₂, *Stud. Surf. Sci. Catal.*, Vol. 77, pp. 389. 1993.
- [29] T. Inui, T. Takeguchi, A. Kohama, K. Tanida, Effective conversion of carbon dioxide to gasoline, *Energy Convers. Mgmt.* Vol. 33, pp. 513. 1992.
- [30] T. Inui, T. Takeguchi, A. Kohama, K. Kitagawa, New Frontiers in Catalysis, in: L. Guszi et al., Eds., *Proc. 10th Int. Congress on Catalysis, Budapest*, pp. 1453. 1992.
- [31] L. Fan, K. Fujimoto, Development of an active and stable ceria-supported palladium catalyst for hydrogenation of carbon dioxide to methanol, *Appl. Catal. A: Gen.*, Vol. 106, pp. L1. 1993.
- [32] K. Fujimoto, Y. Yu, Spillover effect on the stabilization of Cu-Zn catalyst for CO₂ hydrogenation to methanol, *Stud. Surf. Sci. Catal.*, Vol. 77, pp. 393. 1993.
- [33] T. Fujitani, M. Saito, Y. Kanai, T. Watanabe, J. Nakamura, T. Uchijima, Development of an active Ga₂O₃ supported palladium catalyst for the synthesis of methanol from carbon dioxide and hydrogen, *Appl. Catal. A: Gen.*, Vol. 125, pp. L199. 1995.
- [34] Y. Nitta, O. Suwata, Y. Okamoto, Copper-zirconia catalysts for methanol synthesis from carbon dioxide: Effect of ZnO addition to Cu-ZrO₂ catalysts, *Catal. Lett.* Vol. 26, pp. 345. 1994.
- [35] B. Denise, R. P. A. Sneed, B. Beguin, O. Cherifi, Supported copper catalysts in the synthesis of methanol: N₂O-titrations, *Appl. Catal.* Vol. 30, pp. 353. 1987.
- [36] J. S. Lee, K. H. Lee, S. Y. Lee, Y. G. Kim, A Comparative Study of Methanol Synthesis from CO₂/H₂ and CO/H₂ over a Cu/ZnO/Al₂O₃ Catalyst, *J. Catal.* Vol. 144, pp. 414. 1993.
- [37] B. J. Liaw, Y. Z. Chen., Liquid-phase synthesis of methanol from CO₂/H₂ over ultrafine CuB catalysts, *Appl. Catal. A: Gen.*, Vol. 206, pp. 245. 2001.
- [38] <http://www.intertek-cb.com/newsitetest/news/semlab.shtml>
- [39] Y. Zhang, J. Fei, Y. Yu, X. Zheng, Methanol Synthesis from CO₂ hydrogenation over Cu based catalyst supported on zirconia modified γ -Al₂O₃, *Energy Convers. Mgmt.*, Vol. 47, pp. 3360. 2006.

- [40] D. J. Dwyer, G. A. Somorjai, Hydrogenation of CO and CO₂ over iron foils : Correlations of rate, product distribution, and surface composition, *J. Catal.* Vol. 52, pp. 291. 1978.
- [41] G. D. Weatherbee, C.H. Bartholomew, Hydrogenation of CO₂ on group VIII metals : IV. Specific activities and selectivities of silica-supported Co, Fe, and Ru, *J. Catal.* Vol. 87, pp. 352. 1984.
- [42] M.D. Lee, J. F. Lee, C. S. Chang, T.Y. Dong, Effects of addition of chromium, manganese, or molybdenum to iron catalysts for carbon dioxide hydrogenation, *Appl. Catal.* Vol. 72, pp. 267. 1991.
- [43] G.C. Chinchin, K.C. Waugh, D.A. Whan, *Appl. Catal.* 25 (1986) 101.
- [44] G.C. Chinchin, M.S. Spencer, K.C. Waugh, D.A. Whan, *J. Chem. Soc., Faraday Trans.* 83 (1987) 2193.
- [45] W.X. Pan, R. Cao, D.L. Roberts, G.L. Griffin, *J. Catal.* 114 (1988) 440.
- [46] P.B. Rasmussen, M. Kazuta, I. Chorkendorff, *Surf. Sci.* 318 (1994) 267.
- [47] P.B. Rasmussen, P.M. Holmblad, C.V. Askgaard, C.V. Ovesen, P. Stoltze, J.K. Nørskov, I. Chorkendorff, *Catal. Lett.* 26 (1994) 373.
- [48] T.S. Askgaard, J.K. Nørskov, C.V. Ovesen, P. Stoltze, *J. Catal.* 156 (1995) 229.
- [49] R.G. Herman, K. Klier, G.W. Simmons, B.P. Finn, J.B. Bulko, T.P. Kobylinski, *J. Catal.* 56 (1979) 407.
- [50] G.R. Sheffer, T.S. King, *J. Catal.* 115 (1989) 376.
- [51] G.R. Sheffer, T.S. King, *J. Catal.* 116 (1989) 488.
- [52] J. Szanyi, D.W. Goodman, *Catal. Lett.* 10 (1991) 383.
- [53] R. Burch, R.J. Chappel, S.E. Golunski, *J. Chem. Soc., Faraday Trans.* 85 (1989) 3569.
- [54] R. Burch, S.E. Golunski, M.S. Spencer, *J. Chem. Soc., Faraday Trans.* 86 (1990) 2683.
- [55] R. Burch, R.J. Chappell, S.E. Golunski, *Catal. Lett.* 1 (1988) 439.
- [56] J. Yoshihara, C.T. Campbell, *J. Catal.* 161 (1996) 776.
- [57] C.V. Ovesen, B.S. Clausen, J. Schiøtz, P. Stoltze, H. Topsøe, J.K. Nørskov, *J. Catal.* 168 (1997) 133.
- [58] R.A. Hadden, B. Sakakini, J. Tabatabaei, K.C. Waugh, *Catal. Lett.* 44 (1997) 45.

- [59] Y. Kanai, T. Watanabe, T. Fujitani, M. Saito, J. Nakamura, T. Uchijima, *Catal. Lett.* 27 (1994) 67.
- [60] J. Nakamura, Y. Kanai, T. Uchijima, T. Fujitani, *Catal. Today* 28 (1996) 223.
- [61] Y. Kanai, T. Watanabe, T. Fujitani, T. Uchijima, J. Nakamura, *Catal. Lett.* 38 (1996) 157.
- [62] J. Nakamura, I. Nakamura, T. Uchijima, Y. Kanai, T. Watanabe, M. Saito, T. Fujitani, *Catal. Lett.* 31 (1995) 325.
- [63] J. Nakamura, I. Nakamura, T. Uchijima, Y. Kanai, T. Watanabe, M. Saito, T. Fujitani, *J. Catal.* 160 (1996) 65.
- [64] J. Nakamura, I. Nakamura, T. Uchijima, T. Watanabe, T. Fujitani, 11th Int. Congr. Catal., *Stud. Surf. Sci. Catal.* 101 (1996) 1389.
- [65] T. Fujitani, I. Nakamura, T. Uchijima, J. Nakamura, *Surf. Sci.* 383 (1997) 285.
- [66] I. Nakamura, Y. Nakano, T. Fujitani, T. Uchijima, J. Nakamura, *Surf. Sci.* 402/404 (1998) 92.
- [67] I. Nakamura, T. Fujitani, T. Uchijima, J. Nakamura, *Surf. Sci.* 400 (1998) 387.
- [68] G.C. Miller, C.H. Rochester, K.C. Waugh, *J. Chem. Soc., Faraday Trans.* 88 (1992) 1033.
- [69] J.E. Bailie, C.H. Rochester, G.J. Millar, *Catal. Lett.* 31, (1995) 333.
- [70] R. A. Koppel, C. Stocker, A. Baiker, Copper and silver-zirconia aerogels: Preparation, structural properties and catalytic behavior in methanol synthesis from carbon dioxide, *J. Catal.*, Vol. 179, pp. 515. 1998.
- [71] S. Lee, R. Aris, The distribution of active ingredients in supported catalysts prepared by impregnation, *Catal. Rev. Sci. Eng.*, Vol. 27, pp. 208-209. 1985
- [72] J.R. Jensen et al. / *Journal of Catalysis* 218 (2003) 67–77
- [73] P. Erno, *A practical guide to instrumental analysis*, CRC Press Inc, London. 1995.
- [74] A.B. Stiles, T.A.Koch, *Catalyst Manufacture*, Marcell Dekker Inc, New York, 1995.
- [75] J. Zyka, *Instrumentation in analytical chemistry II*, Ellis Horwood Ltd, London. 1994.
- [76] Li J T, Zhang W D, Zhou Y X. Study on high dispersion catalysts for methanol synthesis. *Petrochemical technology*, 1998, 27(1): 1–4.

- [77] Hong Z S, Deng J F, Fan K N, Cao Y. Preparation of methanol synthesis catalyst Cu/ZnO/Al₂O₃ by gel-network co-precipitation method. *Chemical Journal of Chinese Universities*, 2002, 23(4): 706–708.
- [78] Wang J F, Chang J, Yin X L, Lu P M. Preparation of Cu/ZnO/Al₂O₃ catalysts for methanol synthesis by urea-hydrolyzed precipitation method. *Journal of Fuel Chemistry and Technology*, 2004, 32(3): 378–380.
- [79] Li J L, Inui T. Enhancement in methanol synthesis activity of a copper/zinc/aluminum oxide catalyst by ultrasonic treatment during the course of the preparation procedure. *Appl Catal A*, 1996, 139(1–2): 87–96.
- [80] A.B. Stiles, T.A.Koch, *Catalyst Manufacture*, Marcell Deker Inc, New York, 1995.
- [81] H. Agaras, G. Carrella, M. A. Larborde, Copper catalyst for the steam reforming methanol. Analysis of preparation variables, *Appl. Catal.*, Vol. 45, pp. 53-60. 1988.
- [82] Bartholomeow, C.H., Baker, R.T.K. and Dadyburjor, D.B., 1991. Stability of Supported Catalysts: Sintering and Redispersion, J.A. Horsley, *talytica*, Studies Division.
- [83] M.Dunlap, J. E. Adaskaveg, *Introduction to the Scanning Electron Microscope Theory, Practice, & Procedures*, Facility for Advanced Instrumentation, U. C. Davis, 1997
- [84] Presentation, 'Introduction to FESEM Technology', Hi- Tech Instruments, UTP, 2009
- [85] www.scintag.com/Chapter 7- Basics of X-ray Diffraction
- [86] R. O. Idem, N. N. Bakhshi, Production of hydrogen from methanol: Catalyst characterization studies, *Ind. Eng. Chem. Res.*, Vol. 33, pp. 2047-2055. 1994.
- [87] W. R. M. Robinson, J. C. Mol, Characterization and catalytic activity of copper/alumina methanol synthesis catalysts, *Appl. Catal.*, Vol. 44, pp. 165-176. 1988.
- [88] *Instruction Manual, TPD/R/O 1100 Catalyst Surface Analyzer*, Thermo Finnigan Italia S.P.A, 2002
- [89] N. W. Hurst, S. J. Gentry, A. Jones, Temperature programmed reduction, *Catal. Rev. Sci. Eng.*, Vol. 24, pp. 233-309. 1982.
- [90] W. M. W. Wesley, *Thermal analysis*, Chichester: John Wiley & Sons. 1986.

- [91] N. Tyynelä, Master's Thesis: Kinetics of reduction of $\text{CrO}_x/\text{Al}_2\text{O}_3$, University of Technology, Espoo. 2000.
- [92] <http://www.ceinstruments.co.uk/tpd.html>
- [93] P.A. Jacobs, Catal. Rev. Sci. Eng., Vol. 24, pp. 415. 1982.
- [94] H. G. Karge, G. Ohlmann, H. Pfeifer, R. Fricke, Catalysis and adsorption by zeolites, Stud. Surf. Sci. Catal., Vol. 65, pp. 133. 1991.
- [95] A.A. Vasilevich, G.P. Shpiro, A.M. Alekseev, T.A. Semenova, M.I. Markina, T.A. Vasil'eva, O.G. Budkina, Kinet. Catal. 16 (1975) 1363.
- [96] B. Dvorak, J. Pasek, J. Catal. 18 (1970) 108.
- [97] G. Sengupta, D.K. Gupta, M.L. Kundi, S.P. Sen, J. Catal. 67 (1981) 223.
- [98] M. Muhler, L.P. Nielsen, E. Tornqvist, B.S. Clausen, H. Topsøe, Catal. Lett. 14 (1992) 241.
- [99] Th.J. Osinga, B.G. Linsen, W.P. van Beek, J. Catal. 7 (1967) 277.
- [100] A. Dandenkar, M.A. Vannice, J. Catal. 178 (1998) 621.
- [101] S. Sato, R. Takahashi, T. Sodesawa, K. Yuma, Y. Obata, J. Catal. 196 (2000) 195.
- [102] J.W. Evans, M.S. Wainwright, A.J. Bridgewater, D.J. Young, Appl. Catal. 7 (1983) 75.
- [103] G.E. Parris, K. Klier, J. Catal. 97 (1986) 374.
- [104] N. Pernicone, T. Fantinel, C. Baldan, P. Riello, F. Pinna, Appl. Catal. A 240 (2003) 199.
- [105] G.J.J. Bartley, R. Burch, R.J. Chappell, Appl. Catal. 43 (1988) 91.
- [106] J.J.F. Scholten, J.A. Konvalinka, Trans. Faraday Soc. 65 (1969) 2465.
- [107] G.C. Chinchin, C.M. Hay, H.D. Vandervell, K.C. Waugh, J. Catal. 103 (1987) 79.
- [108] A. Gervasini, S. Bennici, Appl. Catal. A: 281 (2005) 199–205
- [109] P. Gabbott, Principle and Applications of Thermal Analysis, Balckwell Publishing, 2008
- [110] C. Duval, R.E. Gesper, Inorganic Thermogravimetric Analysis, Elsevier, 1963
- [111] H.M. Mc Nair, J.M. Miller, Basic Gas Chromatography, Joh Wiley and Sons Inc, 1997
- [112] <http://www.chem.agilent.com>

- [113] R.H. Perry, D.W. Green, Perry's Chemical Engineering Handbook, McGraw Hill, 1999
- [114] M.J Rhodes., A.T. Bell ., The effects of Zirconia morphology on methanol synthesis from CO and H₂ over Cu/ZrO₂ catalysts, LBNL.57001_Pt_1, 2005
- [115] Guo X J, Li L M, Liu S M, Bao G L, Hou W H, J Fuel Chem Technol, , 35(3), 29–333, 200
- [116] L.Sunggyu, Methanol Synthesis Technology, CRC Press, 1990.
- [117] G.C. Chinchén, P.J. Denny, J.R. Jennings, M.S. Spencer, K.C. Waugh, Appl. Catal. 36, (1988), 1
- [118] K.C. Waugh, Catal. Lett. 58 (1999) 163.
- [119] T.S. Askgaard, J.K. Nørskov, C.V. Ovesen and P. Stoltze, A kinetic model of methanol synthesis, *Journal of Catalysis* **156** (1995), pp. 229–242.
- [120] *Federal Specification O-M 232 F*, U.S. Government Printing Office, Washington, D.C., June 5, 1975.
- [121] H.F. Rase, Handbook of commercial catalysts: heterogeneous catalysts, pg 93, CRC Press LLC, 2000.
- [122] T.N. Sorrell, Organic chemistry, pg488, University Science Books, 1996.
- [123] Wender, in *Catalysis and Surface Science* (H. Heinemann and G. A. Somorjai, eds.) ,p. 321, Marcel Dekker, New York,1984.
- [124] N. Iwasa, O. Yamamoto, T. Akazawa, S. Ohyama, and N. Takezawa, *J. Chem. Soc., Chem. Commun.*(18):13221323 (1991).
- [125] A. Aguilo and T. Horlenko, *Hydrocarbon Proc., November*:120130 (1980).
- [126] Y.R.Luo, Comprehensive Handbook of Chemical Bond Energies, pg 681&1030 - CRC Press, 2007
- [127] J. Guo, H. Lou, X. Zheng, The deposition of coke from methane on a Ni/MgAl₂O₄ catalyst, Carbon 45 (2007) 1314–1321

APPENDIX A

CALCULATION EXAMPLES

A-1 Calculation of Metal amount/Chemical Amount for Desired Metal Ratio

E.g. Catalyst **Sample C** calculation,

Table A-1: Catalyst Sample C Metal Composition Calculation

	Mol Ratio (atomic ratio)	Metal Molecular Weight	Mass, g	Mol	Atomic Metal %
Cu	4.5	63.546	5	0.078683	40.91
Zn	5	65.39	5.716768605	0.087426	45.45
Al	1	26.965	0.47148942	0.017485	9.09
Zr	0.5	91.224	0.797532496	0.008743	4.55

1. Set mol ratio of each element in catalysts sample C:

$$Cu: Zn: Al: Zr = 4.5:5:1:0.5$$

2. Set mass of Cu metal desired in catalyst sample C.

$$Mass\ Cu = 5g.$$

3. Calculate mol of metal Cu desired in catalyst sample C.

$$Mol\ Cu = \frac{Mass\ Cu}{MW_{Cu}} = \frac{5g}{63.546\frac{g}{mol}} = 0.07868mol$$

4. From determined mol ratio, calculate the mol of other elements, Zn, Zr, Al

$$\begin{aligned} (i)\ mol\ Zn &= \frac{mol\ ratio\ Zn}{mol\ ratio\ Cu} \times mol\ Cu \\ &= \frac{5}{4.5} \times 0.07868 \\ &= 0.08743 \end{aligned}$$

$$\begin{aligned}
 \text{(ii) } \text{mol Zr} &= \frac{\text{mol ratio Zr}}{\text{mol ratio Cu}} \times \text{mol Cu} \\
 &= \frac{0.5}{4.5} \times 0.07868 \\
 &= 0.00874
 \end{aligned}$$

$$\begin{aligned}
 \text{(iii) } \text{mol Al} &= \frac{\text{mol ratio Al}}{\text{mol ratio Cu}} \times \text{mol Al} \\
 &= \frac{1}{4.5} \times 0.07868 \\
 &= 0.01749
 \end{aligned}$$

5. From the mol of each elements, Calculate the,

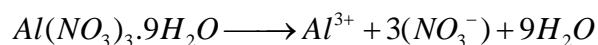
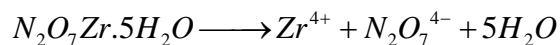
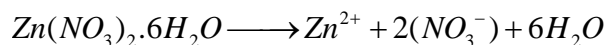
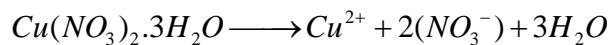
a) Mass of each metal in the desired product:

$$\begin{aligned}
 \text{(i) } \text{Mass Zn} &= \text{mol Zn} \times MW_{\text{Zn}} \\
 &= 0.08743 \times 65.39 \\
 &= 5.7168
 \end{aligned}$$

$$\begin{aligned}
 \text{(ii) } \text{Mass Zr} &= \text{mol Zr} \times MW_{\text{Zr}} \\
 &= 0.00874 \times 91.224 \\
 &= 0.7975
 \end{aligned}$$

$$\begin{aligned}
 \text{(iii) } \text{Mass Al} &= \text{mol Al} \times MW_{\text{Al}} \\
 &= 0.01749 \times 26.965 \\
 &= 0.4715\text{g}
 \end{aligned}$$

b) Mass of chemical required to produce desired product metal ratio:



Thus;

$$(i) \text{ Mass } Cu(NO_3)_2 \cdot 3H_2O = \text{ mol } Cu(NO_3)_2 \cdot 3H_2O \times MW_{Cu(NO_3)_2 \cdot 3H_2O}$$

$$\rightarrow \text{ mol } Cu(NO_3)_2 \cdot 3H_2O = \text{ mol } Cu^{2+} = 0.07868$$

$$\begin{aligned} \rightarrow MW_{Cu(NO_3)_2 \cdot 3H_2O} &= \sum_i^N MW_i = MW_{Cu} + 2MW_{NO_3} + 3MW_{H_2O} \\ &= 63.546 + 2 \times 62.00 + 3 \times 18.00 \\ &= 241.546 \end{aligned}$$

$$\begin{aligned} \text{Mass } Cu(NO_3)_2 \cdot 3H_2O &= 0.07868 \times 241.546 \\ &= 19.01\text{g} \end{aligned}$$

$$(ii) \text{ Mass } Zn(NO_3)_2 \cdot 6H_2O = \text{ mol } Zn(NO_3)_2 \cdot 6H_2O \times MW_{Zn(NO_3)_2 \cdot 6H_2O}$$

$$\rightarrow \text{ mol } Zn(NO_3)_2 \cdot 6H_2O = \text{ mol } Zn^{2+} = 0.08743$$

$$\begin{aligned} \rightarrow MW_{Zn(NO_3)_2 \cdot 6H_2O} &= \sum_i^N MW_i = MW_{Zn} + 2MW_{NO_3} + 6MW_{H_2O} \\ &= 65.39 + 2 \times 62.00 + 6 \times 18.00 \\ &= 297.39 \end{aligned}$$

$$\begin{aligned} \text{Mass } Zn(NO_3)_2 \cdot 6H_2O &= 0.08743 \times 297.39 \\ &= 26.01\text{g} \end{aligned}$$

$$(iii) \text{ Mass } N_2O_7Zr \cdot 5H_2O = \text{ mol } N_2O_7Zr \cdot 5H_2O \times MW_{N_2O_7Zr \cdot 5H_2O}$$

$$\rightarrow \text{ mol } N_2O_7Zr \cdot 5H_2O = \text{ mol } Zr^{4+} = 0.00874$$

$$\begin{aligned} \rightarrow MW_{N_2O_7Zr \cdot 5H_2O} &= \sum_i^N MW_i = MW_{Zr} + MW_{N_2O_7} + 5MW_{H_2O} \\ &= 91.224 + 140 + 6 \times 18.00 \\ &= 339.224 \end{aligned}$$

$$\begin{aligned} \text{Mass } Cu(NO_3)_2 \cdot 3H_2O &= 0.00874 \times 339.224 \\ &= 2.965\text{g} \end{aligned}$$

$$\begin{aligned}
 \text{(iv) } Mass \text{ Al(NO}_3)_3 \cdot 9\text{H}_2\text{O} &= mol \text{ Al(NO}_3)_3 \cdot 9\text{H}_2\text{O} \times MW_{\text{Al(NO}_3)_3 \cdot 9\text{H}_2\text{O}} \\
 \rightarrow mol \text{ Al(NO}_3)_3 \cdot 9\text{H}_2\text{O} &= mol \text{ Al}^{3+} = 0.01749 \\
 \rightarrow MW_{\text{Al(NO}_3)_3 \cdot 9\text{H}_2\text{O}} &= \sum_i^N MW_i = MW_{\text{Al}} + 3 \times MW_{\text{NO}_3} + 9MW_{\text{H}_2\text{O}} \\
 &= 26.965 + 3 \times 62 + 9 \times 18.00 \\
 &= 374.965
 \end{aligned}$$

$$\begin{aligned}
 Mass \text{ Al(NO}_3)_3 \cdot 9\text{H}_2\text{O} &= 0.01749 \times 374.965 \\
 &= 6.559 \text{ g}
 \end{aligned}$$

6. Atomic Metal % calculation,

$$\begin{aligned}
 \text{Metal Atomic \%} &= \frac{\text{Atoms}_{\text{Metal}}}{\sum_i^N \text{Atoms}_i} \\
 &= \frac{\text{Mol}_{\text{Metal}} \times N_A}{N_A \times \sum_i^N \text{Mol}_i} \\
 &= \frac{\text{Mol}_{\text{Metal}}}{\sum_i^N \text{Mol}_i} = \frac{\text{Mol Ratio}_{\text{Metal}}}{\sum_i^N \text{Mol Ratio}_i}
 \end{aligned}$$

$$\begin{aligned}
 \text{a. Cu Atomic \%} &= \frac{\text{Mol Ratio Cu}}{\sum_i^N \text{Mol Ratio}_i} \times 100\% \\
 &= \frac{4.5}{4.5 + 5 + 1 + 0.5} \times 100\% = 40.9\%
 \end{aligned}$$

$$\begin{aligned}
 \text{b. Zn Atomic \%} &= \frac{\text{Mol Ratio Zn}}{\sum_i^N \text{Mol Ratio}_i} \times 100\% \\
 &= \frac{5}{4.5 + 5 + 1 + 0.5} \times 100\% = 45.45\%
 \end{aligned}$$

$$\begin{aligned} \text{c. Zr Atomic \%} &= \frac{\text{Mol Ratio Zr}}{\sum_i^N \text{Mol Ratio } i} \times 100\% \\ &= \frac{0.5}{4.5 + 5 + 1 + 0.5} \times 100\% = 4.55\% \end{aligned}$$

$$\begin{aligned} \text{d. Al Atomic \%} &= \frac{\text{Mol Ratio Al}}{\sum_i^N \text{Mol Ratio } i} \times 100\% \\ &= \frac{1}{4.5 + 5 + 1 + 0.5} \times 100\% = 9.09\% \end{aligned}$$

A-2: Calculation of Metal Surface Area, Dispersion and Mean Particle Size

Table A-2: Catalyst Sample C Copper sites physical properties

Copper metal density, ρ_{Cu}	8.92 g/cm ³
SK (Cu constant-spherical or cubic)	6
Copper Molecular Weight, MW_{Cu}	63.546
Stoichiometric Factor, SF--> Cu ₂ O	2.00
Stoichiometric Factor, SF --> CuO	1
Avogadro No. N_A	6.022x10 ²³ no atoms/ mol atoms
No Cu atoms per square meter, c_m	1.47x10 ¹⁹ no. atoms/m ²
Calibrated Signal to gas mol factor , FC	0.000106745 $\mu\text{mol/mV}$

Example: Catalyst Sample C properties calculation:

1. Obtain Data from MSA analysis, Sample C

Table A-3: Low and High Temperature Peak Signal magnitude, s-TPR analysis

Cu wt% in catalyst, W_{Cu}	41.71
Catalyst Mass (g)	0.17
Low T peak ads ,mV (Cu ₂ O)	32185
High T peak ads ,mV (CuO)	377731
sum(low and high T peak)	409916

2. Calculate mol of H₂ adsorbed at Low T, High T and their sum.

i) Low T Peak, Cu₂O:

$$\begin{aligned}\text{mol H}_2 \text{ adsorbed} &= \frac{\text{Signal(mV)} \times \text{FC}(\mu\text{mol/mV})}{\text{Catalyst Mass(g)}} \\ &= \frac{32185 \times 0.000106745}{0.17} \\ &= 20.04 \mu\text{mol/g}_{\text{cat}}\end{aligned}$$

ii) High T Peak, CuO:

$$\begin{aligned}\text{mol H}_2 \text{ adsorbed} &= \frac{\text{Signal(mV)} \times \text{FC}(\mu\text{mol/mV})}{\text{Catalyst Mass(g)}} \\ &= \frac{377731 \times 0.000106745}{0.17} \\ &= 237.18 \mu\text{mol/g}_{\text{cat}}\end{aligned}$$

iii) Sum T Peak, CuO & Cu₂O:

$$\begin{aligned}\text{mol H}_2 \text{ adsorbed} &= \text{Low T} + \text{High T} \\ &= 20.04 + 237.18 \\ &= 257.22 \mu\text{mol/g}_{\text{cat}}\end{aligned}$$

3. Calculate Metal Surface Areas, MSA at Low T, High T and their sum

i) Low T Peak, Cu₂O:

$$\begin{aligned}
 MSA(m^2/g_{Cu}) &= \frac{\text{mol H}_2 \times \text{S.F} \times N_A}{10^4 \times c_m \times W_{Cu}} \\
 &= \frac{20.04 \left(\frac{\mu\text{mol}}{g_{\text{cat}}} \right) \times 2 \times 6.022 \times 10^{23} \left(\frac{\text{no atoms}}{\text{mol atoms}} \right)}{10^4 \left(\frac{\mu\text{mol}}{\text{mol}} \times \frac{\text{Ratio}}{100 \text{ wt\%}} \right) \times 1.47 \times 10^{19} \left(\frac{\text{no atoms}}{m^2} \right) \times 41.71(\text{wt\%})} \\
 &= 3.94 \text{ m}^2/g_{Cu}
 \end{aligned}$$

(ii) High T Peak, CuO:

$$\begin{aligned}
 MSA(m^2/g_{Cu}) &= \frac{\text{mol H}_2 \times \text{S.F} \times N_A}{10^4 \times c_m \times W_{Cu}} \\
 &= \frac{237.18 \left(\frac{\mu\text{mol}}{g_{\text{cat}}} \right) \times 1 \times 6.022 \times 10^{23} \left(\frac{\text{no atoms}}{\text{mol atoms}} \right)}{10^4 \left(\frac{\mu\text{mol}}{\text{mol}} \times \frac{\text{Ratio}}{100 \text{ wt\%}} \right) \times 1.47 \times 10^{19} \left(\frac{\text{no atoms}}{m^2} \right) \times 41.71(\text{wt\%})} \\
 &= 23.10 \text{ m}^2/g_{Cu}
 \end{aligned}$$

(iii) Sum T Peak, CuO & Cu₂O:

$$\begin{aligned}
 MSA(m^2/g_{Cu}) &= \text{LowT} + \text{High T} \\
 &= 23.10 + 3.94 \\
 &= 27.04 \text{ m}^2/g_{Cu}
 \end{aligned}$$

4. Calculate Mean Particle Diameter, ϕ for catalysts sample C

$$\begin{aligned}
 \phi_{av} \text{ (nm)} &= \frac{10^3 \times \text{SK}}{\text{MSA}(\text{sum}) \times \rho_{Cu}} \\
 &= \frac{10^3 \times 6}{27.04 \left(\frac{m^2}{g_{Cu}} \right) \times 8.92 \left(\frac{g_{Cu}}{cm^3} \right)} \\
 &= 24.88 \text{ nm}
 \end{aligned}$$

5. Calculate Cu Metal Dispersions DCu^1 and DCu^2

$$\begin{aligned}
 D_{Cu}^1 &= \frac{\text{Surface Cu (Cu}_2\text{O)}}{\text{Surface Cu (Cu}_2\text{O)} + \text{Bulk Cu (CuO)}} \times 100\% \\
 &= \frac{\text{MSA Low T}}{\text{Sum MSA}} \times 100\% \\
 &= \frac{3.94}{27.04} \times 100\% \\
 &= 14.57\%
 \end{aligned}$$

$$\begin{aligned}
 D_{Cu}^2 &= \frac{\text{adsorbing Cu atoms}}{\text{total Cu atoms}} = \frac{\text{MSA (sum)} \times \text{MW}_{Cu} \times c_m}{N_A} \times 100\% \\
 &= \frac{27.04 \text{ m}^2/\text{g}_{Cu} \times 47.41 (\text{wt}\%) \times 1.47 \times 10^{19} (\text{no atoms}/\text{m}^2)}{6.022 \times 10^{23} (\text{no atoms}/\text{mol atoms})} \times 100\% \\
 &= 4.19\%
 \end{aligned}$$

A-3: CO Conversion and Selectivities Calculation

Example: Catalyst Sample C activity calculation:

1. Obtain Reaction data from Gas Chromatograph for catalyst sample C.

Table A-4: Catalyst Sample C Reaction Product Composition in mol%

time(hr)	Reactant		Product (mol %)					
	CO	H2	CH3OH	Ethanol	DME	Methyl Formate	CO2	CH4
0	35.750	71.866	0.000	0.000	0.000	0.000	1.023	0.000
0.5	35.311	71.169	0.083	0.000	0.000	0.002	7.757	0.006
1	35.592	71.139	1.393	0.015	0.000	0.009	0.622	0.006
1.5	35.516	71.254	2.296	0.020	0.000	0.012	1.625	0.006
2	35.302	71.095	2.715	0.022	0.000	0.013	1.591	0.006
2.5	35.465	71.514	3.119	0.024	0.000	0.014	1.566	0.005
3	35.664	71.609	3.051	0.026	0.000	0.013	0.951	0.005
3.5	35.736	71.500	2.947	0.026	0.000	0.014	0.000	0.005

2. Calculate CO conversion, X_{CO} for Catalyst sample C.

$$X_{CO} = \frac{(n_{CO})^i - (n_{CO})^f}{(n_{CO})^i \times g_{cat}} \times 100\%$$

E.g. At time 1 hour:

$$X_{CO} = \frac{35.75 - 35.59}{35.75 \times 1} \times 100\% \\ = 0.447\%$$

3. Calculate MeOH Selectivity, S_{MeOH} for Catalyst sample C

$$S_{MeOH} = \frac{(n_{MeOH})^f}{\sum (n_x)^f} \times 100\%$$

E.g. At time 1 hour:

$$S_{MeOH} = \frac{1.393}{(1.393 + 0.015 + 0.000 + 0.009 + 0.622 + 0.006)} \times 100\% \\ = 68.13\%$$

4. Calculate MeOH Yield, Y_{MeOH} for Catalyst sample C

$$Y_{CH_3OH} = \frac{(n_{CH_3OH})^f}{(n_{CO})^i} \times 100\%$$

E.g. At time 1 hour:

$$Y_{CH_3OH} = \frac{1.393}{35.75} \times 100\% \\ = 3.897\%$$

Table A-5: CO Conversion, MeOH Yield and Selectivity, Catalyst Sample C

Time(hr)	CO conversion (%)	Methanol Selectivity (%)	MeOH Yield (%)
	-	-	0.00
0	1.23	1.05	0.23
0.5	0.44	68.13	3.90
1	0.65	57.98	6.42
1.5	1.25	62.46	7.60
2	0.80	65.96	8.72
2.5	0.24	75.41	8.53
3	0.09	98.55	8.50
3.5	0.04	98.47	8.24

5. Calculate Yields and Selectivities for Ethanol, DME, Methyl Formate, CH₄ and CO₂ for Catalyst sample C.

$$S_x = \frac{(n_x)^f}{\sum_i (n_i)^f} \times 100\%$$

Table A-6: Yields of Byproducts, Catalyst Sample C

Time(hr)	DME Yield (%)	Ethanol Yield (%)	MF Yield (%)	CO ₂ Yield (%)	CH ₄ Yield (%)
0	0.0000	0.0000	0.0000	2.8616	0.0011
0.5	0.0000	0.0000	0.0063	21.9677	0.0167
1	0.0000	0.0434	0.0241	1.7462	0.0167
1.5	0.0000	0.0572	0.0346	4.5751	0.0182
2	0.0000	0.0620	0.0370	4.5067	0.0166
2.5	0.0000	0.0688	0.0385	4.4167	0.0150
3	0.0000	0.0722	0.0375	2.6657	0.0135
3.5	0.0000	0.0739	0.0391	0.0000	0.0152

$$Y_x = \frac{(n_x)^f}{(n_{CO})^i} \times 100\%$$

Table A-7: Selectivities of Byproducts, Catalyst Sample C

Time(hr)	DME Selectivity (%)	Ethanol Selectivity (%)	MF Selectivity (%)	CO ₂ Selectivity (%)	CH ₄ Selectivity (%)
0	-	-	-	-	-
0.5	0.00	0.00	0.03	98.84	0.08
1	0.00	0.76	0.42	30.40	0.29
1.5	0.00	0.51	0.31	41.03	0.16
2	0.00	0.50	0.30	36.60	0.13
2.5	0.00	0.52	0.29	33.12	0.11
3	0.00	0.64	0.33	23.50	0.12
3.5	0.00	0.34	0.47	0.00	0.18

APPENDIX B XRD SPECTRUMS

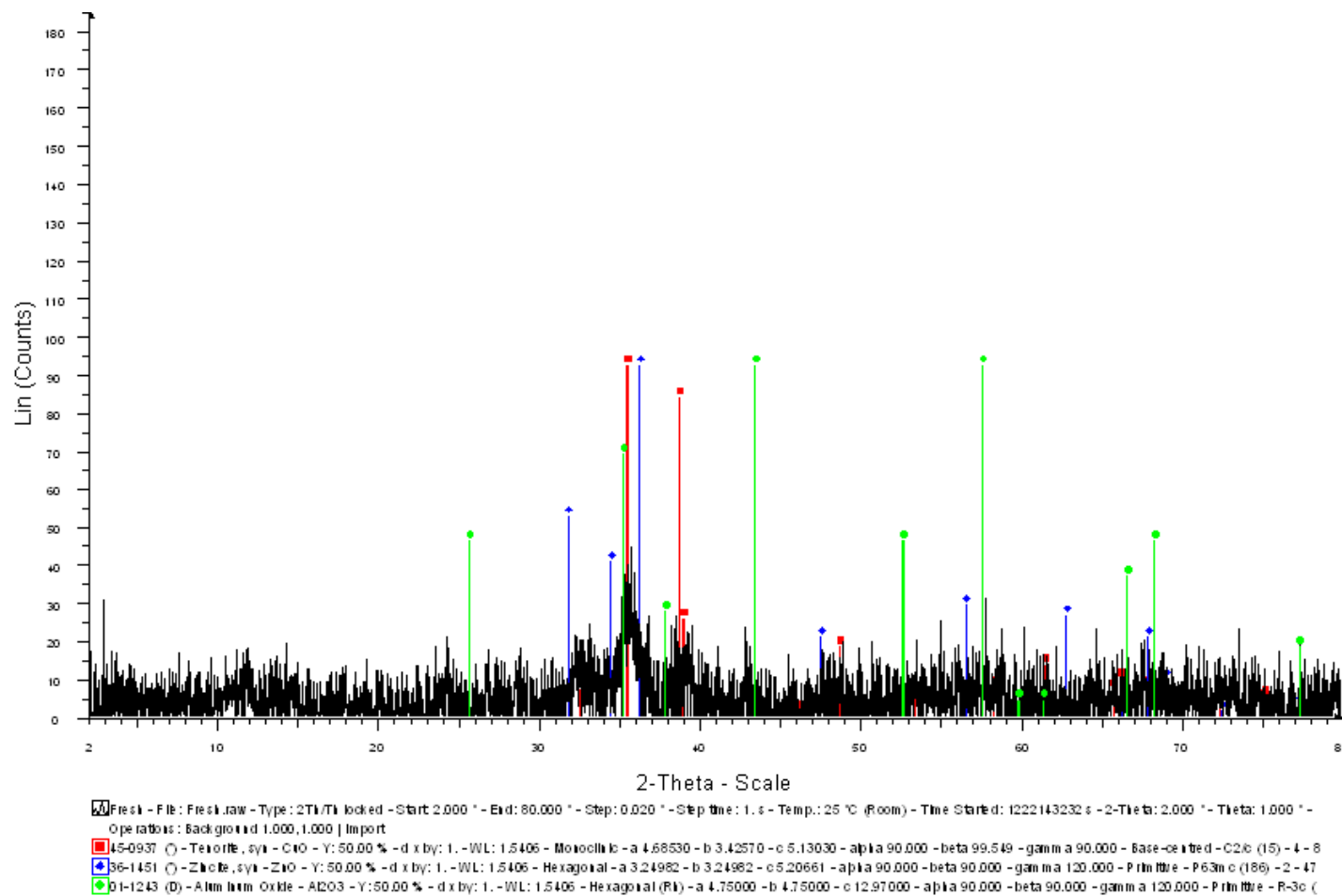


Figure B-1: XRD Spectrum of commercial Catalyst Sample, Ind

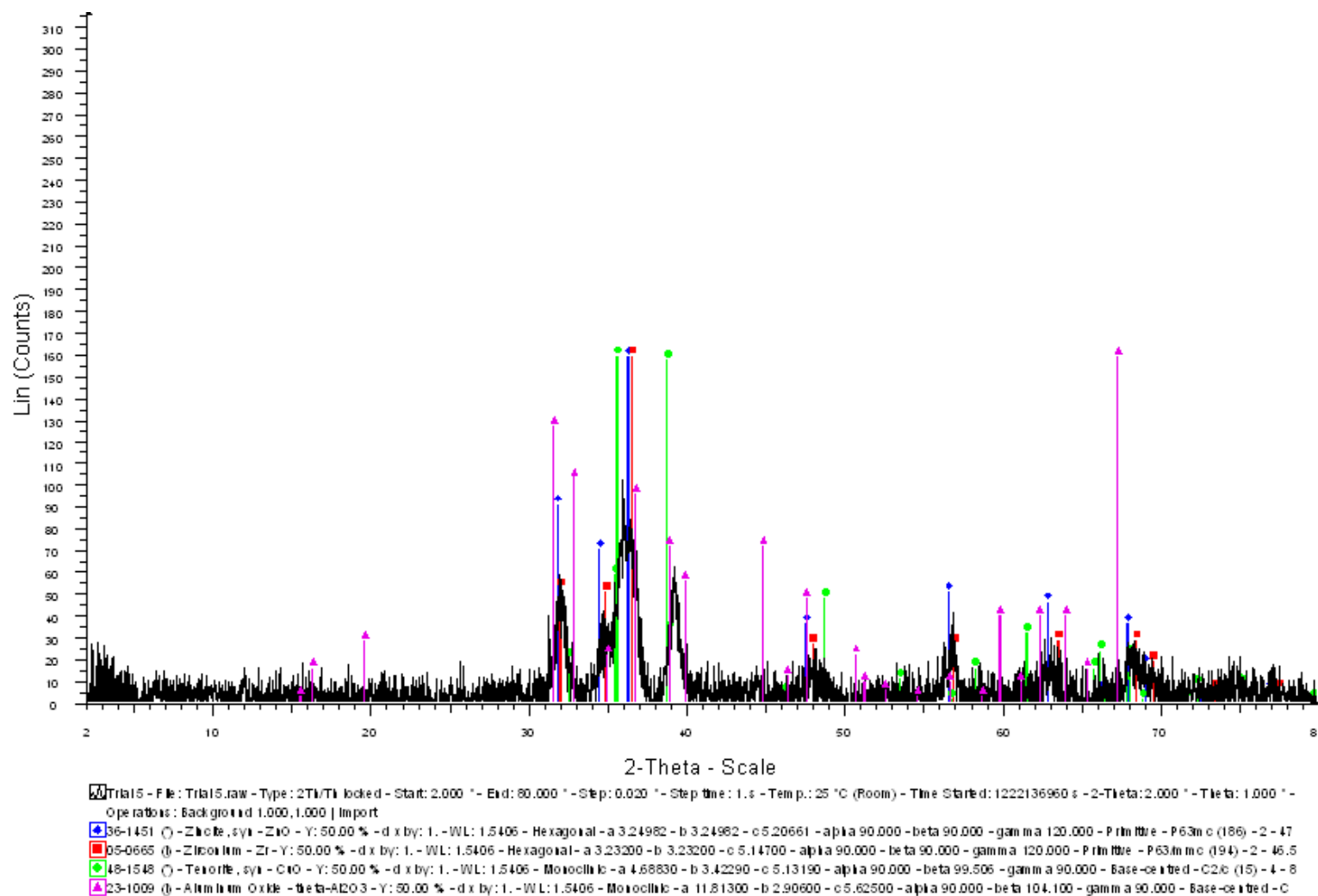


Figure B-2: XRD Spectrum of prepared Catalyst Sample A

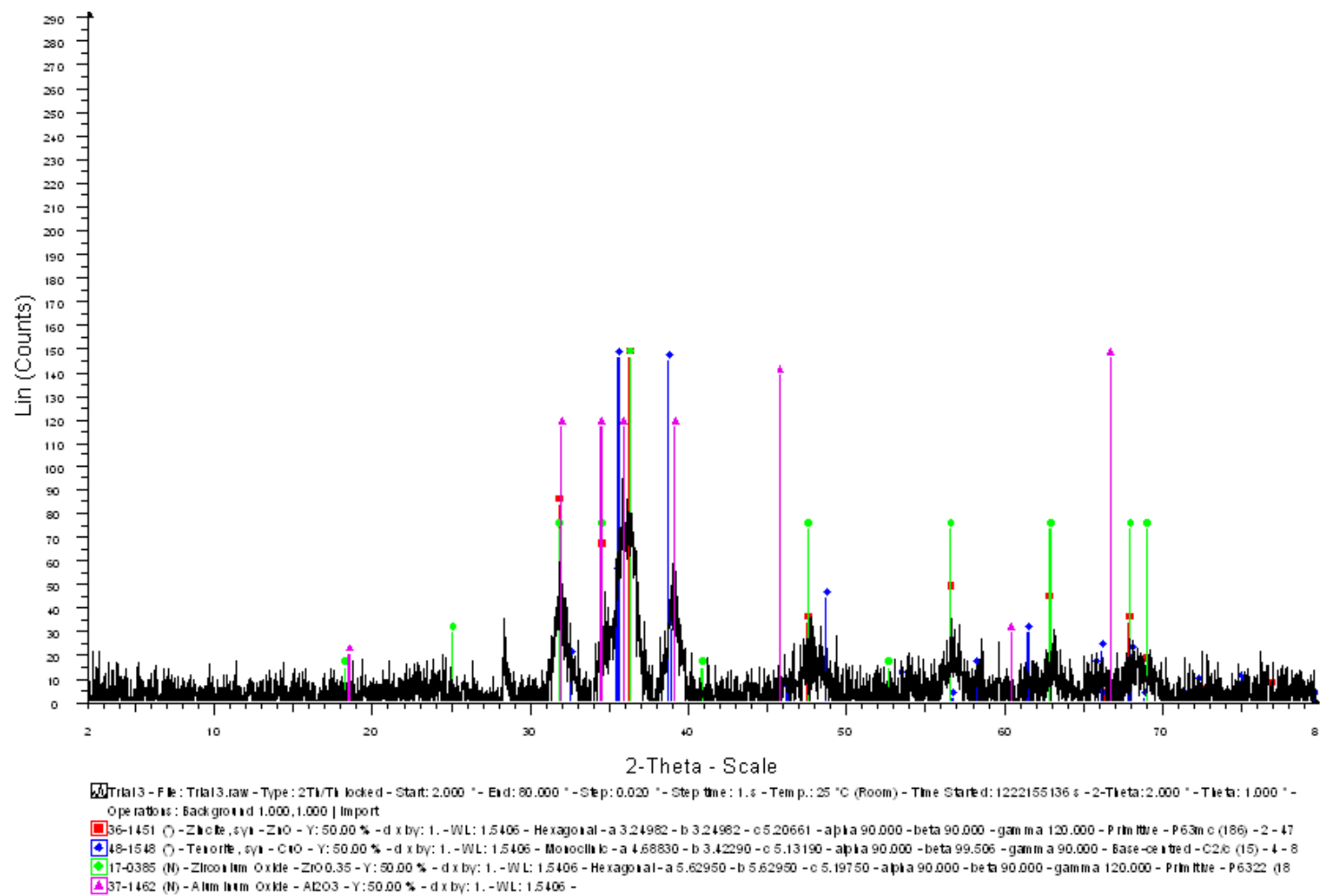


Figure B-3: XRD Spectrum of prepared Sample B

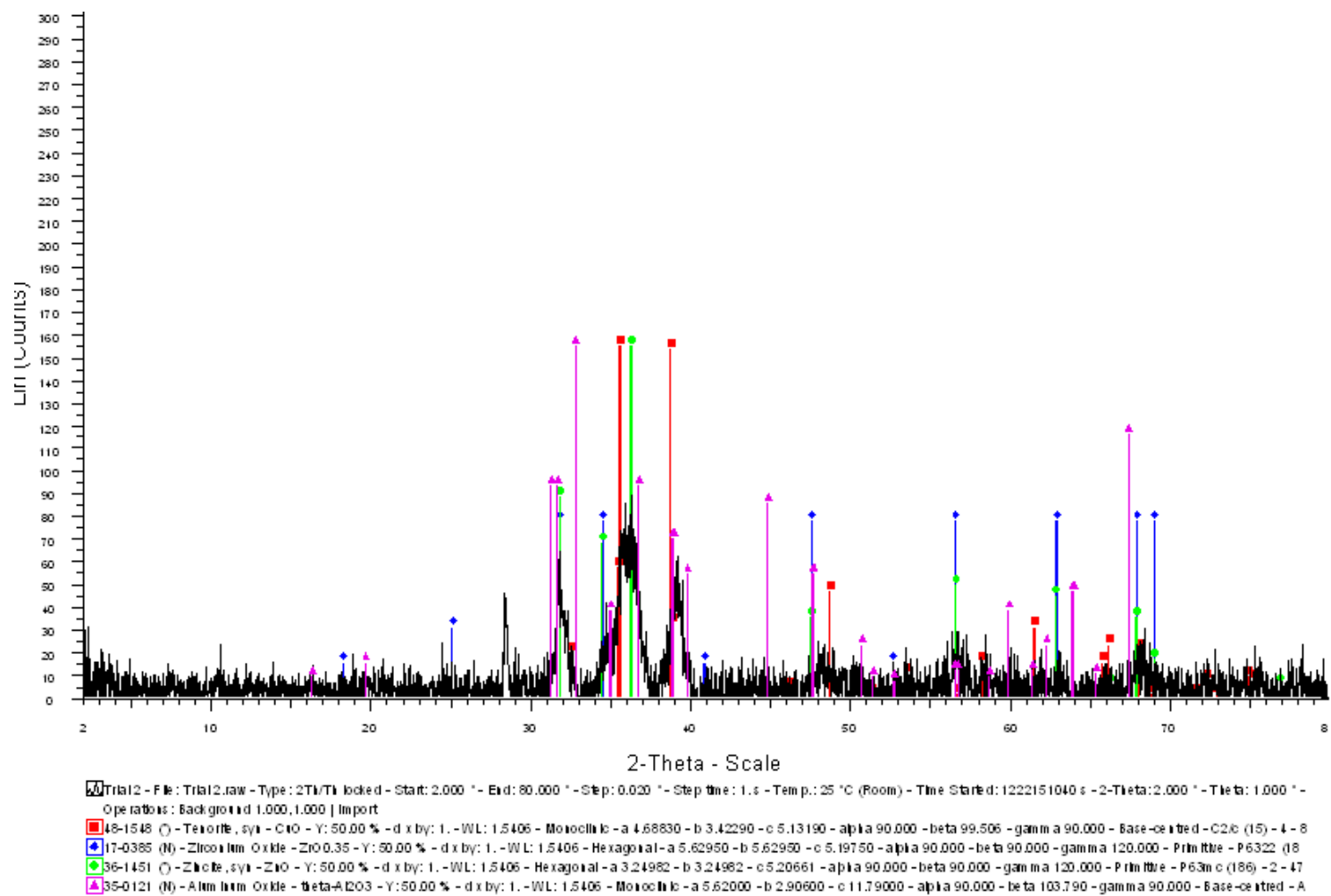


Figure B-4: XRD Spectrum of prepared Sample C

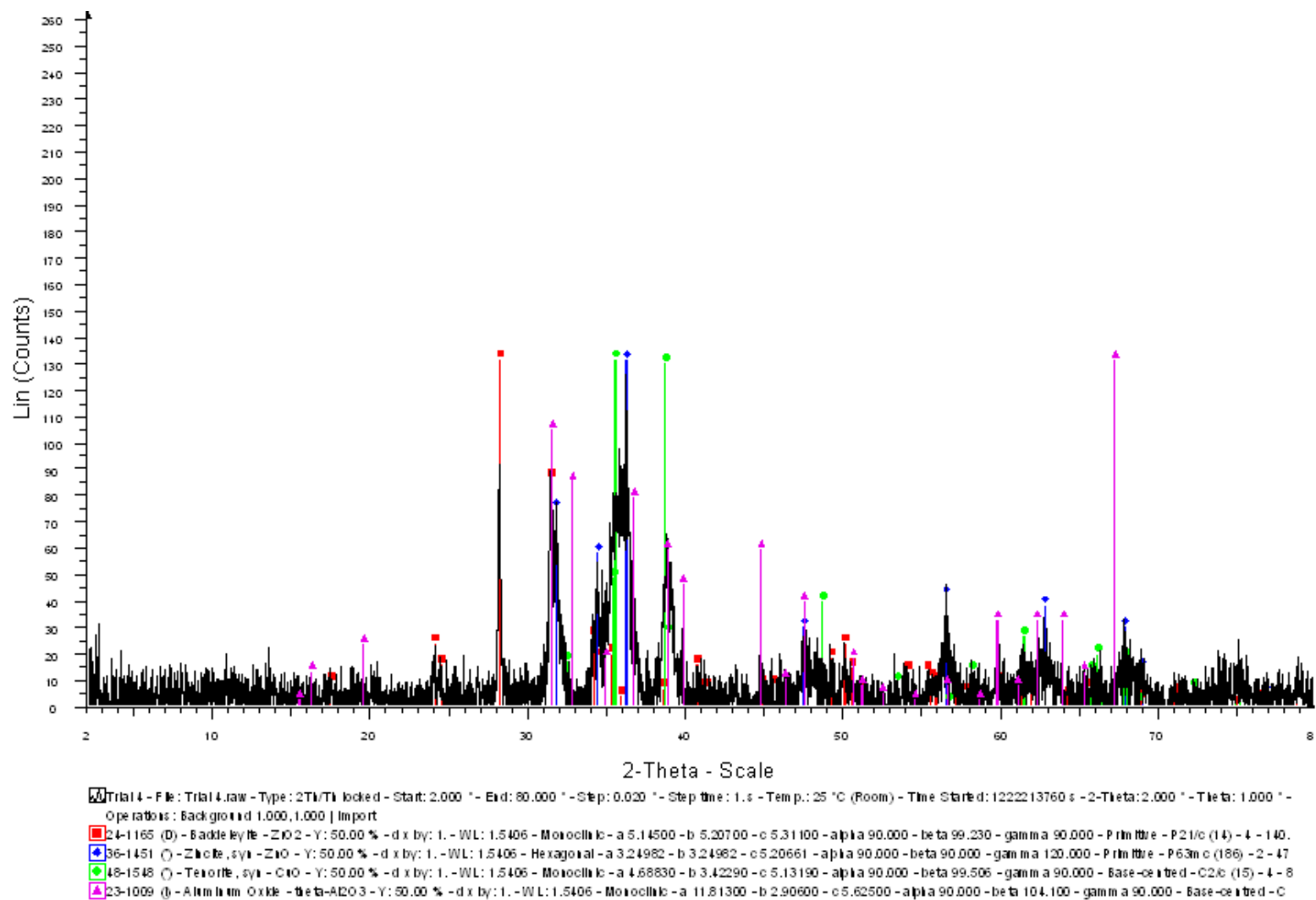


Figure B-5: XRD Spectrum of prepared Sample D

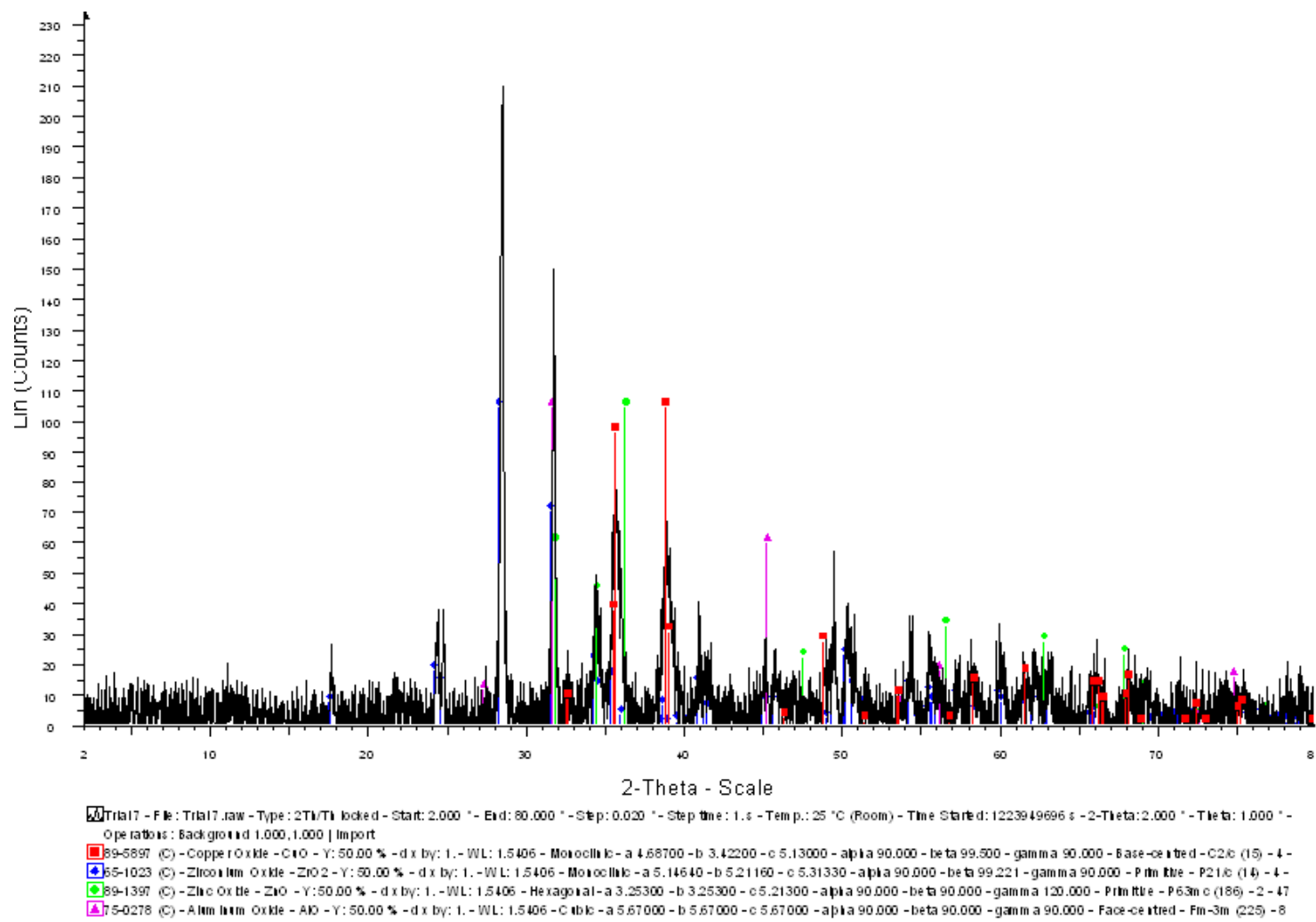


Figure B-6: XRD Spectrum of prepared Sample F

APPENDIX C

TGA Plots

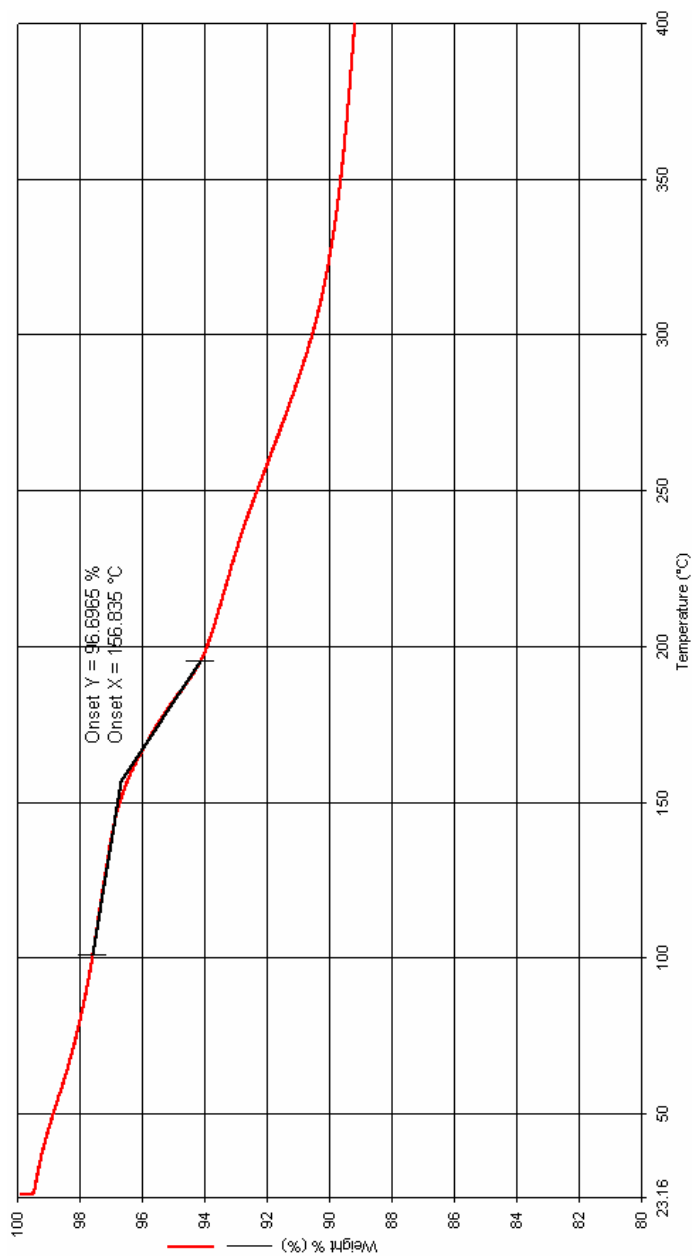


Figure C-1: TGA plot of Weight change (wt %) vs. Temperature (°C), Sample A calcined

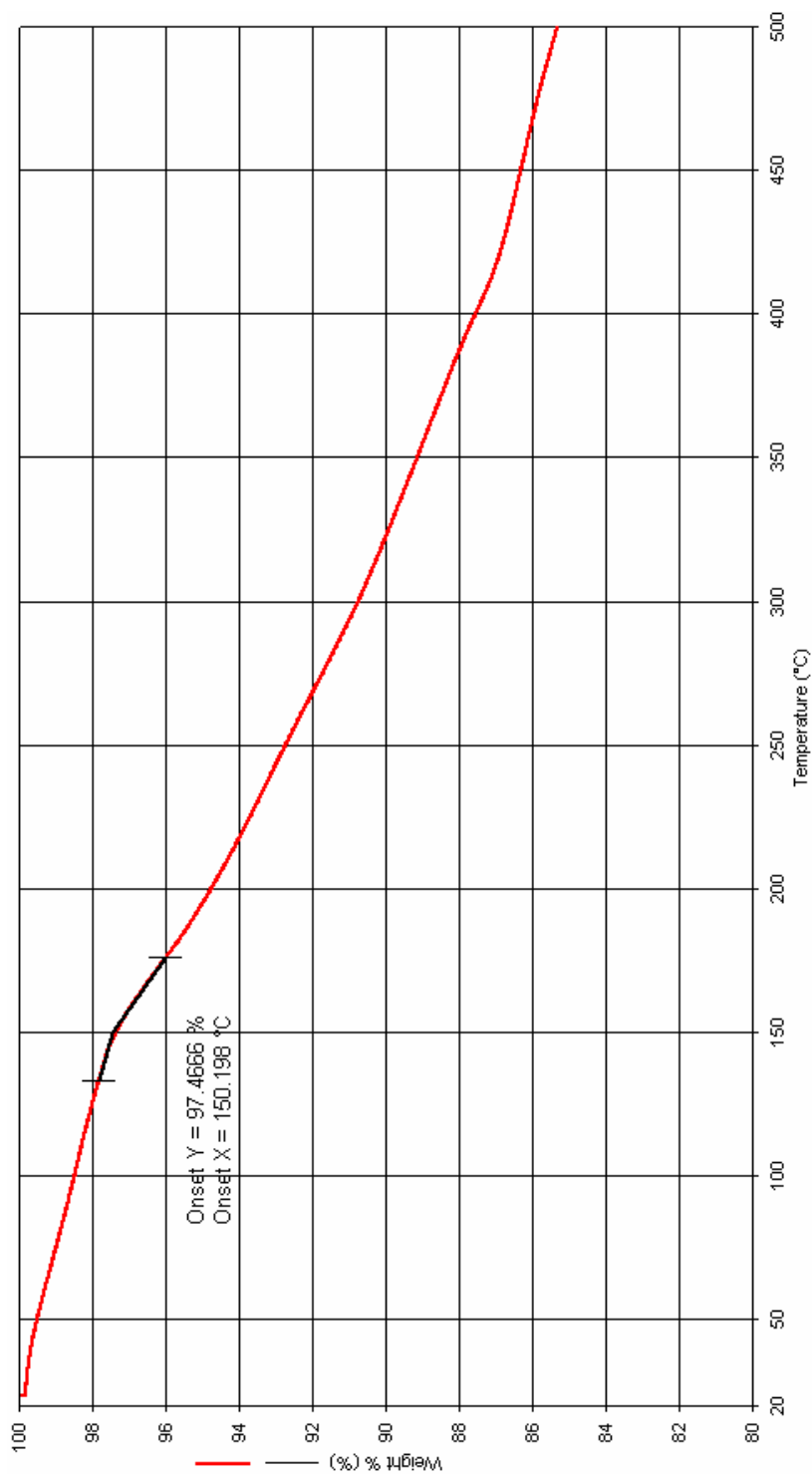


Figure C-2: TGA plot of Weight change (wt %) vs. Temperature (°C), commercial Sample Ind calcined

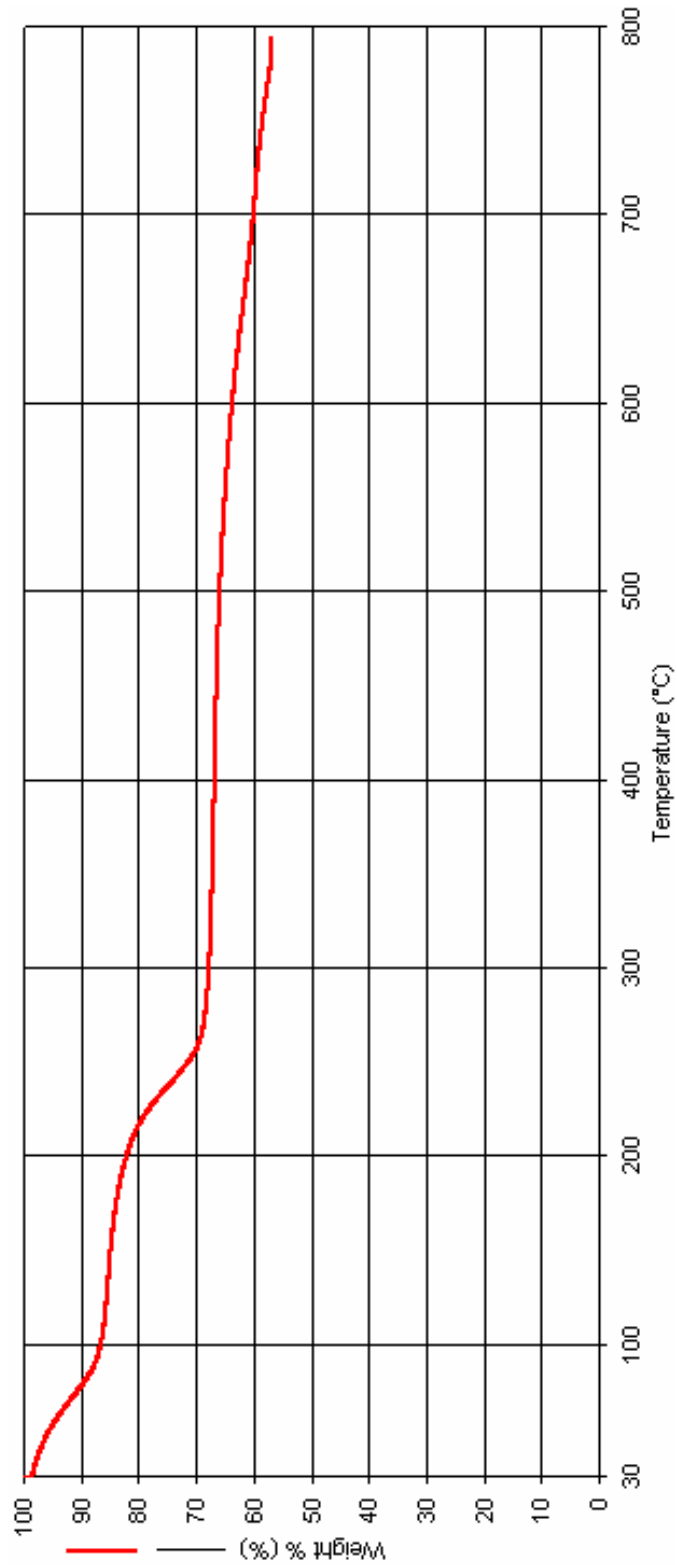


Figure C-3: TGA plot of Weight change (wt %) vs. Temperature (°C), commercial Sample C Dried

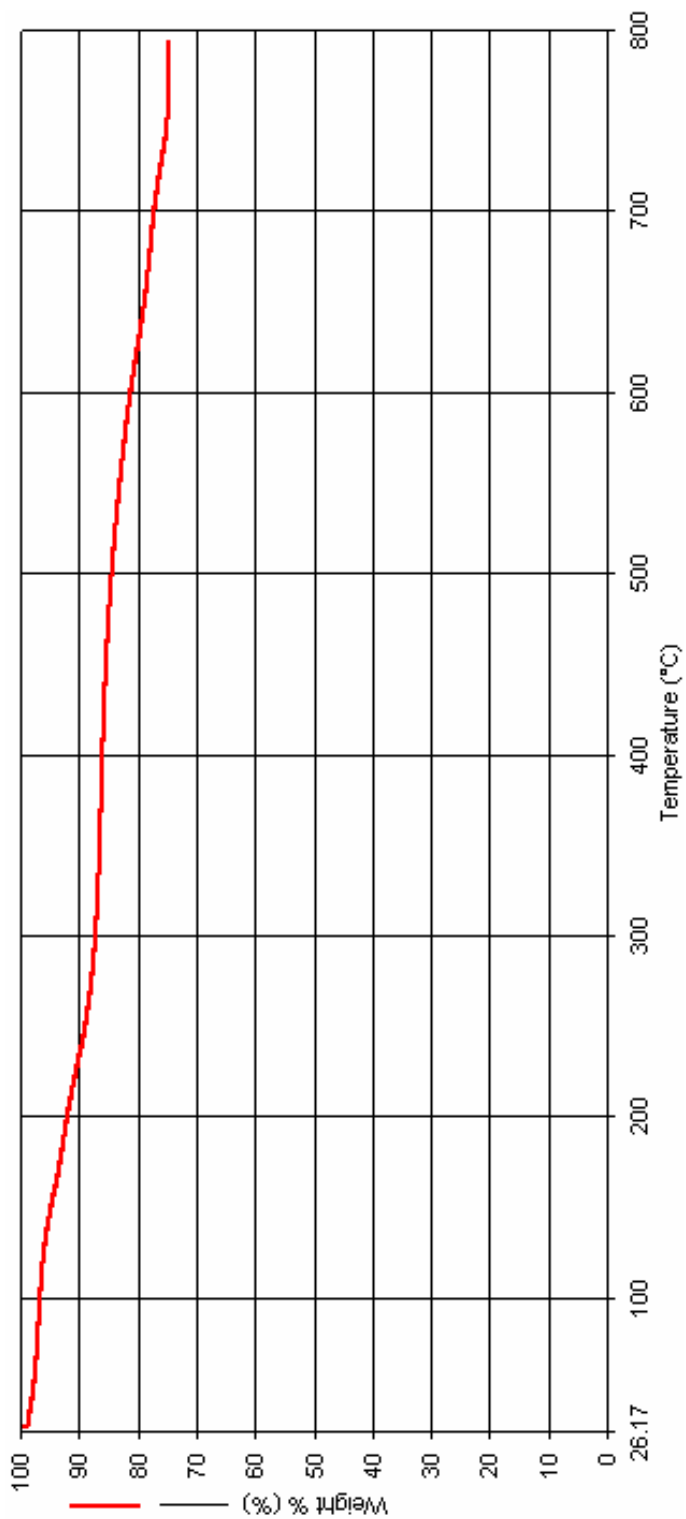


Figure C-4 TGA plot of Weight change (wt %) vs. Temperature (°C), commercial Sample C Calcined at 350°C

APPENDIX D

Reactor Standard Operating Procedure

I. Catalysts Sample Loading Into Reactor

1. Open glass door panel to expose the reactor
2. Use Allen key to loosen tubular reactor shell from its support
3. Remove the Inner shell from the Outer shell and lock the filter to the base of the Inner shell tube
4. Insert Alumina balls into Inner shell until $\frac{1}{2}$ of tube length is full
5. Insert $\frac{1}{2}$ cm thick layer of Quartz wool and then insert 1g of catalysts sample
6. Insert another $\frac{1}{2}$ cm thick layer of Quartz wool and then insert alumina balls until catalysts is firmly placed in the middle of the reactor tube.
7. Insert Inner shell into the Outer shell and Screw the Reactor tube back to its support
8. Clamp heater arms on both side and shut the glass door panel tight
9. CAUTION: Since the thermocouple is located on the bottom of the reactor, beware not to accidentally drop the reactor while removing reactor from its support.

II. Reactor Initiation

1. Turn the main switch 'ON' located on the control panel
2. Ensure that all gas lines are tightly connected to the reactor inlet.
3. Perform a Pressure Leak test by flowing Nitrogen gas at 3 bars into the pressure monitoring the drop for 15 minutes. If there is rapid Pressure drop in th reactor ,

perform leak test along the lines to detect leak site. If there is one, STOP all operation and repair the leaking pipeline.

4. If there is no Pressure drop, purge Nitrogen gas from the Pressure relief valve
5. To start reduction process, set the desired Temperature at the Temperature controller located on the control panel
6. Open the Needle valve located beside the reactor manually as well as the check valve switch located on the control panel for desired gas flow line.
7. Open gas flow from cylinder and set regulator to desired Pressure in the reactor
8. Monitor the Pressure gauge on the reactor to obtain the desired Reactor Pressure
9. Switch the heater on from the control panel to begin heating process
10. Reduction conditions are : 1bar, sample specific Temperatures (see Section 4.1.5) and additional 1 hour of heating after reaching set point
11. After reduction, Inert (Nitrogen) gas is flowed at 10 bars for 1 hour to cool sample to 250°C (change Temperature controller set point to 250°C) and remove excess reduction gas (5% H₂ in N₂). Flow line should be changed from reduction to inert gas line.
12. Reaction is then commenced at 250°C , 30 bars. Line is changed to reactant gas line.
13. Outlet gas line is maneuvered either to GC for analysis or effluent vacuum.

III. System Shutdown

1. Close gas flows from cylinder
2. Heater is turned off by control panel switch
3. Release gas to vacuum effluent line by switching ON the pressure relief valve.
4. Ensure there is no pressure reading from regulator
5. Switch off the valves' and heater switches on control panel
6. Close all needle valves beside the reactor
7. Turn off main switch on control panel
8. Allow reactor to cool down overnight before commencing the next sample loading

